AD-A085 707 AIR FORCE INST OF TECH WRIGHT-PATTERSON AFB OH SCHOO--ETC F/G 20/5
COMPARISON OF CONTROL METHODS IN A FREQUENCY STABILIZED LASER.(U)
JAN 80 R D LUZITANO
UNCLASSIFIED AFIT/GE/EE/80-2 NL

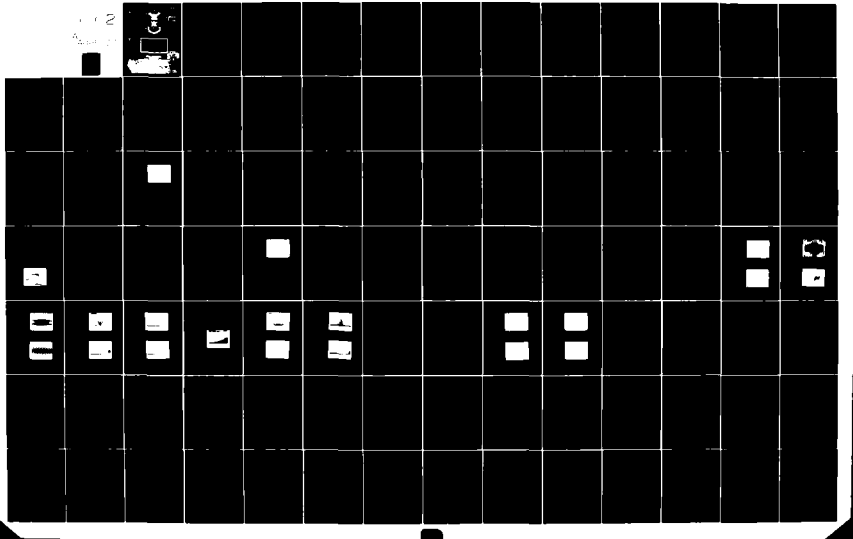

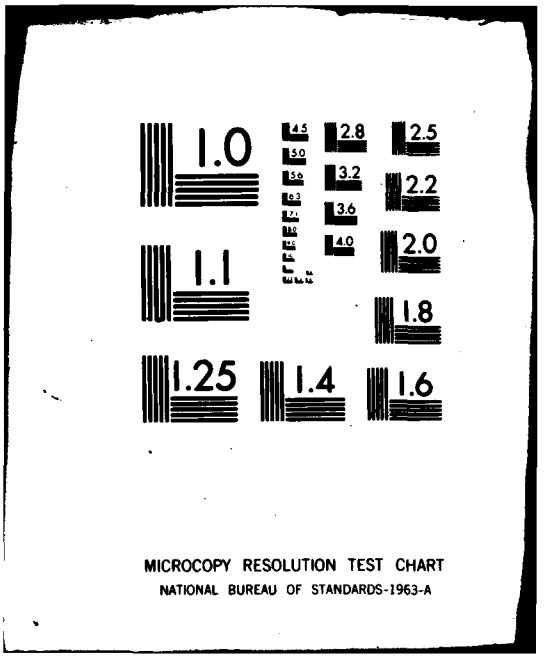
1.0
1.1
1.25
1.4
1.6
1.8
2.0
2.2
2.5
2.8
3.2
3.6
4.0
4.5
5.0
5.6
6.3
MICROCOPY RESOLUTION TEST CHART
NATIONAL BUREAU OF STANDARDS-1963-A

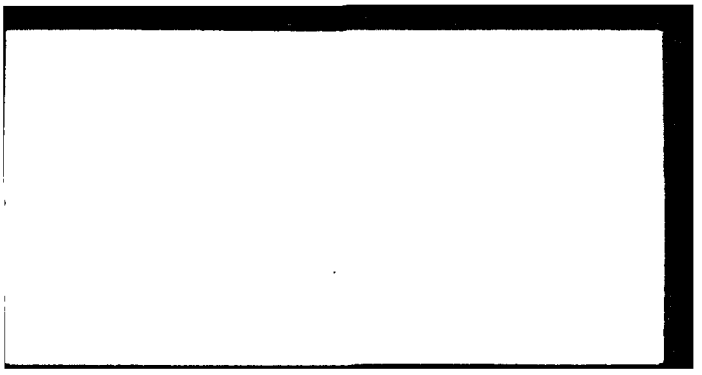

COMPARISON OF CONTROL METHODS IN A FREQUENCY STABILIZED LASER

THESIS

AFIT/GE/EE/80-2 Robert D. Luzitanc
Capt USAF

AFIT/GE/EE/80-2

COMPARISON OF CONTROL METHODS IN A FREQUENCY STABILIZED LASER

THESIS

Presented to the Faculty of the School of Engineering
of the Air Force Institute of Technology
Air University
in Partial Fulfillment of the
Requirements for the Degree of
Master of Science

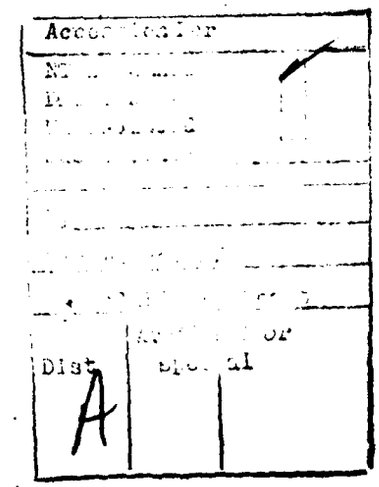

by

Robert D. Luzitano, B.S.
Capt USAF
Graduate Electrical Engineering
January 1980

Approved for public release; distribution unlimited.

Preface

The purpose of this thesis is to compare two different types of control methods that can be used to frequency stabilize a laser. This study should help solve some of the problems associated with the passive ring laser gyro work being done in the Navigation Laboratory at the Air Force Institute of Technology (AFIT).

My thanks are extended to Major Salvatore Balsamo for suggesting this area of research to me and for providing me with the necessary background knowledge and guidance during my studies. I also thank Dr. Kent Stowell of the Avionics Laboratory for sponsoring this thesis and for providing me with much of the equipment required during my research. In addition, special gratitude is extended to Mr. Carl Shortt and his personnel of the Model Fabrication Shop, and to Mr. Robert Durham and his personnel of the AFIT Electrical Engineering Laboratory for providing me with the fabricated components and technical expertise required during my research work. Finally, I thank my wife and family for their help, understanding, and devotion during this period.

Table of Contents

List of Figures

List of Figures

List of Figures

List of Figures

List of Figures

List of Tables

List of Symbols

Symbol	Definition
Å	Angstrom, equal to 10^{-10} meters
λ	Wavelength of helium-neon laser. Equal to 6328 Å
μ	Micro, equal to 10^{-6}
(s)	Indicates Laplace domain
ν	Laser resonant frequency
ν_R	Noise corrupted reference frequency
ν_C	Correction frequency
$\Delta\nu$	Axial mode spacing
$\Delta\nu_T$	Change in laser frequency per change in ^oF
$\Delta\nu_{PZT}$	Change in laser frequency due to a change in PZT length
$\Delta\nu_I$	Interferometer sensitivity in MHz/volt
$\Delta\nu_A$	Calculated value of the laser axial mode spacing
$\Delta\nu_M$	Measured value of the laser axial mode spacing
ΔL_T	Change in laser cavity length per ^oF
ΔL_{SB}	Change in length of the laser spacer bar per ^oF
ΔL_{EP}	Change in length of the laser end plates per ^oF
ΔL_{PZTM}	Change in length of the PZT mounts per ^oF
ΔL_{PZT}	Change in length of the PZT per ^oF
ΔL_{FW}	Change in length of the fiberglass washer per ^oF
ΔL_{SW}	Change in length of the steel washer per ^oF
ΔL_M	Change in length of a laser mirror per ^oF

List of Symbols

Symbol	Definition
ΔT	Change in temperature in ^{o}F
ΔT_C	Maximum temperature that can be compensated for
A	Operational Amplifier
C	Capacitor
c	Speed of light, $3x10^{10}$cm/sec
db	Decibel
D	Denominator of M_1
D_2	Desired closed loop denominator for variation 2 of method I
D_{3a}	Desired denominator of the closed loop transfer function using only the PZT_1 portion of method II
D_3	Desired closed loop denominator using method II
E	Error signal
e(t)ss	Steady state error signal
FSR	Laser free spectral range
Gc_1	Compensator used for variation 1 of method I
Gc_2	Compensator used for variation 2 of method I
Gc_3	Compensator used for method II
Gc_{3a}	Long PZT loop portion of Gc_3
Gc_{3b}	Short PZT loop portion of Gc_3
Gc_x	Dummy compensator
Gc_1N	Numerator of Gc_1
Gc_1D	Denominator of Gc_1

List of Symbols

Symbol	Definition
$Gc_{3b}N$	Numerator of Gc_{3b}
$Gc_{3b}D$	Denominator of Gc_{3b}
G_{X1}	Open loop transfer function for the single PZT controller without a compensator
G'_{X1}	Open loop transfer function using Gc_1 for variation 1 of method I
G''_{X1}	Open loop transfer function using Gc_2 for variation 2 of method I
G_{X2}	Open loop transfer function using the dual PZT controller Gc_3 for method II
G_{LIA}	LIA transfer function
$G_{HVA/PZT}$	Combined transfer function of HVA and PZT
ζ	Resonator parameter
HVA	High voltage amplifier
Hz	Hertz
K	Killo, 10^3
K_{LIA}	Unique LIA constant
K'_{LIA}	General LIA constant
K_{X1}	Numerator constant for G_{X1}
Kc_1	Numerator constant for Gc_1
Km_2	Numerator constant for M_2
Km_{3a}	Numerator constant for M_{3a}
Km_{3b}	Numerator constant for M_{3b}
K_{HVA}	HVA gain setting

List of Symbols

Symbol	Definition
K'	Variable gain of Gc_1
K''	Variable gain of Gc_2
$K''a$	Variable gain of Gc_{3a}
$K''b$	Variable gain of Gc_{3b}
L	Optical distance between laser mirrors
LIA	Lock-In-Amplifier
LIA_S	LIA sensitivity setting
$m_{1,2}$	Laser mirrors
M	Meg, 10^6
m	Milli, 10^{-3}
M_2	Control ratio for method I, variation 2
M_{3a}	Control ratio for method II using only Gc_{3a}
M_3	Control ratio for method II using Gc_3
N_2	Desired closed loop numerator for variation 2 of method I
N_3	Desired closed loop numerator of method II
N_{3a}	Desired closed loop numerator using only the PZT_1 portion of method II
PZT	Piezoelectric transducer
PSD	Phase sensitive detector
q	Laser frequency integer mode number
$r_{1,2}$	Laser mirror radius of curvature

List of Symbols

Symbol	Definition
R	Resistor
sec	Seconds
v	Volts
Vd	Detector output voltage
∞	Infinity

Abstract

The purpose of this research is to compare two types of control methods that can be used to frequency stabilize a laser. The first method uses a single piezoelectric transducer (PZT) to control the cavity length of a helium-neon laser. The second method employs dual PZT controllers of different lengths so that a fast response time can be achieved with the benefit of a large dynamic range. Two variations of the first method are compared to the second method. The first variation uses an integrator with gain as a compensator in an electronic feedback control loop and is designed using steady state analysis. The second variation uses a more sophisticated compensator that is designed using frequency analysis. Frequency analysis is also used in the compensator design for the second method. Each compensator is tested in a laser control loop and the results of each method are compared.

I Introduction

Over the last two decades, laser application has extended into the field of inertial navigation. Advancement in laser gyro technology now puts laser gyros on a competitive level with their counterpart, the mechanical gyro. Although the laser gyro does not have errors associated with moving parts, other error sources exist that effect its accuracy. A recent study by Olkowski and Holland concerning errors in a passive ring laser gyroscope, indicates a need for a frequency stabilized laser in order to overcome temperature and mechanically induced changes in the laser cavity (Ref 1:42). The following section explains how a laser resonant frequency may vary and introduces a method that can be used to stabilize the laser.

Background

The frequency spectrum associated with a true sinusoid is a narrow line while deviations from a true sinusoid cause a broadening of that line. The helium-neon lasers used in most laser gyros display a spectrum lineshape that is inhomogeneously broadened. This means that the collection of atoms in the laser medium can exhibit several resonant frequencies for the same laser transition. The laser output intensity versus frequency plot has a gaussian like shape, so variations in frequency also cause

variations in intensity.

The actual output frequency of a laser is determined by the optical distance between the laser mirrors which is known as the cavity length. O'Shea, Callen, and Rhodes show that the length of the laser cavity is equal to an integral number of laser half wavelengths (Ref 4:91). Written in terms of frequency,

$$\nu = q\left(\frac{c}{2L}\right) \tag{1.1}$$

where ν is the resonant frequency, q is an integer, c is the speed of light, and L is the optical cavity length. Since q can be any integer, there are many frequencies or axial modes that a laser may resonate at providing that ν is within the gaussian shaped intensity vs frequency plot. The axial mode frequency separation, $\Delta\nu$, is given by

$$\Delta\nu = \frac{c}{2L} \tag{1.2}$$

Figure 1.1 shows the relationship between the laser transition intensity, the axial mode spacing, and the laser output.

From the discussion and equations just presented, it is evident that any deviation in the cavity length will cause a deviation in the output frequency and intensity. In order then to control the frequency, the cavity length

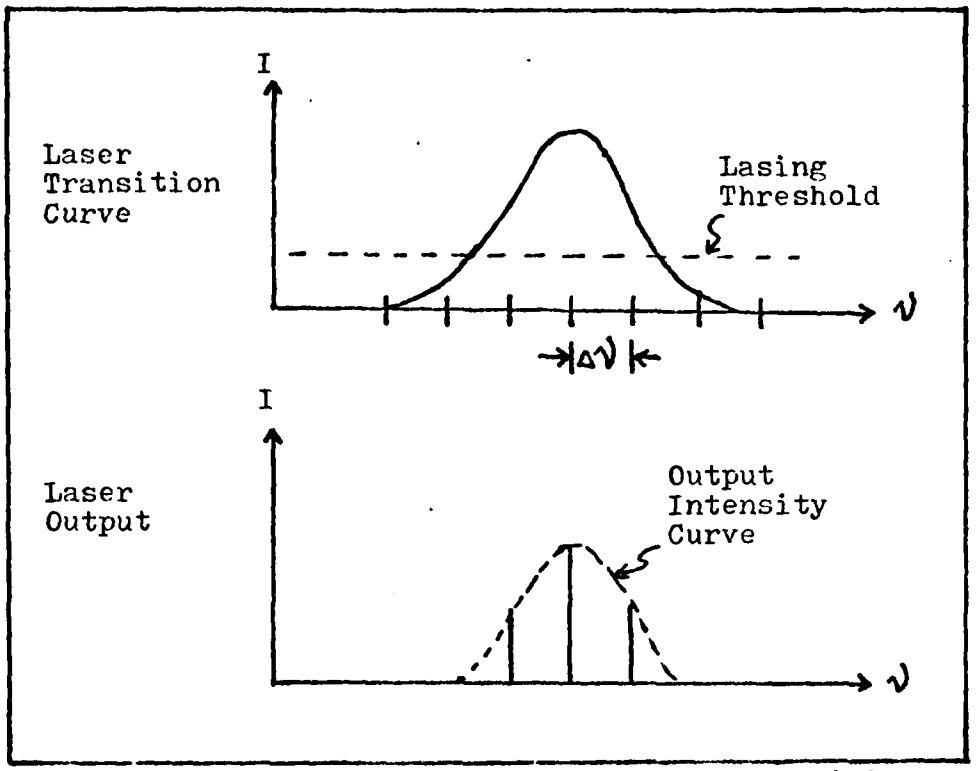

Figure 1.1 Relationship Between a Laser Transition Curve, Axial Mode Spacing, and Laser Output Intensity

must be controlled. A common approach used, and followed in this research, is to sample the laser output and compare it to a reference frequency. Deviations from the reference frequency are converted into an electrical signal. The signal is then routed through an electronic control loop to a piezoelectric transducer (PZT) that adjusts the length of the cavity to cancel the disturbance noise. The limitation on the feedback system is primarily due to the mechanical resonances of the PZT (Ref 3:346). For this reason, a method of control using two PZTs of different lengths looks very attractive. A long PZT is

needed to accommodate a large dynamic range to control disturbances such as temperature drifts. A short PZT with a fast response time is needed to control higher frequency noises.

Problem Statement

The purpose of this research is to ascertain the effectiveness of two control methods that can be employed to frequency stabilize a laser. The first method is a standard approach and uses a single PZT to control the length of a laser cavity. The control range of this method is limited by the length of the PZT. A long PZT is desired to provide a large control range, however, the added mass and length increases the response time. To overcome this limitation the second method uses dual PZT controllers. A long PZT is used to provide the desired control range and a short PZT is used to provide a fast response time. To ascertain the effectiveness of each control method, the magnitude and phase of the closed loop error signal must be recorded and analyzed.

Method of Approach

The method of approach starts with the selection of a basic control loop scheme. Laser frequency stabilization has been studied since the early sixties and, over the last two decades, many favorable schemes have been presented.

The basic scheme used in this research is similar to the one presented by P.W. Smith (Ref 3:343). An interferometer cavity is used as a frequency reference to which the laser output is compared. Frequency deviations are converted into an electrical signal and routed through an electronic feedback loop that controls the movement of a PZT to which one of the laser mirrors is attached. In this manner, noise disturbances causing frequency instability are sensed and countered by moving the PZT, thereby correcting the cavity length.

The next step in the approach was to design and build a laser. This was followed by a noise source study that included literature research and equipment experimentation. The laser control system was then modeled and transfer functions for each component were determined. Variations of method I included the design of a first compensater from steady-state analysis and the design of a second compensator using frequency analysis. The compensator for method II was also designed using frequency analysis. Finally, each compensator was used in the control loop and a spectrum analysis was made of the error signal. Results of each test were recorded and a comparison was made of the two control methods.

Order of Presentation

A description and results of the research are

presented in the following manner. First, the frequency stabilization theory is presented in Chapter II and is followed by a discussion of the laser design in Chapter III. Next, noise sources are analyzed in Chapter IV and system model parameters are determined in Chapter V. The compensators are designed in Chapter VI, and performance results and comparisons are presented in Chapter VII. Finally, conclusions and recommendations are made in Chapter VIII. In order to fully comprehend this material the reader should have a basic knowledge of the techniques used to frequency stabilize a laser.

II Frequency Stabilization

General Description

As pointed out in Chapter I, the output of a laser can contain many discrete frequencies separated by $\Delta\nu$. It was also pointed out that changes in the cavity length cause variations in the frequency output of the laser. Environmental noises such as temperature drift, acoustic noise, and table vibrations all contribute to fluctuations in the cavity length. Properties of the laser itself also contribute to frequency fluctuations, termed as output noise. The following two control methods are designed to reduce the effects of these noise disturbances.

Method I is a standard method and consists of a single PZT that controls the cavity length. As mentioned in the introduction, the limitation on the feedback system is primarily due to the mechanical resonances of the PZT. A long PZT is desired for its large dynamic range; however, the added length and mass lower the mechanical resonance and increases the response time. For this reason a second method of control is studied.

Method II consists of dual PZTs of different lengths to control the laser cavity length. A long PZT is used for its dynamic range and a short one is used to provide a fast response time.

The theory for each method is described in the

following sections, but first, the Fabry-Perot interferometer theory will be explained as it establishes the frequency reference for the control loop.

Fabry-Perot Interferometer

The Fabry-Perot interferometer shown in Figures 2.1 and 2.3 acts as a frequency reference to which the laser output is compared. As described by O'Shea, Callen, and Rhodes, a Fabry-Perot interferometer is an optical resonant cavity that consists of a pair of highly reflective mirrors parallel to each other, and whose separation can be varied (Ref 4:33). They further show that for most wavelengths only a small percentage of the light entering the cavity is transmitted. For certain wavelengths, however, nearly 100% of the light is transmitted. This transmission occurs when the optical distance between the mirrors equals an integral number of half-wavelengths of the incident light. The condition for resonance then is

$$\nu_I = m\left(\frac{c}{2d}\right) \qquad (2.1)$$

where ν_I is a resonant frequency of the interferometer, m is an integer, c is the speed of light, and d is the optical distance between the mirrors. Notice that Eq (2.1) is similar to Eq (1.1) as both the interferometer cavity and the laser cavity work on the same principle.

For a confocal cavity (radius of curvature of the mirrors equals the optical cavity length) with the reflectance of both mirrors close to unity, the transmittance, I_T, of an interferometer near a resonant frequency is (Ref 8:5)

$$I_T = \frac{1}{\left(1 + A/T\right)^2\left[1+\left(\frac{4\pi d}{\lambda(1-R)}\right)^2\left(\nu_N - \nu_I\right)^2\right]} \qquad (2.2)$$

where A is the dissipative mirror loss, T is the mirror transmittance, R is the mirror reflectivity, d is the optical distance between the cavity mirrors, ν_I is the cavity resonant frequency, and ν_N is a frequency close to resonance. For the Jodon SA-1500 interferometer used in this research $A<0.2\%$, $T\approx 0.8\%$, $R\approx 99\%$, $d=5$cm.

At resonance, the last term in the denominator of Eq (2.2) is zero and the transmittance becomes

$$I_T = \frac{1}{(1 + A/T)^2} \qquad (2.3)$$

Using the values shown for the Jodon SA-1500 interferometer,

$$I_T = 64\% \qquad (2.4)$$

It is easy to see from the denominator of Eq (2.2) that a small relative change in the frequency of the

incident light will create a large change in I_T. As an example, if $(\nu_N - \nu_I) \doteq 2$ MHz, which is small considering that ν for a helium-neon laser is $4.74\ 10^{14}$ Hz, then

$$I_T = \frac{1}{\left(1+\frac{0.002}{0.008}\right)^2\left[1+\left(\frac{4\pi\ 5\text{ cm}}{3\times10^{10}(1-0.99)}\right)^2\left(2\times10^6\text{ Hz}\right)^2\right]}$$

$$= 54.4\% \qquad (2.5)$$

This is a 9.6% decrease in I_T. This rapid drop in output intensity for a slightly off-resonance condition makes the Fabry-Perot interferometer an excellent device to use as a frequency standard in a control loop.

From Eq (2.1), if the cavity length is swept over a range of several wavelengths, the interferometer acts as a spectrum analyzer and can be used to show the spectral content of a laser as shown in Figure 2.0. The sharp peaks in Figure 2.0 represent the output frequencies of the laser that was built for this research.

In order to sweep the cavity length over several wavelengths, a slow varying ramp voltage is applied to a PZT mounted inside the interferometer housing. The PZT has one of the interferometer mirrors mounted to it so that a change in PZT length, caused by an external voltage, changes the optical cavity length and thus changes the condition for resonance.

The range of frequencies that can be swept through

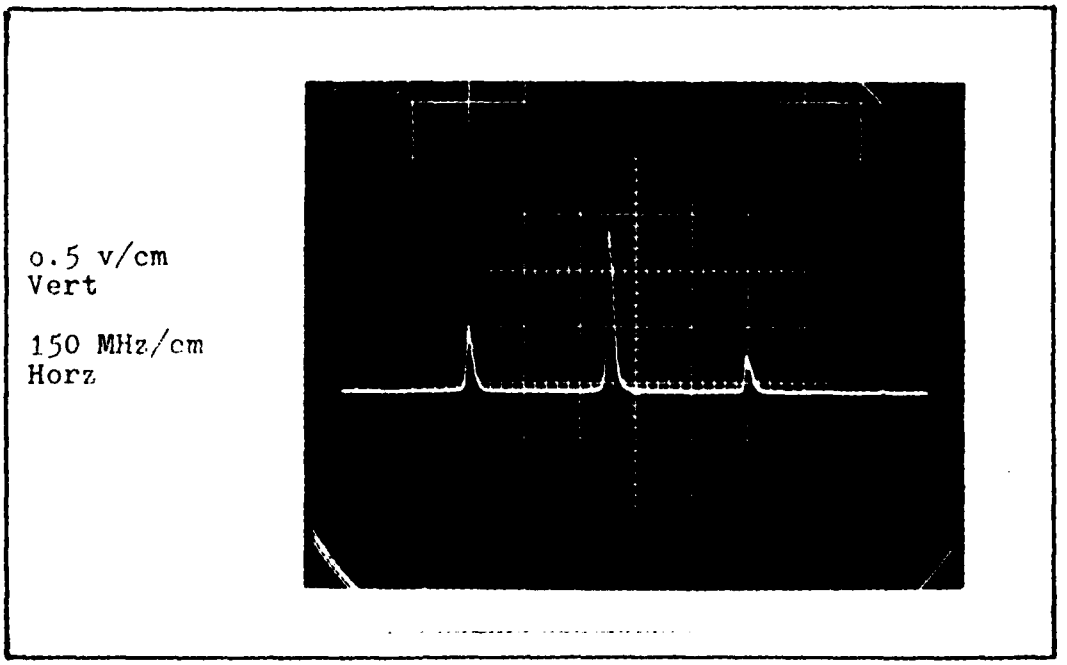

Figure 2.0 Laser Output Scanned With the Reference Interferometer

without repetition is known as the free spectral range (FSR), where

$$FSR = \frac{c}{2d} \tag{2.6}$$

The FSR for the laser used in this research is 1500 MHz. A Fabry-Perot interferometer is used as a frequency reference in both control methods I and II as seen in the following sections.

Control Method I

A control loop block diagram for the system used in method I is shown in Figure 2.1. The control loop model

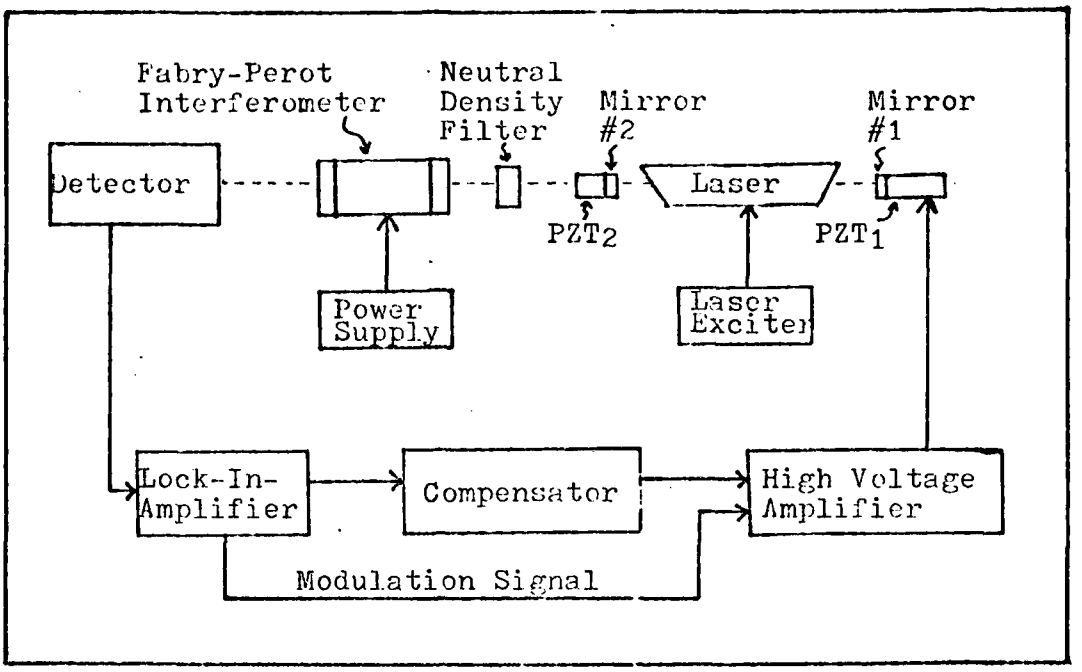

Figure 2.1 Control Loop Block Diagram for Control Method I

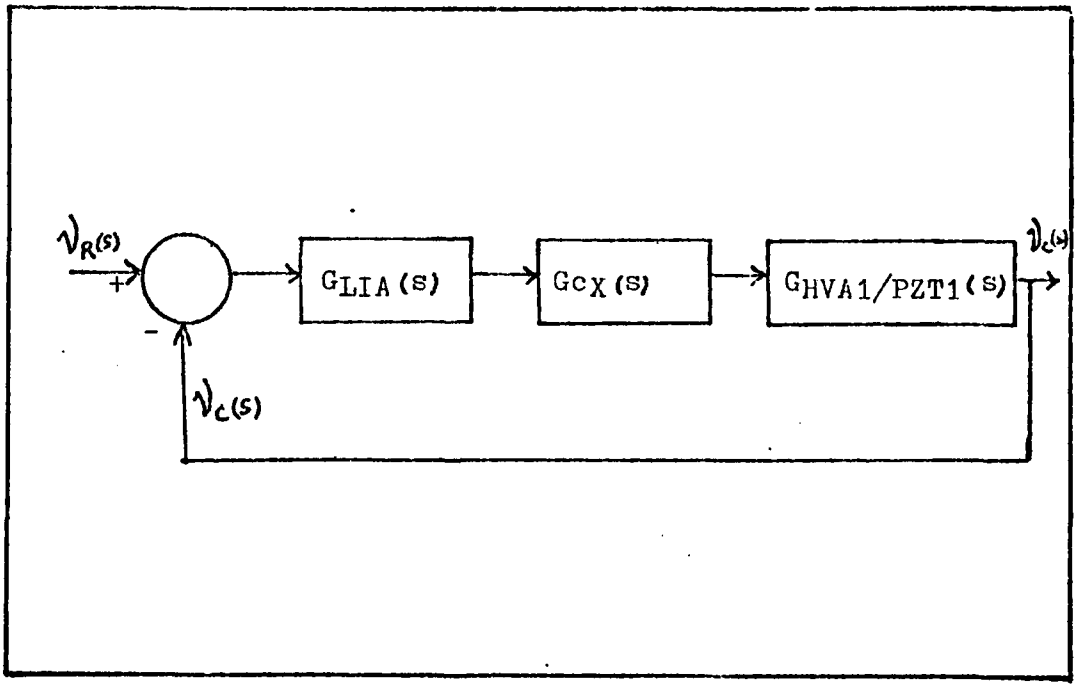

Figure 2.2 Control Loop Model for Control Method I

Table 2.1

Control Loop Symbol Definitions for Figures 2.2 and 2.4

Symbol	Definition
ν_R	Noise corrupted reference signal
ν_C	Control loop correction signal
G_{LIA}	Lock-In-Amplifier transfer function
$G_{HVA1/PZT1}$	High Voltage Amplifier #1/Piezoelectric Transducer #1 transfer function
$G_{HVA2/PZT2}$	High Voltage Amplifier #2/Piezoelectric Transducer #2 transfer function
G_{cX}	Compensators

for the system is shown in Figure 2.2 with symbols defined in Table 1.1.

Looking at Figure 2.1, light from the laser is passed through a neutral density filter and enters the Fabry-Perot interferometer. The neutral density filter reduces the intensity of the laser light in order to keep the detector in its linear region. The interferometer PZT is used to match the interferometer resonant cavity to a laser mode that has been positioned at the top of the laser output intensity curve with PZT_1. A frequency deviation in the laser output causes an off-resonant condition in the interferometer as explained earlier. The detector senses a sharp decrease in the intensity from the interferometer which results in a decrease in

voltage to the lock-in-amplifier (LIA). The LIA is the heart of the control loop and produces an error signal that locks the laser to the interferometer resonant frequency. A modulation technique is used within the LIA which locks the laser frequency to the interferometer resonance. This technique will be discussed in full detail in the following section. With reference to Figure 2.1, the error signal from the LIA is routed through a compensator that is designed in Chapter VI. The signal then goes to high voltage operational amplifier 1 (HVA_1). Note that the modulation frequency used in the LIA is also routed directly to HVA_1. The HVA sends a final correction signal to PZT_1 that has laser mirror m_1 mounted to it. Movement of the PZT by the loop counters the noise disturbance that caused the original frequency fluctuation in the laser output. In this manner, the laser is locked to the interferometer resonant frequency and noise that is within the bandwidth of the loop is suppressed.

The operation of control method II is similar to that just presented and is discussed in the following section.

Control Method II

A control loop block diagram for control method II is shown in Figure 2.3. The model for the system is shown in Figure 2.4 with symbol definitions as shown in Table 2.1.

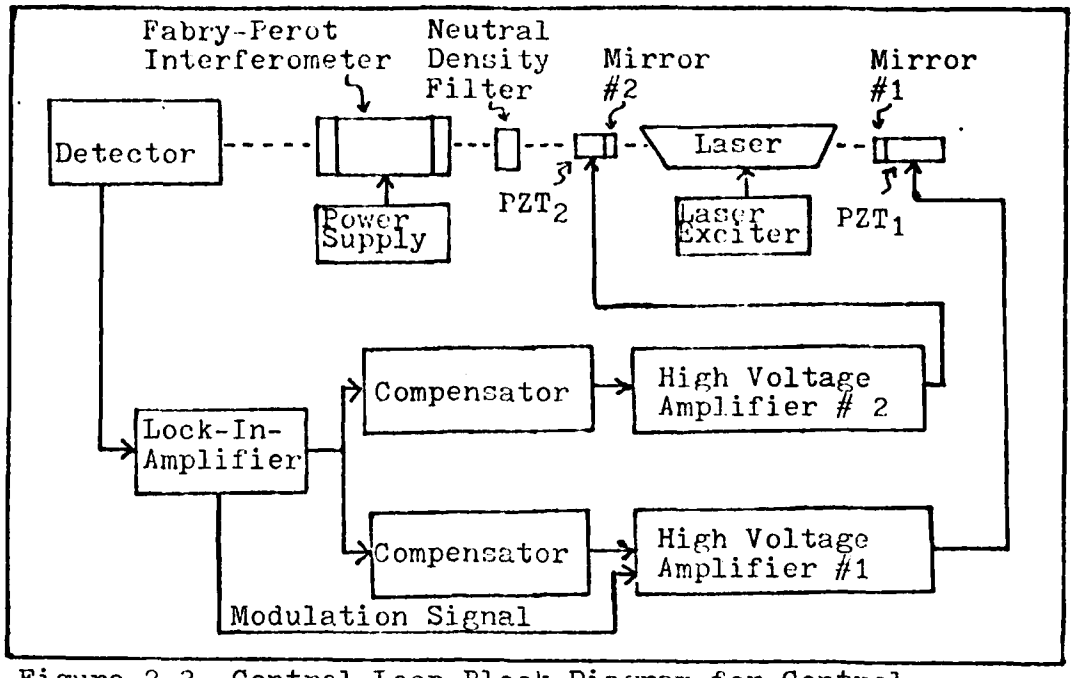

Figure 2.3 Control Loop Block Diagram for Control Method II

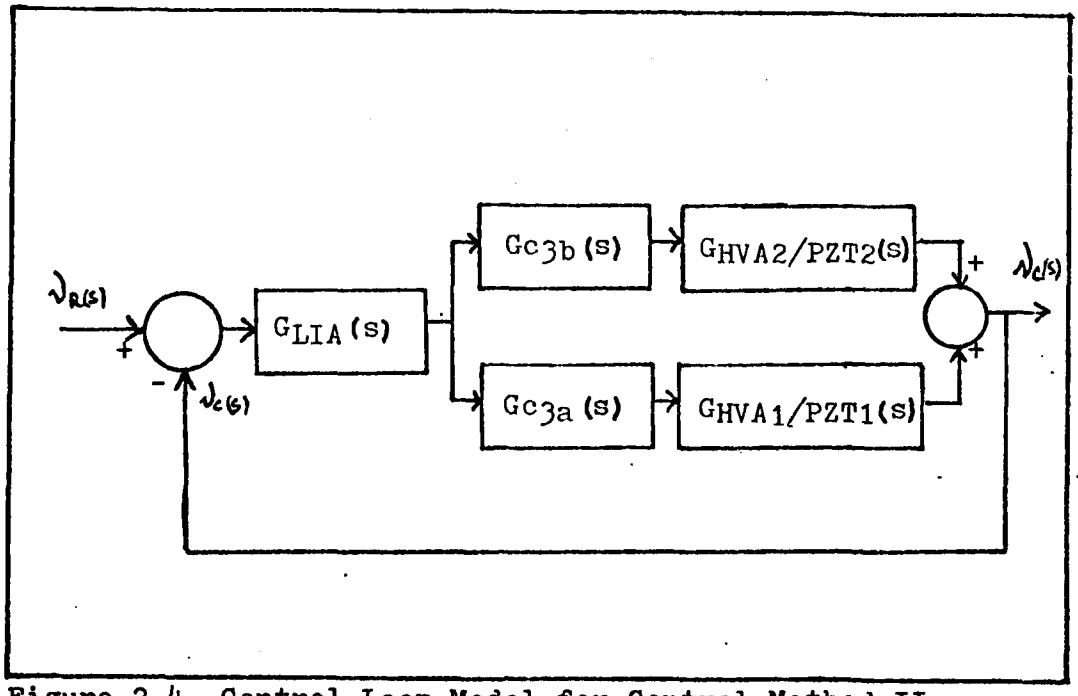

Figure 2.4 Control Loop Model for Control Method II

The theory used in control method II is the same as that for method I; however, the signal from the LIA is now split and goes to two different compensation networks. The design of these networks are quite different from each other and are fully described in Chapter VI. Correction signals leave each of the compensators and are amplified by HVA_1 and HVA_2 that control respective PZTs. Note that the modulation signal still goes to HVA_1 as in the previous section. The modulation technique is the same for both control methods and is described in the next section.

Modulation Technique

As stated earlier, the LIA is used to lock the laser frequency to the interferometer resonance. It accomplishes this by comparing the phase of a modulation signal to the phase of the returned signal from the detector and creates an error voltage proportional to the phase difference. A 41 KHz modulation signal is selected, as it is a resonant frequency of PZT_1 and is well beyond the bandwidth of the control loop.

Figures 2.5 through 2.8 are used to illustrate the reaction of the LIA to a frequency shift in the laser. When the laser cavity length is such that the laser frequency corresponds to point A in Figure 2.5, the output of the interferometer is at a maximum. As the PZT is

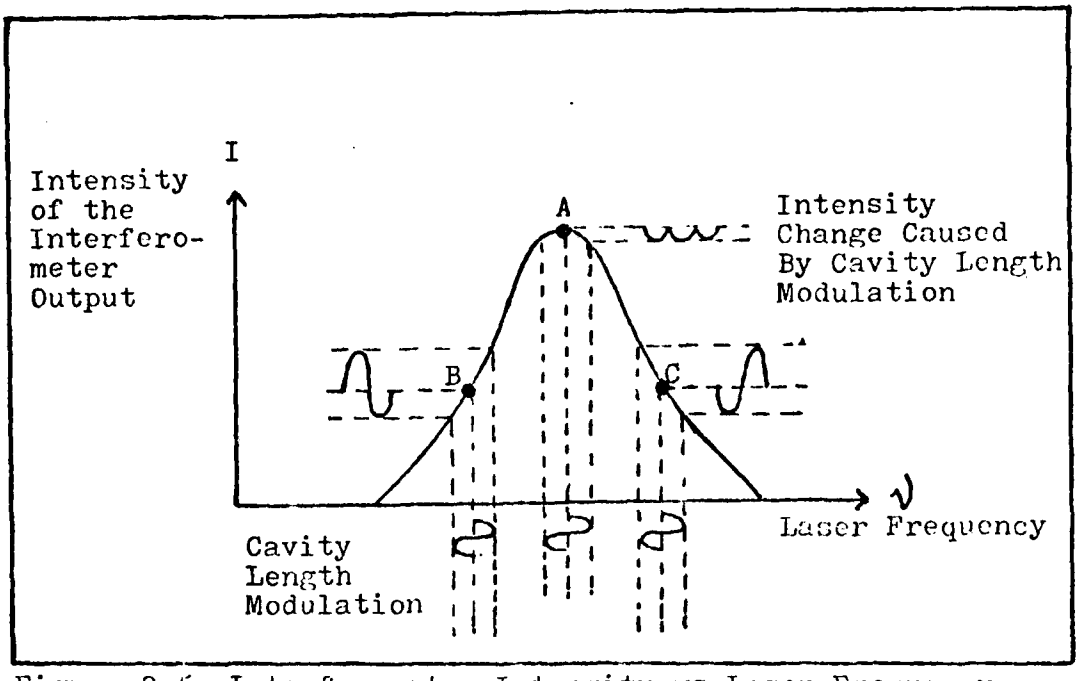

Figure 2.5 Interferometer Intensity vs Laser Frequency

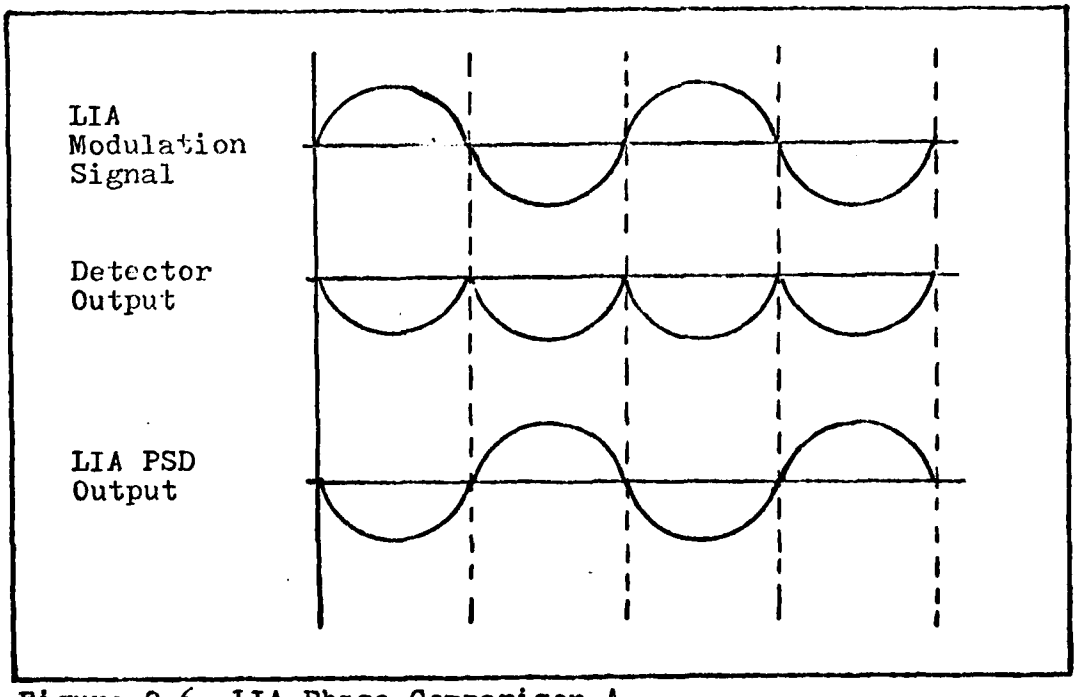

Figure 2.6 LIA Phase Comparison A

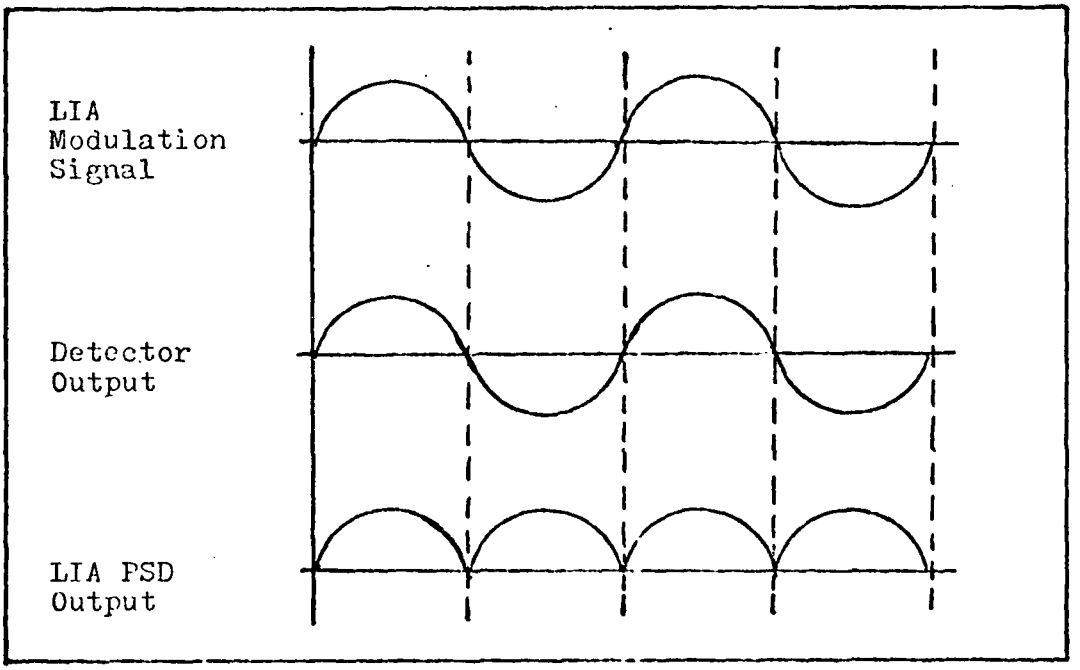

Figure 2.7 LIA Phase Comparison B

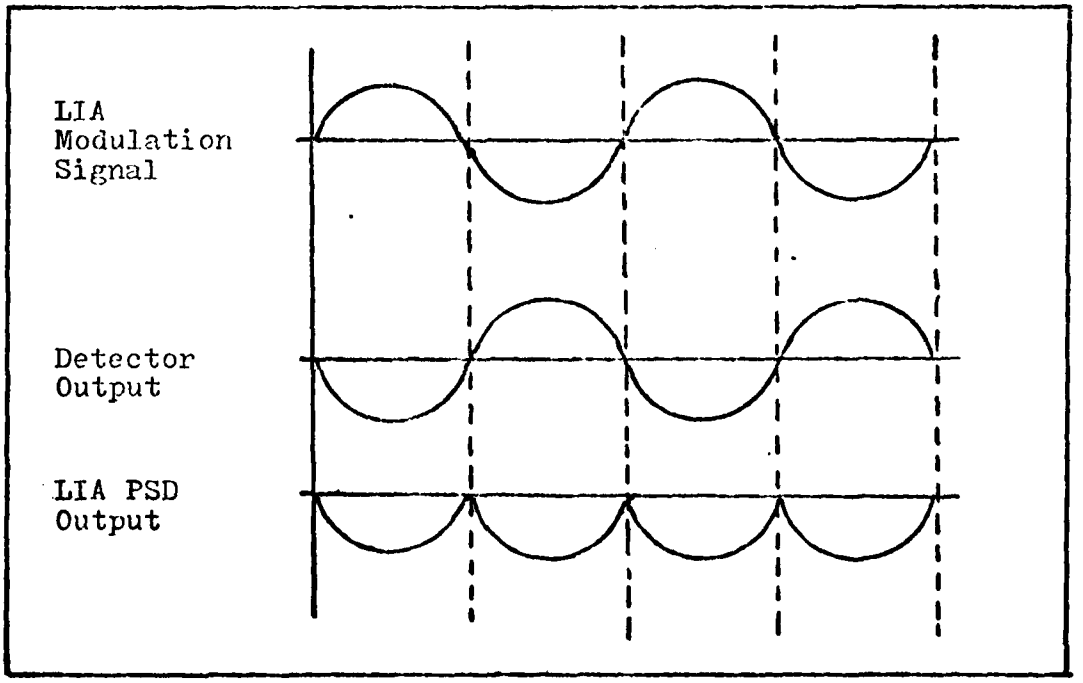

Figure 2.8 LIA Phase Comparison C

dithered by the modulation signal, it causes the laser to oscillate about point A which produces the detector output as shown in Figure 2.6. The modulation signal and the output of the detector are mixed in the LIA. The mixer, called a phase sensitive detector (PSD), produces the signal shown in Figure 2.6. The PSD signal is sent through a low pass filter inside the LIA which results in a zero DC level error signal. The laser cavity length thus remains unchanged.

When the laser cavity length produces a frequency corresponding to point B in Figure 2.5, the output of the interferometer is less than maximum. The modulation signal then causes the detector output to vary as shown in Figure 2.7. The LIA PSD produces a net positive signal as shown. This results in a positive DC level error signal. The error signal is routed to the PZT and causes it to lengthen thus increasing the laser frequency until it corresponds to point B in Figure 2.5.

When the laser cavity length produces a frequency corresponding to point C, the action is the same as that shown for point B, with signals as shown in Figure 2.8. For this case, the LIA produces a negative DC level error signal which results in an increase in cavity length and a lowering of the laser frequency to that corresponding to point B in Figure 2.5.

In the manner just described the laser frequency is

locked to the Fary-Perot interferometer resonant frequency. As noise causes the laser frequency to shift, the LIA and feedback loop always drives the frequency back to point B in Figure 2.5.

As stated in the introduction the limitation on the feedback system is primarily due to the PZT. The type of control compensation can also affect the control loop and is discussed in the following section.

Compensators

By adding compensators to the feedback loop, parameters of the loop can be altered. Three different types of compensators are designed, built, and tested with comparisons of the results made in Chapter VII.

The first compensator is used in the first variation of method I. It is designed using steady state analysis and consists of an integrator with gain. The presence of the integrator in the loop creates a type I system and, as pointed out by A.D. White, the system steady state error is expected to be zero for a step input and finite for a ramp input (Ref 2:350). White also points out that this may not be the most desirable compensator as it does nothing for the bandwidth of the loop.

The second compensator is used in the second variation of control method I. It is designed using the Guilleman-Truxal design procedure presented by D'Azzo and

Houpis (Ref 7:408). The compensator is basically an extension of the first design with additional circuitry to provide a closed loop bandwidth of 2 KHz. The second compensator is expected to increase the bandwidth of the control loop as compared to the first.

The third compensator is quite different from the first two as two PZTs are now used to control the cavity length. Different size PZTs are used in the laser design to accommodate both quick response and a large dynamic range. The compensator for the long PZT loop is designed first for a closed loop bandwidth of 100 Hz and ignores the short PZT loop. The compensator for the short PZT loop is then designed for a total system closed loop bandwidth of 2 KHz.

The overall step-by-step design of the compensators is presented in Chapter VI, but before that is done, the laser designed and built for this research will be described in the next chapter.

III Laser Design

General Description

A diagram of the laser is shown in Figure 3.1. The laser cavity is made up of two carbon steel end plates and utilizes four super-invar rods as spacer bars. Stainless steel mounting blocks are held to the end plates with four corner screws and alignment is accomplished with shims. PZT_1 is 1.5 inches long, and PZT_2 is 0.5 inches long. They are secured in their respective mounting blocks using set screws and epoxy glue. The laser mirrors are each glued to steel washers that are in turn glued to fiberglass insulators. Each of these combinations are glued to a PZT with the output mirror attached to PZT_2. The laser gain tube is held in place by two carbon steel support blocks that are suspended from the four spacer bars. The total cavity length, L (optical distance between mirrors), is equal to 39 cm. Scale drawings of the laser hardware are included in Appendix A. Figure 3.2 is a picture of the assembled laser and includes the reference interferometer.

A discussion concerning each critical component in the laser design is presented in the following sections.

Laser Gain Tube

A Spectra-Physics model 120 helium-neon gain tube is

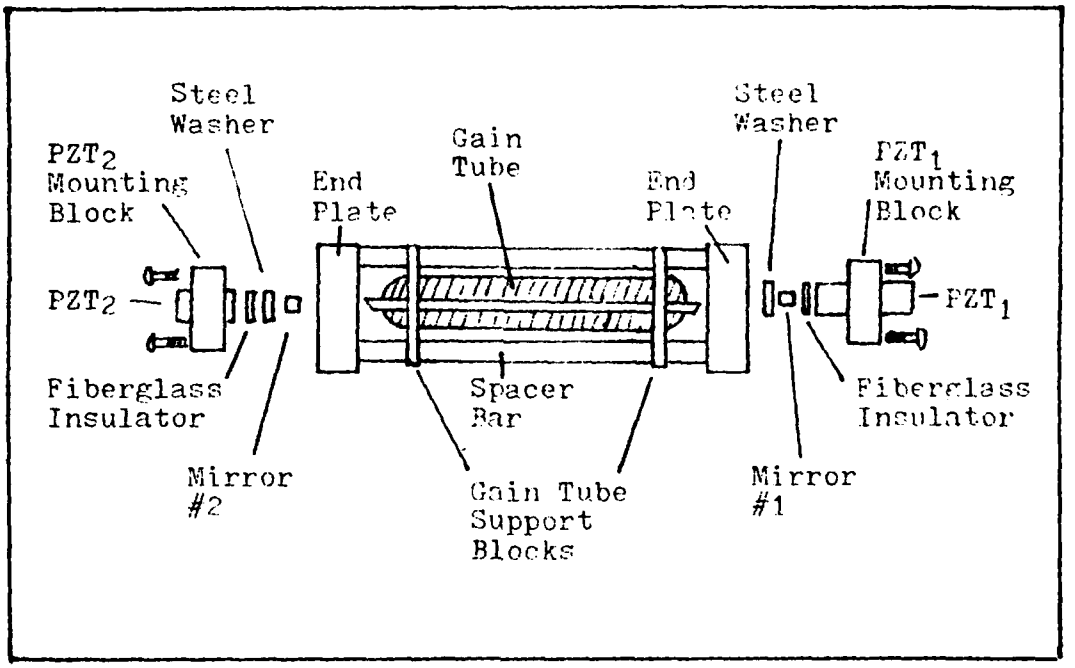

Figure 3.1 Laser Design

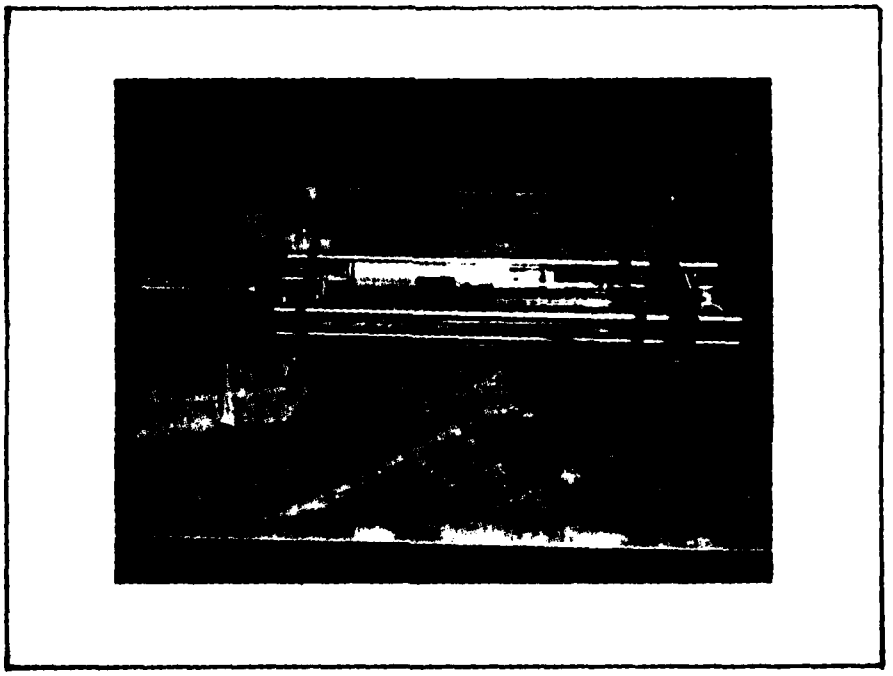

Figure 3.2 Assembled Laser With Interferometer

used as the heart of the laser and is pumped by a Spectra-Physics model 249 power supply. The gain tube draws approximately 6.0 ma and is designed for a 5 mw output.

Laser Mirrors

The laser mirrors were selected from parts on-hand in accordance with the following stability criteria. For stability,

$$0 < g_1 g_2 < 1 \qquad (3.1)$$

where g_1 and g_2 are dimensionless quantities and are the g-parameters of the resonator. The resonator g-parameters are

$$g_1 = 1 - \frac{L}{r_1} \text{ and } g_2 = 1 - \frac{L}{r_2} \qquad (3.2)$$

where r_1 and r_2 represent the radii of curvature of mirrors m_1 and m_2 and equal ∞ and 85 cm respectively. Solving Eq (3.2), $g_1=1$, and $g_2=0.541$. Eq (3.1) then becomes

$$0 < 0.541 < 1 \qquad (3.3)$$

and the stability criteria is met.

The transmittance of m_1 and m_2 are 0.01% and 2.0% respectively where m_2 is the output mirror.

Piezoelectric Transducers (PZTs)

The PZTs selected to adjust the cavity length are tubular transducers with wall thicknesses of 1/4 inches. One PZT is 1/2 inch long and the other is 1-1/2 inches long. The PZTs are center mounted, as shown in Figure 3.1, to eliminate reaction movement by the mount. Although data specifications such as bandwidth and sensitivity for the PZTs are given by the manufacturer, mounting methods make it necessary to experimentally obtain all required data. This is accomplished in Chapter V.

End Plate Spacer Bars

Super-invar is used as the spacer bar material because of its very low temperature expansion coefficient The importance of this can be seen by looking at Eq 4.1, Table 4.1, the Eqs that follow Table 4.1, and the following example.

If mild steel was used instead of super-invar, ΔL_{SB} from Table II would be 94.75×10^{-6} inches instead of 3.00×10^{-6} inches. This would result in ΔL_T equal to 257.1×10^{-6} cm/^{o}F instead of the value 24.06×10^{-6} cm/^{o}F found in Eq (4.2). The output frequency drift would then be -3125 MHz/^{o}F rather than the value -292.5 MHz/^{o}F shown in Eq (4.6). Using Eq (4.8), the range of temperature controllable by the laser would only be 0.03^{o}F instead of 0.32^{o}F as shown. With a controllable range this small,

it would be very difficult to keep the laser frequency stabilized.

Axial Mode Spacing

The calculated axial mode spacing $\Delta\nu_A$ is determined from Eq (1.2) and the measured value of L which is 39 cm. Then

$$\Delta\nu_A = \frac{3\times10^{10}\,cm/sec}{(2)(39cm)}$$

$$= 385cm \qquad (3.5)$$

It must be noted here that the determination of L was crude and will only be used to verify the much more accurate measured value of the axial mode spacing, $_M$.

Figure 3.3 is a picture of the laser output when scanned with the reference interferometer. The FSR of 1500 MHz is spread over 10 cm so that each cm equals 150 MHz. Since axial modes are shown to be 2.5 cm apart, the mode spacing is

$$\Delta\nu_M = \frac{(1500\,MHz)(2.5cm)}{10\,cm}$$

$$= 375\ MHz \qquad (3.6)$$

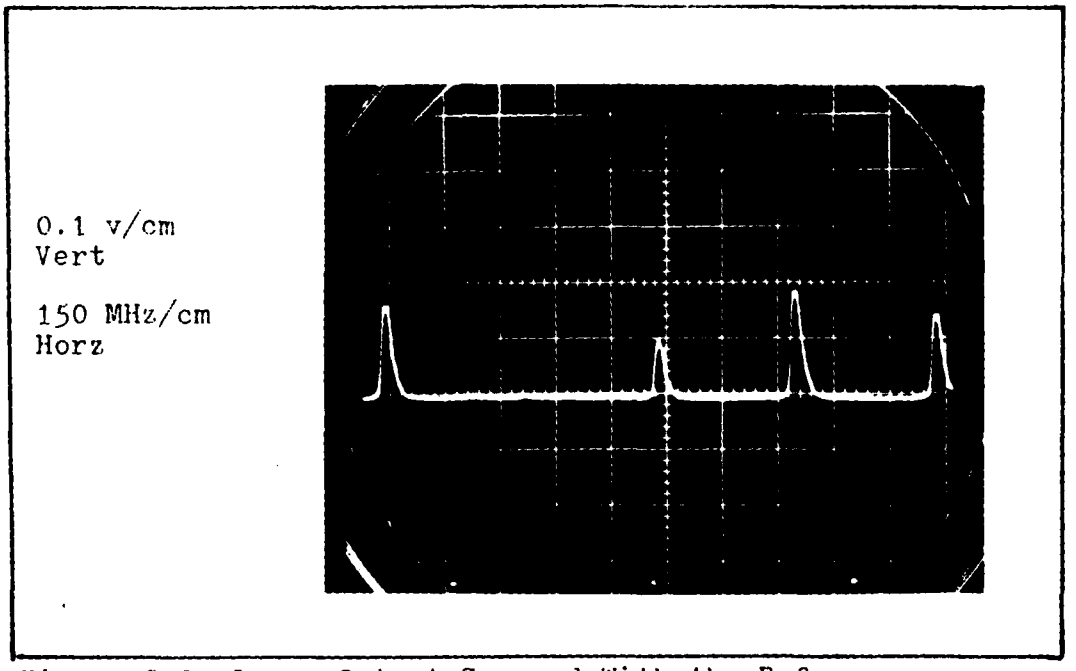

Figure 3.3 Laser Output Scanned With the Reference Interferometer for FSR Calculations.

Since it is difficult to perform this measurement due to laser drift, $\Delta\nu_M$ was determined several times and equation 3.6 is the average of those measurements. This is within 3% of the calculated value. The result of Eq (3.6) will be used in later calculations.

Although the laser is designed with noise suppression in mind, it is still subject to many disturbances that cause output noise. Some of these sources are studied in the following chapter.

IV Laser Noise Sources

General Discussion

Noise sources that cause frequency fluctuations in a laser can be grouped into three catagories: environmental noises, noises from the gain tube, and noises from the control loop. Environmental noises are the predominant ones and consist of temperature drifts, acoustical noise, and table vibrations. Noises from the gain tube are caused by such things as variations in the index of refraction of the active gas, variations in the gas pressure and temperature, and variations in the discharge conditions. Noise from the control loop is emitted from the electronic components and is very small.

Most of the noises can be calculated and will be analyzed in the following sections. From the results, it is expected that the spectral content of appreciable laser noise will be well below 3 KHz and will be controllable.

Laser Noise due to Temperature Changes

Temperature drift or fluctuation is low frequency in nature and is by far the largest contributor to laser frequency noise. The biggest affect is on the cavity length, and this is the reason invar material was chosen for the spacer bars. The change in cavity length, ΔL_T, due to temperature change, ΔT, in degrees Fahrenheit is

Table 4.1

Temperature Affects on the Laser Components

Component	Component Length	Temp. Coef. 10^{-6} in/in F	L due to T	
			10^{-6} in	Symbol
Super Invar Spacer Bars	15.040	0.2	3.008	ΔL_{SB}
Mild Steel End Plates	11.000	6.3	6.3	ΔL_{EP}
Stainless Steel PZT Mounts	0.375	9.6	3.6	ΔL_{PZTM}
PZTs	1.000	1.18	1.18	ΔL_{PZT}
Fiberglass Washer	0.026	5.5	0.143	ΔL_{FW}
Mild Steel Washer	0.097	6.3	0.611	ΔL_{SW}
Mirror	o.250	6.0	1.5	ΔL_M

calculated using Eq (4.1), as follows:

$$\Delta L_T = \Delta L_{SB} + \Delta L_{EP} + \Delta L_{PZTM} - \Delta L_{PZT} - \Delta L_{FW} - \Delta L_{SW} - \Delta L_M \qquad (4.1)$$

The terms in Eq (4.1) are defined in Table 4.1. Using the values from Table 4.1 and converting them to cm yields

$$\Delta L_T = 24.06 \times 10^{-6} \text{ cm/°F} \qquad (4.2)$$

The change in frequency, $\Delta\nu_T$, due to Δ_T can be calculated from Eq (1.1).

The effect on ν caused by a small change in L is

$$\delta\nu = \frac{-q c}{2L^2}\,\delta L \tag{4.3}$$

If ΔL_T and $\Delta\nu_T$ are assumed to be small then they can be substituted into Eq (4.3) so that

$$\Delta\nu_T = \frac{-q c}{2L^2}\,\Delta L_T \tag{4.4}$$

Substituting $q\lambda$ for 2L, Eq (4.4) becomes

$$\Delta\nu_T = \frac{-c}{\lambda L}\,\Delta L_T \tag{4.5}$$

Then

$$\Delta\nu_T = \frac{-(3\times10^8\ m/sec)}{(6328\times10^{-10}m)(39cm)}\left(24.06\times10^{-6}cm/^\circ F\right)$$

$$= -292.5\ MHz/^\circ F \tag{4.6}$$

The sensitivity of PZT_1 from Chapter V is used to calculate the controllability of the laser due to temperature changes. From Eq (5.1), the PZT_1 sensitivity in terms of ν is 0.1875 MHz/volt. With 500 volts available from the HVA, the change in laser frequency, $\Delta\nu_{PZT1}$, due to a maximum change in length of PZT_1, is

$$\Delta\nu_{PZT1(max)} = 93.75\ MHz \tag{4.7}$$

Using Eqs (4.6) and (4.7) to solve for the maximum temperature change that can be compensated for using PZT_1 yields:

$$\Delta T_c = \frac{\Delta \nu_{PZT1}}{\Delta \nu_T}$$

$$= \frac{93.75\ MHz}{292.5\ MHz/°F}$$

$$= 0.32\ °F \qquad (4.8)$$

It must be noted that a change in temperature also changes the cavity length of the interferometer. For this reason, the interferometer was thermally wrapped with styrofoam and tape to reduce the effect of temperature changes during an experiment.

Laser Noise Due to Acoustical Noise and Table Vibration

Since actual measurments of acoustical and vibrational affects were not made, an experiment by Haruhiko Nagai was used to estimate their affects and is presented here (Ref 6). The construction of Nagai's laser and the one used in this research are very similar. The major differences are that his cavity length is about one third the size of the one used here, and his mirror holders use spring loaded adjustment screws where the holders used here are hard mounted with shims.

In part of Nagai's experiment, he determines the lowest natural frequency of each mechanical element in the cavity by the use of sound pressures generated by a loud speaker. He compares the results with those obtained analytically to show that the mirror holder system's natural frequency has components of 40 Hz and 100 Hz, while the frequency of the spacer system is 3 KHz (Ref 6:863). Since the mirror holders on the laser used here are hard mounted, it is assumed that the noise content will not be any greater then found by Nagai. Also, since the spacer system used here is three times longer, the spacer system resonant frequency is expected to be smaller than 3 KHz.

Nagai shows that his laser frequency fluctuations due to acoustical noise was about 9.6 KHz and that due to vibrations was about 110 KHz (Ref 6:863). Care was taken during this research to isolate the laser work-plate by placing it on foam rubber. Also, a plastic shield was used to cover the laser in order to isolate the laser from acoustical noise. With the precautions taken, it is assumed that the affects of vibration and acoustical noise would not be very much greater than that found by Nagai.

Laser Noise from the Gain Tube Noises

Gain tube noises are very small compared to the others presented. Nagai points out that variations in

the refractive index of active gas is about 1 MHz/ma for a laser tube very similar to the one used in this research (Ref 6:858). Since the laser power supply has less than a 0.3 ma variation, a laser noise of less than 300 KHz is expected. Other noises previously mentioned are troublesome only when stability requirements are greater than 1 part in 10^{10} (Ref 5.11).

Noises from the Control Loop

Noises from the control loop are very small, as seen in Figures 4.1 to 4.5 found at the end of this section, and have little affect on the laser frequency. This is due to a very high signal-to-noise ratio in the circuitry and also to the fact that almost all of the gain in the loop is put into the preamplifier of the LIA.

An example of a typical open loop signal-to-noise ratio achieved in the loop can be given by looking at the noise from the LIA shown in Figure 4.3. The maximum peak-to-peak amplitude is about 0.1 volts. The expected error signal produced from a 1 MHz shift in the laser frequency is 12 volts, as shown by Eq (5.4). This equates to a signal-to-noise ratio of about 120 to 1. With a large gain at the front end of a closed loop, noise created in the loop is effectively reduced providing it is within the bandwidth of the loop.

Figures 4.6 to 4.10, located at the end of this

section, show the frequency spectrum of the noise from each of the control loop components. Most of the noise from the components is less than 500 Hz/sec. The LIA has the largest spectral spread and decays exponentially to about 20 db between zero and two KHz as seen in Figure 4.8.

HVA_2 has a noise component of 1.2 MHz, as seen in Figure 4.5, which is outside the bandwidth of the control loops. This noise, however, has little affect on the laser frequency because of its small amplitude and because it is far beyond the mechanical response limit of the PZTs.

A noise source that is critical is the interferometer power supply as it causes fluctuations in the reference frequency. The noise level is shown to be about 0.006 volts as seen in Figure 4.1 and has a 60 Hz/sec spectral content. Using Eq (5.1), the reference frequency fluctuations are about 41 KHz and will occur at a 60 Hz/sec rate. This is only significant for a stability requirement greater than 1 part in 10^{10}.

In summary, a control loop with a 2.0 KHz bandwidth should be able to reduce all of the critical noises shown in this section.

Identification of noise sources is a major step in the design of a good control network. Determination of control loop parameters is also a major step and is accomplished in the following chapter.

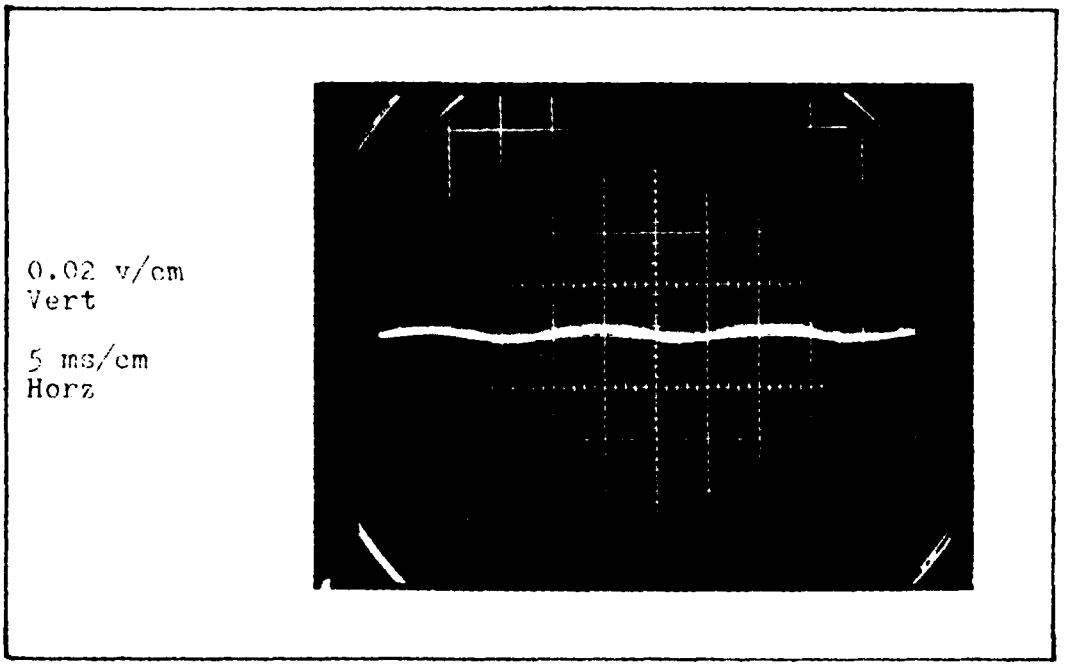

Figure 4.1 Noise from the Interferometer Power Supply

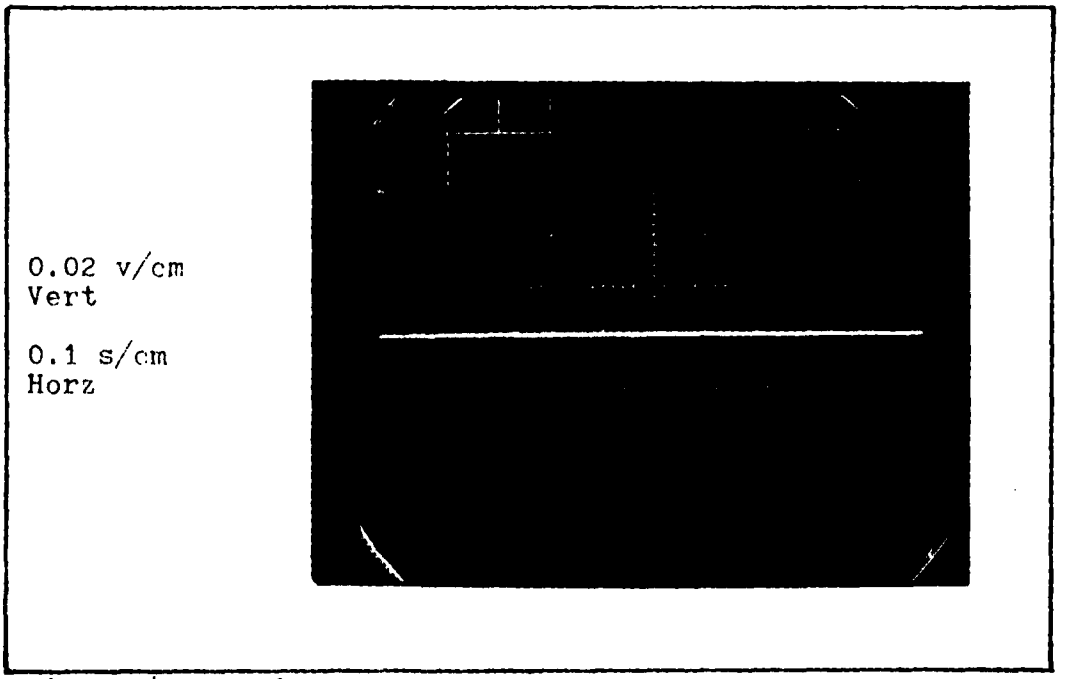

Figure 4.2 Noise from the Detector With the Laser Blocked

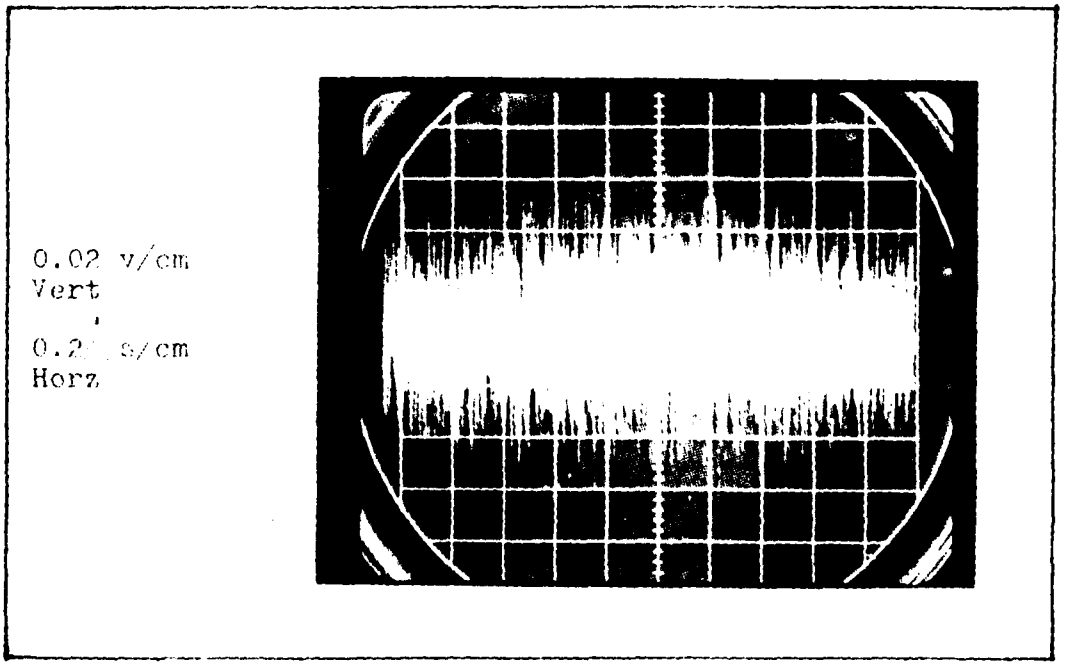

Figure 4.3 Noise from the LIA

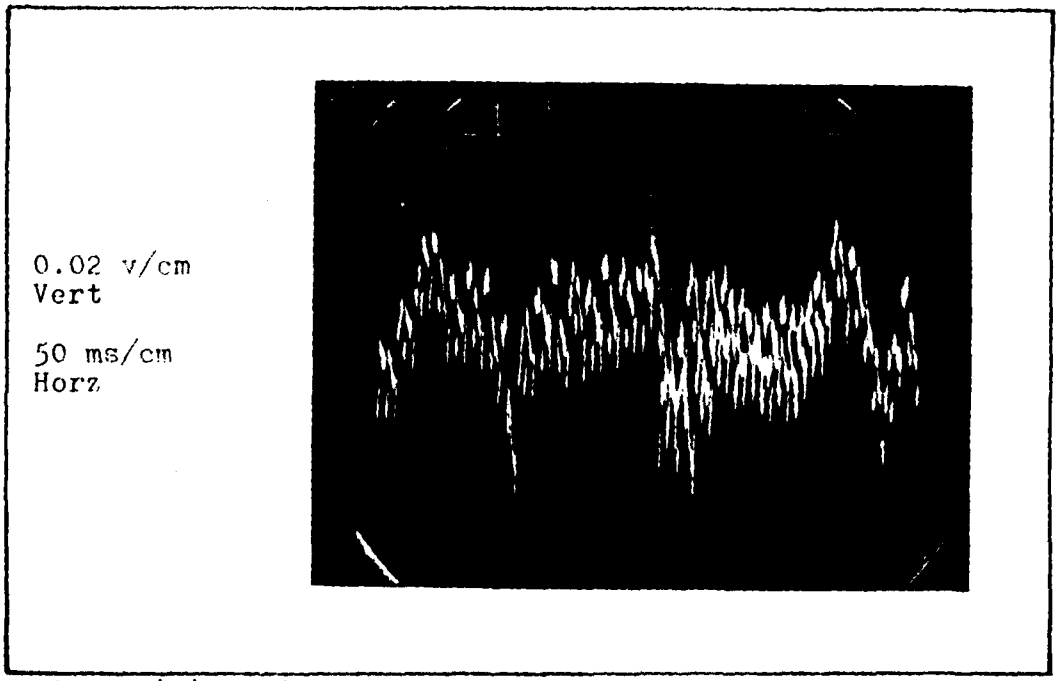

Figure 4.4 Noise from HVA1

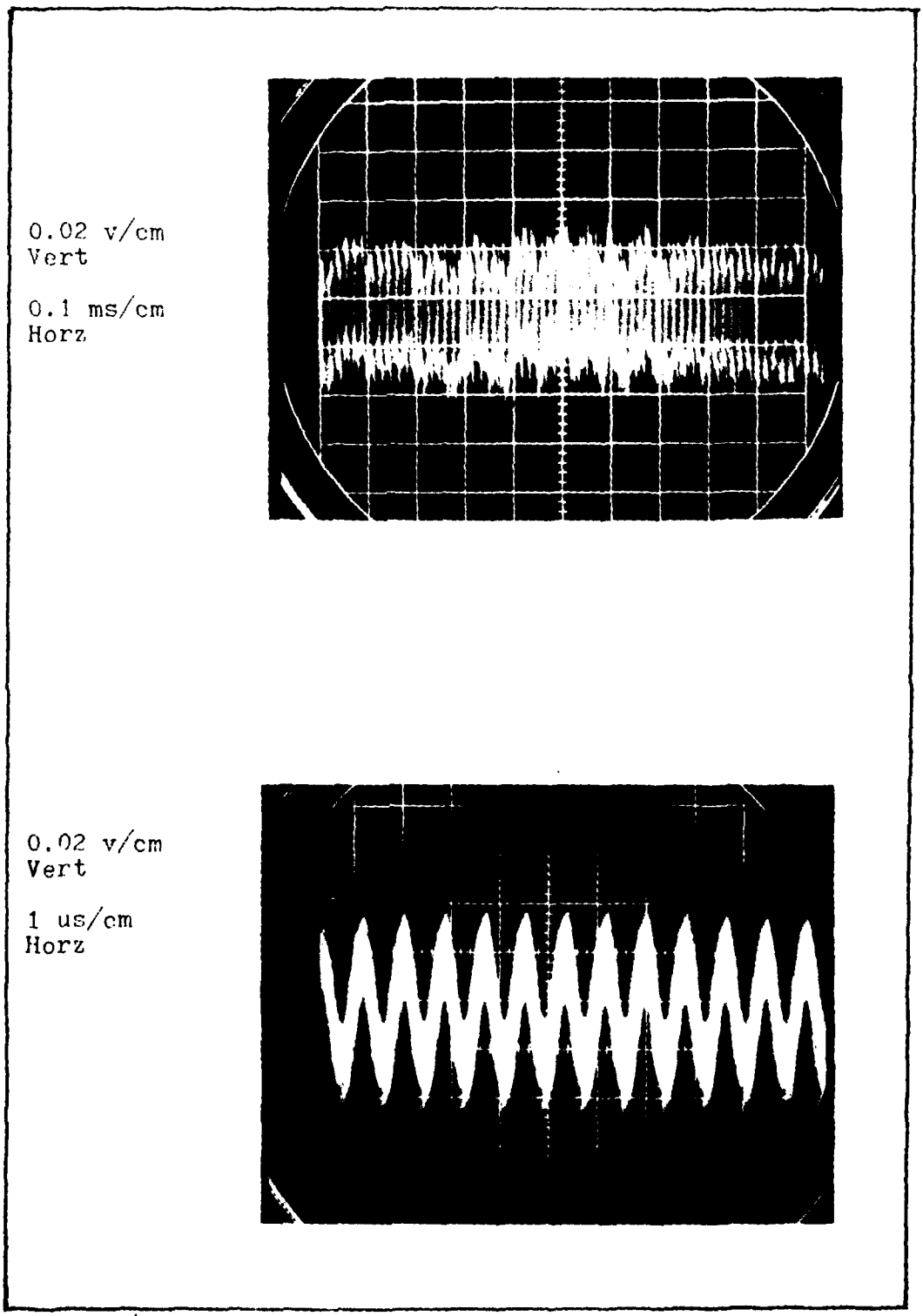

Figure 4.5 Noise from HVA_2

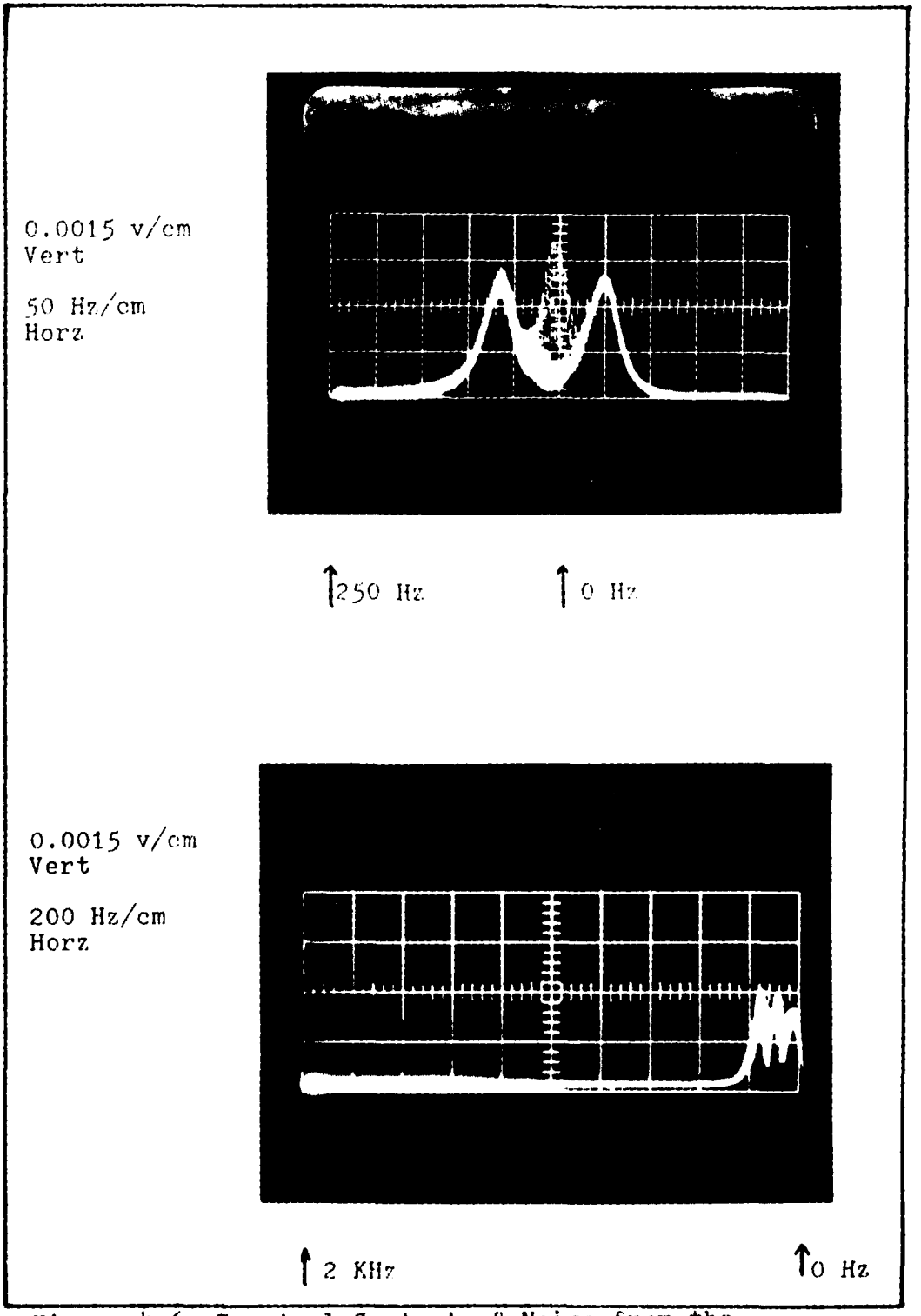

Figure 4.6 Spectral Content of Noise from the Interferometer Power Supply

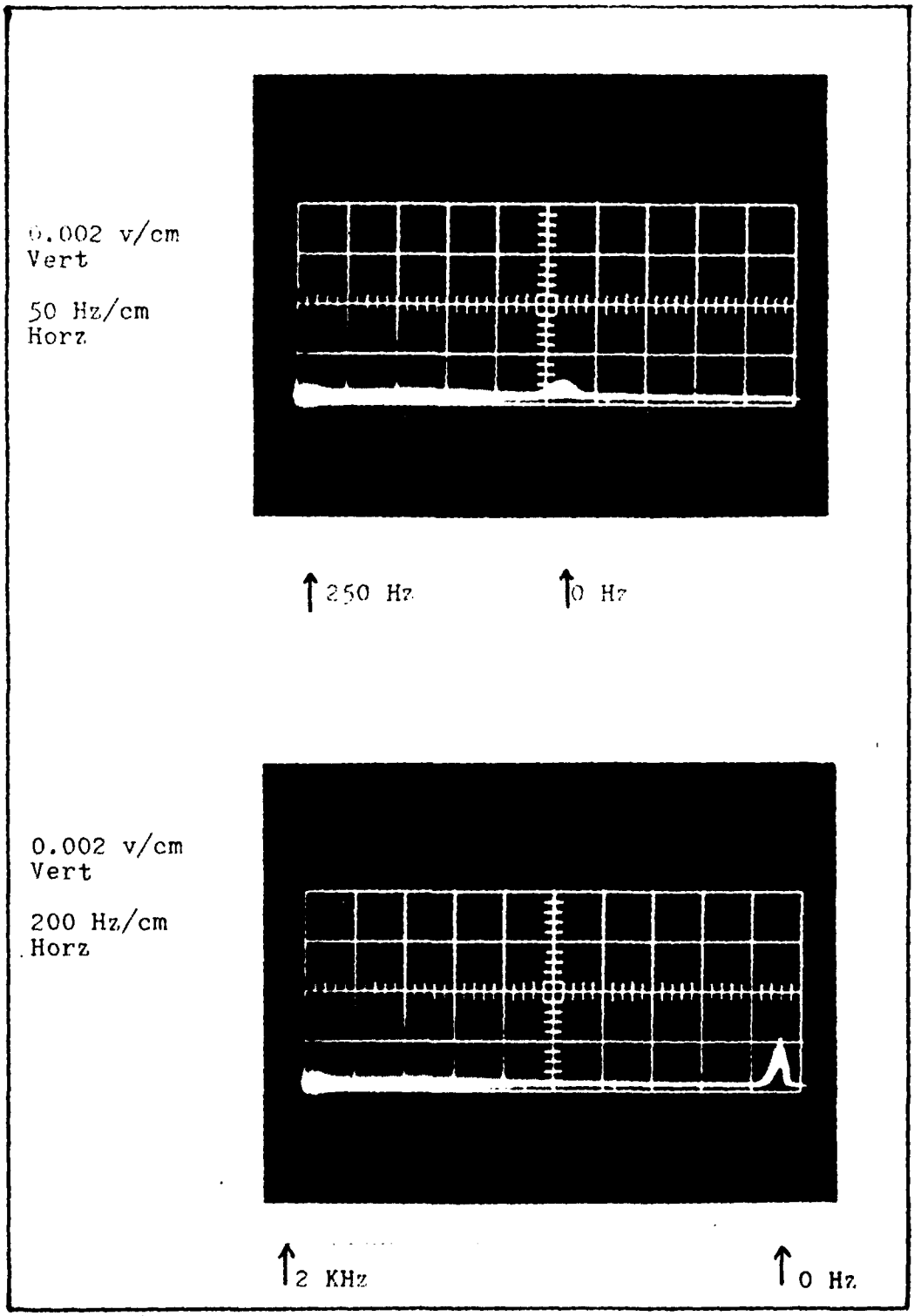

Figure 4.7 Spectral Content of Detector Noise with the Laser Blocked

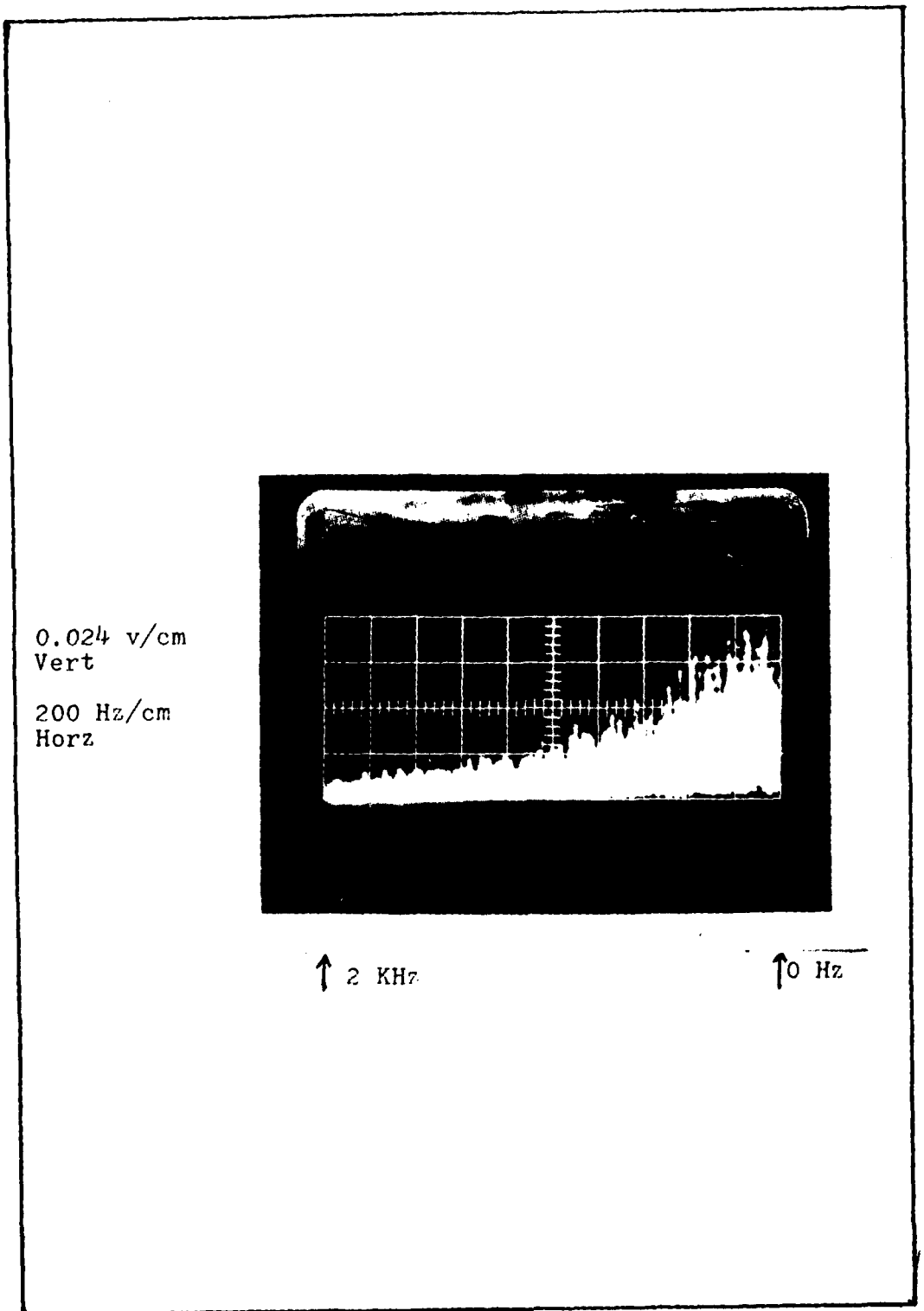

Figure 4.8 Spectral Content of Noise from the LIA

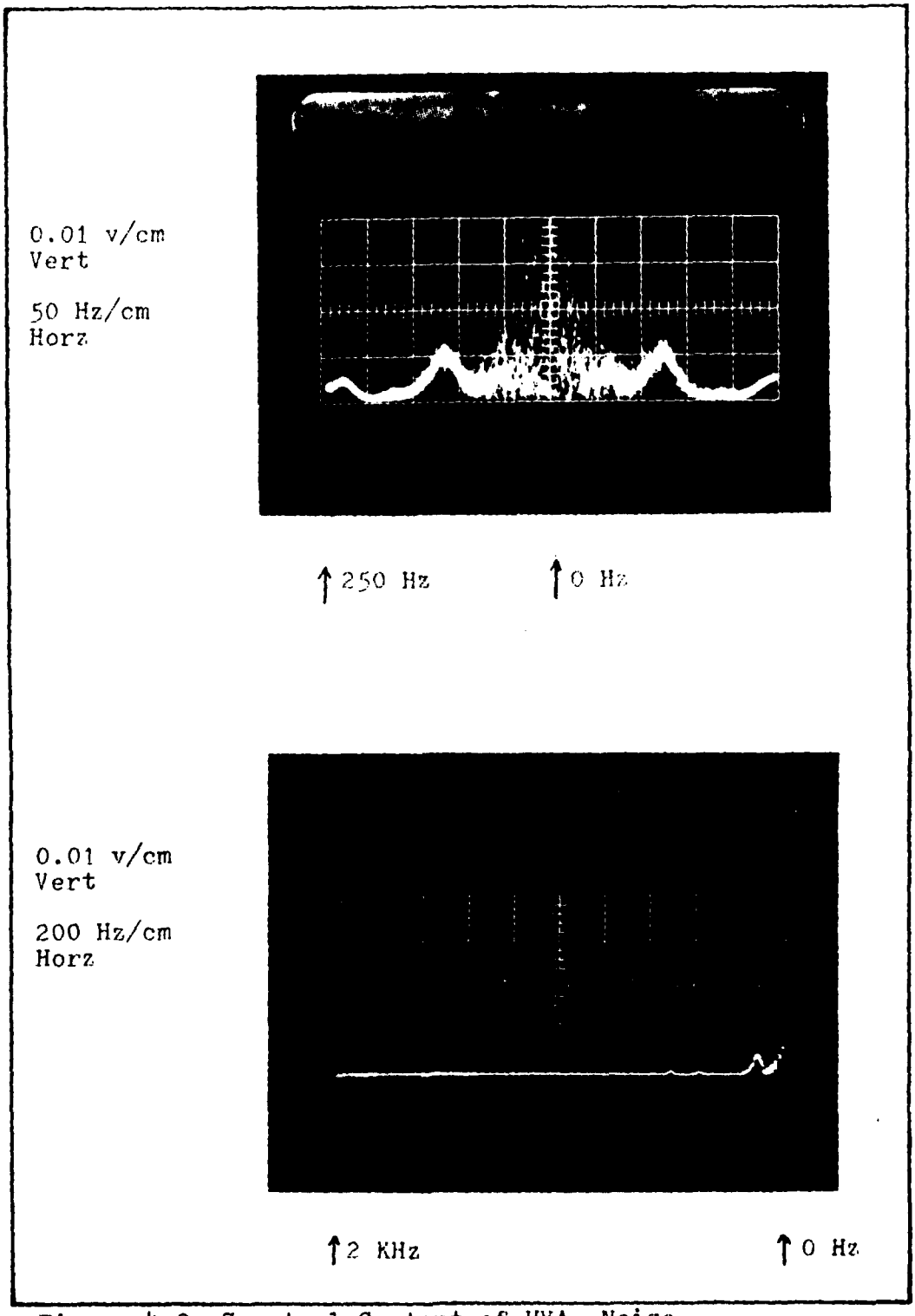

Figure 4.9 Spectral Content of HVA_1 Noise

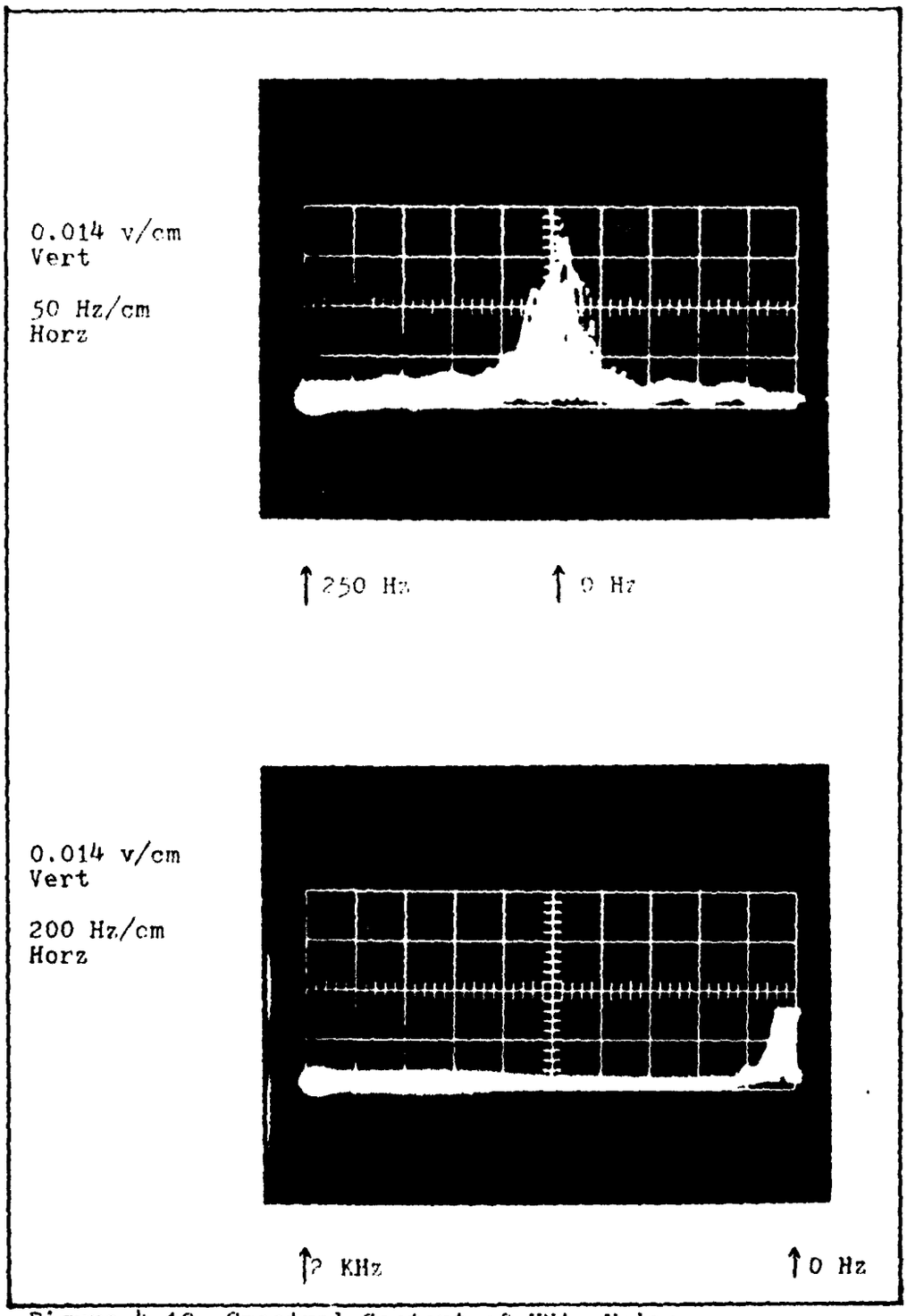

Figure 4.10 Spectral Content of HVA_2 Noise

V System Model Parameters and Transfer Functions

General Discussion

This chapter deals with solving the system model parameters. First the interferometer sensitivity is determined and is followed by the determination of PZT_1 and PZT_2 sensitivities. Next, the LIA constant is determined and the frequency characteristics are found for the LIA and HVA/PZT combinations.

Interferometer Sensitivity ($\Delta\nu_I$)

The interferometer sensitivity, $\Delta\nu_I$, in MHz/volt, was determined using the equipment set-up shown in Figure 5.1. The interferometer resonance was matched to a laser mode by adjusting the interferometer's internal PZT with HVA_2. When resonance was achieved, as indicated by a maximum voltage on the oscilloscope, the voltage setting of HVA_2 was recorded. HVA_2 was then slowly adjusted until a new interferometer resonance matched the next mode. The new voltage setting of HVA_2 was recorded and the difference between the two settings was determined. This experiment was performed several times for an average differance voltage of 55 volts. Since the laser mode spacing, $\Delta\nu_M$, from Eq (3.6) equals 375 MHz, the interferometer sensitivity becomes

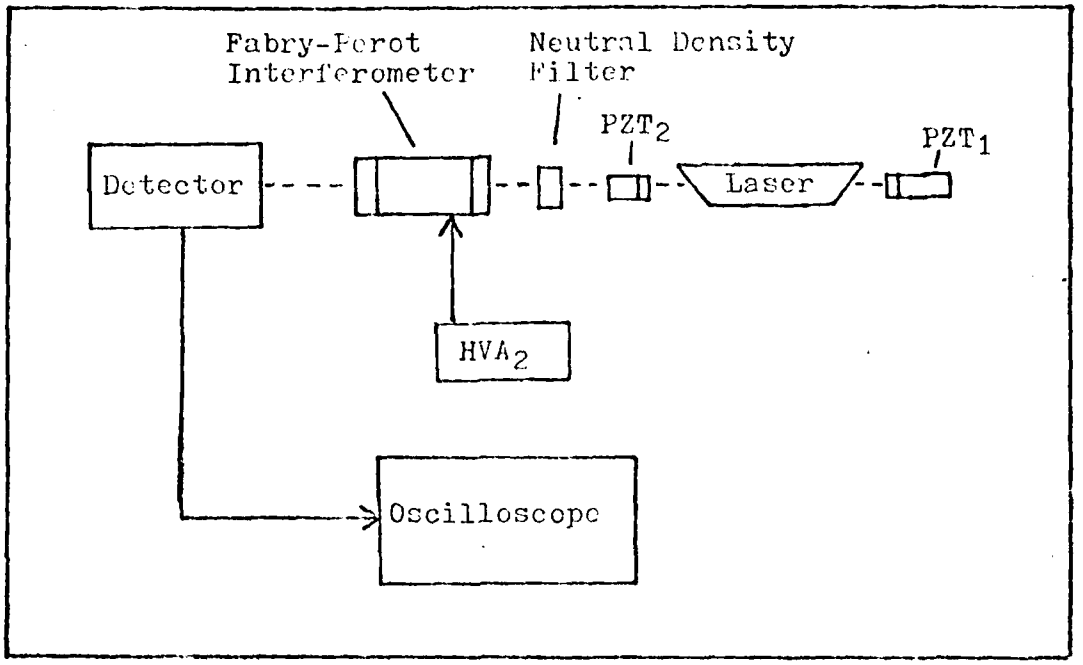

Figure 5.1 Block Diagram of the Interferometer Sensitivity Test

$$\Delta\nu_I = \frac{375\ \text{MHz}}{55\ \text{v}}$$

$$= 682\ \text{MHz/volt} \qquad (5.1)$$

PZT_1 Sensitivity ($\Delta\nu_{PZT_1}$)

The sensitivity of PZT_1, in MHz/volt, was determined by scanning the laser output with the interferometer and observing the mode shift for a particular change in PZT_1 voltage. Figure 5.2 shows a pattern shift to the left of 1.1 cm for a change in HVA_1 voltage of 880 volts. The oscilloscope is calibrated to 150 MHz/cm by spreading the FSR over 10 cm. The mode shift then is 165 MHz which yields

0.05 v/cm
Vert

150 MHz/cm
Horz

HVA_1=
880 volts

0.05 v/cm
Vert

150 MHz/cm
Horz

HVA_1=
0 volts

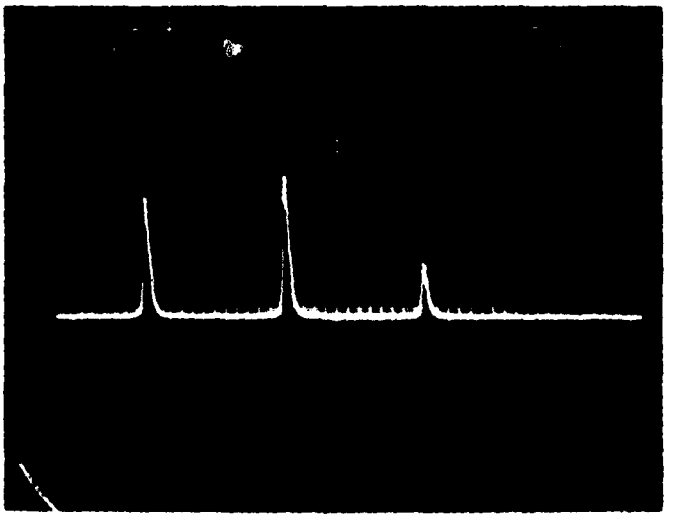

Figure 5.2 PZT_1 Sensitivity

0.05 v/cm
Vert

150 MHz/cm
Horz

HVA1=
622 volts

0.05 v/cm
Vert

150 MHz/cm
Horz

HVA_1=
0 volts

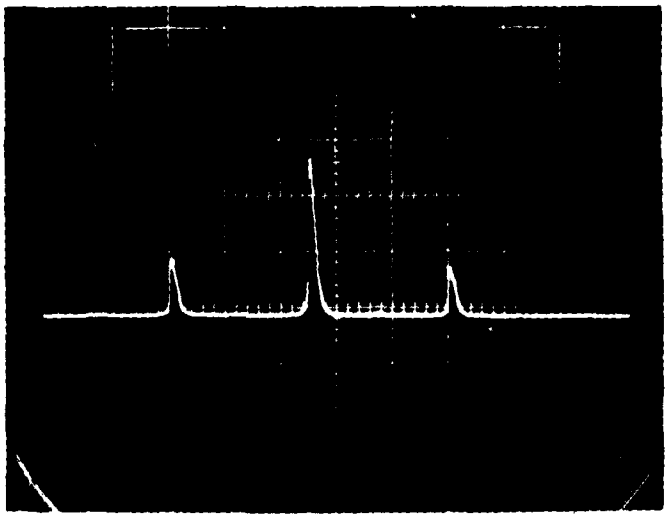

Figure 5.3 FZT_2 Sensitivity

$$\Delta\nu_{PZT1} = \frac{165\ MHz}{880\ v}$$

$$= 0.1875\ MHz/volt \qquad (5.2)$$

PZT_2 Sensitivity ($\Delta\nu_{PZT2}$)

The sensitivity of PZT_2 was found in the same manner as it was for PZT_1. Figure 5.3 shows a 2 cm shift to the right for a 622 volt decrease in HVA_2 voltage. Thus, the mode shift is -300 MHz. Then

$$\Delta\nu_{PZT2} = \frac{-300\ MHz}{622\ v}$$

$$= -0.482\ MHz/volt \qquad (5.3)$$

The negative sign in Eq (5.3) was verified by several other experiments.

LIA Constant (K_{LIA})

The LIA constant converts frequency to voltage across the LIA. A block diagram of the test set up to accomplish this is shown in Figure 5.4. The horizontal sweep voltage from the oscilloscope causes the laser output to sweep across the interferometer resonance. This produces an error signal out of the LIA that is routed to channel B of the chart recorder. The HVA_1 output is recorded on channel A with results shown in Figure 5.5. A linear section of the error signal from Figure 5.5 is matched

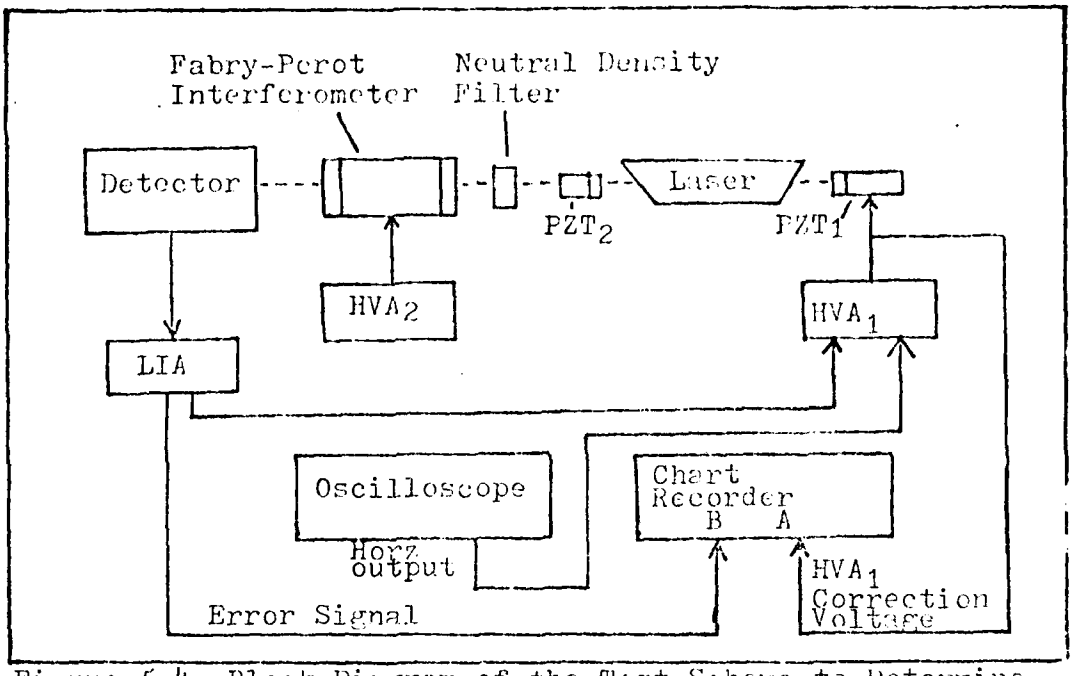

Figure 5.4 Block Diagram of the Test Scheme to Determine the LIA Constant

to the voltage ramp from channel A. As seen in Figure 5.5, a 4.0 volt sweep from HVA_1 causes a 9.0 volt change in the error signal. Using Eq (5.2) to convert the HVA_1 voltage to frequency, and solving for K_{LIA},

$$K_{LIA} = \frac{9 \text{ volts}}{(4 \text{ volts})(\Delta\nu_{PZT1})}$$

$$= \frac{9 \text{ volts}}{(4 \text{ volts})(0.1875 \text{ MHz/volt})}$$

$$= 12 \text{ volts/MHz} \qquad (5.4)$$

During this measurment the LIA Sensitivity was set to 500 μv, the REF ATTN was set to 0.1v calibrated, and

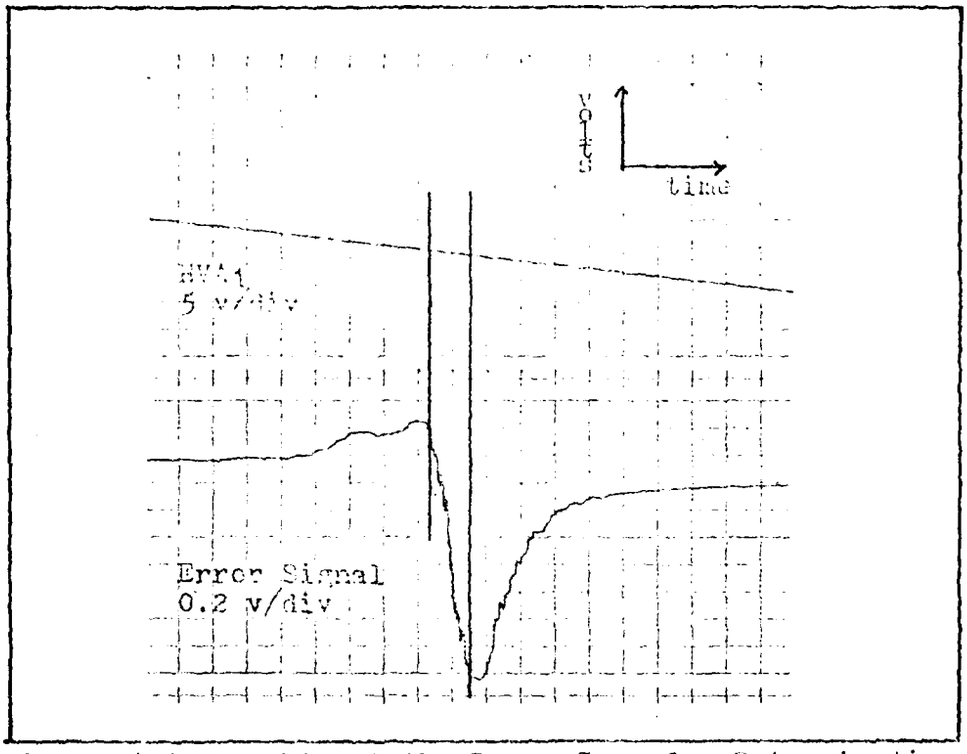

Figure 5.5 Results of the Laser Scan for Determination of the LIA Constant

the detector signal peaked at 0.2 volts. The REF ATTN setting is always kept at 0.1v, however, the other parameters are subject to change so a general equation for K_{LIA} is

$$K'_{LIA} = \left(12\text{v/MHz}\right)\left[\frac{Vd}{0.2\text{v}} \cdot \frac{500\times10^{-6}}{LIA_S}\right]$$

$$= \left(0.03\right)\left[\frac{Vd \text{ volts/MHz}}{LIA_S}\right] \qquad (5.5)$$

where Vd is the detector voltage and LIA_S is the LIA sensitivity setting.

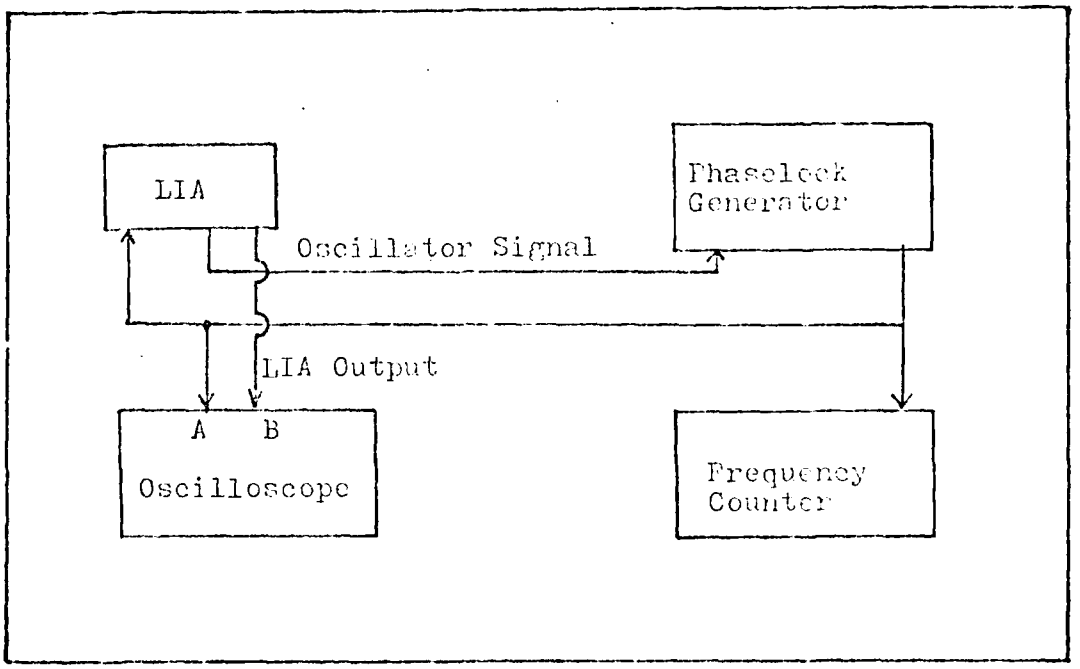

Figure 5.6 Block Diagram of Equipment Scheme used to Determine LIA Frequency Response

LIA Frequency Analysis and Transfer Function

Figure 5.6 is a block diagram of the equipment scheme used to determine the frequency characteristics of the LIA. The LIA oscillator signal was set to 41 KHz and modulated by the phaselock generator with a variable modulation frequency. The LIA output was then compared in phase and amplitude to the phaselock generator output using the oscilloscope shown in Figure 5.6. The frequency response of the LIA is shown in Figure 5.7.

The transfer function in radians/sec, which includes K'_{LIA} from Eq (5.5), is

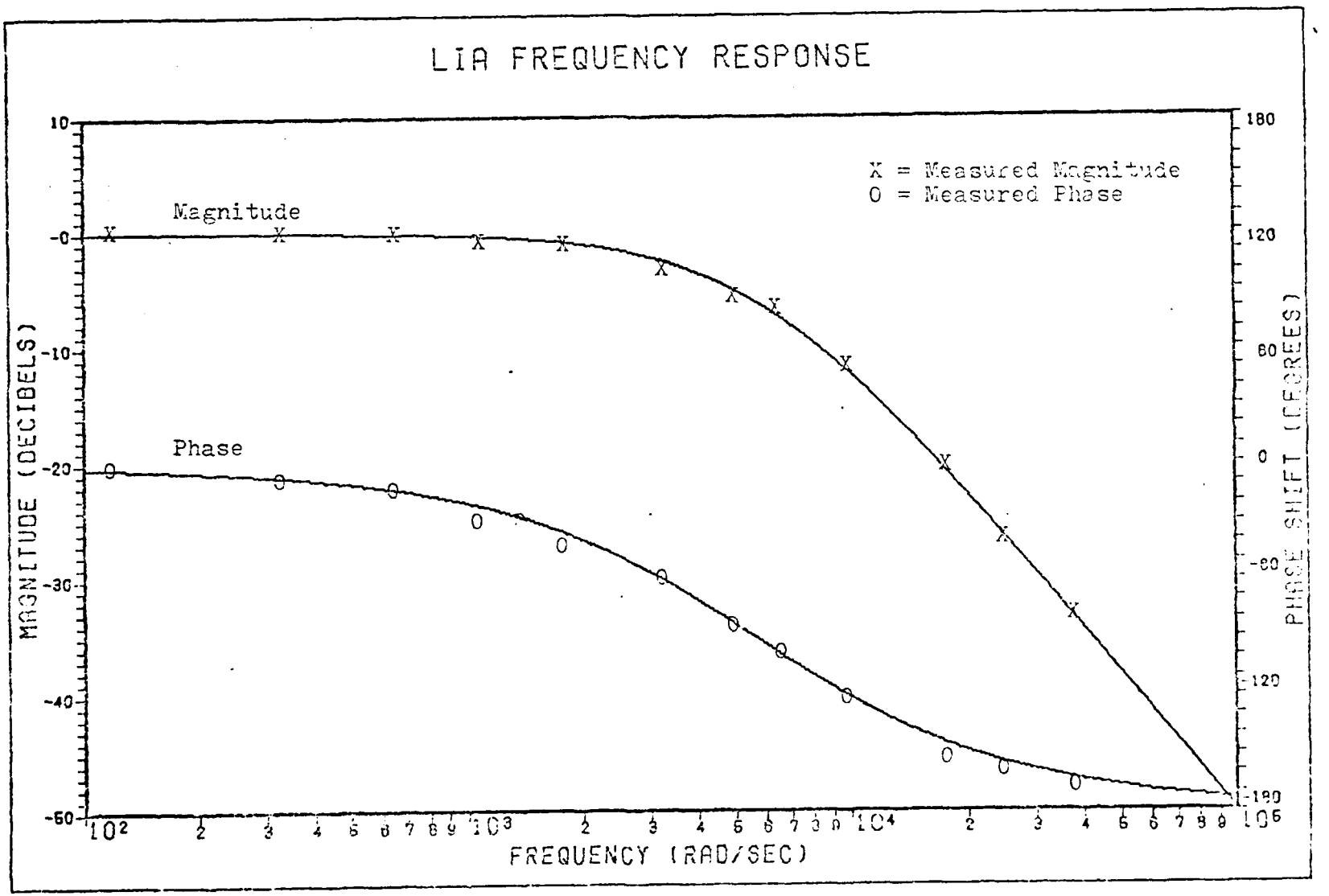

Figure 5.7 LIA Frequency Response

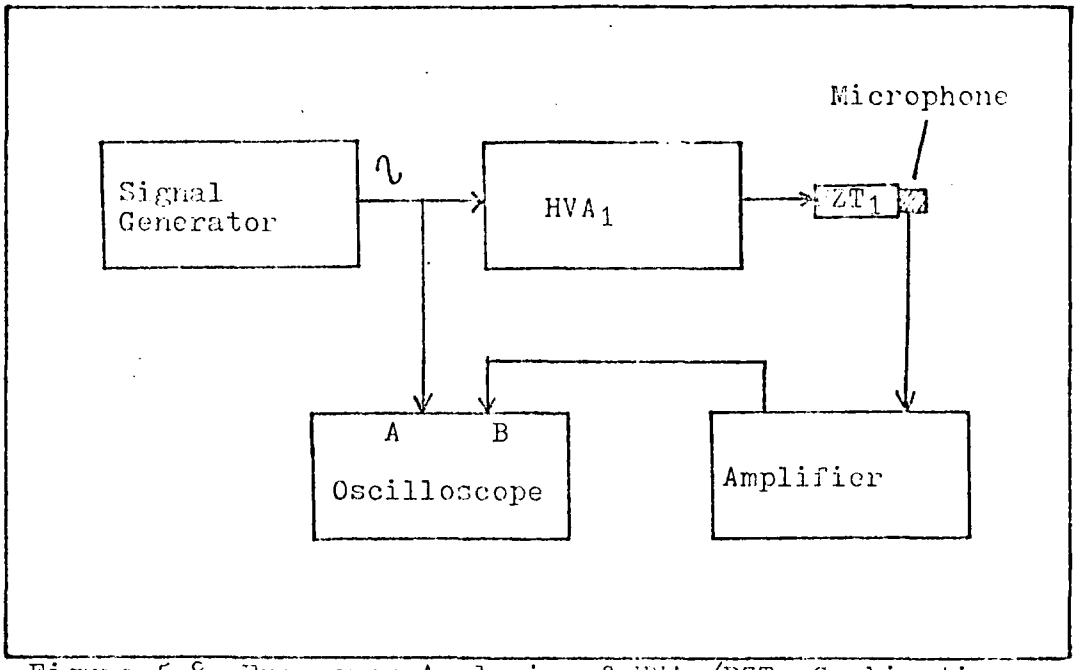

Figure 5.8 Frequency Analysis of HVA_1/PZT_1 Combination Using a Condenser Microphone

$$G_{LIA} = \frac{K'_{LIA}}{(s+5654)^2}$$

$$= \frac{(0.03)(V_o/LIA_s\ v/MHz)}{(s+5654)^2} \qquad (5.6)$$

HVA_1/PZT_1 Frequency Analysis and Transfer Function

In order to determine the frequency response for PZT_1, HVA_1 had to be used, therefore, the frequency response for the HVA_1/PZT_1 combination was determined using the test scheme shown in Figure 5.8.

The frequency response of the HVA_1/PZT_1 combination was estimated by comparing the magnitude and phase of the

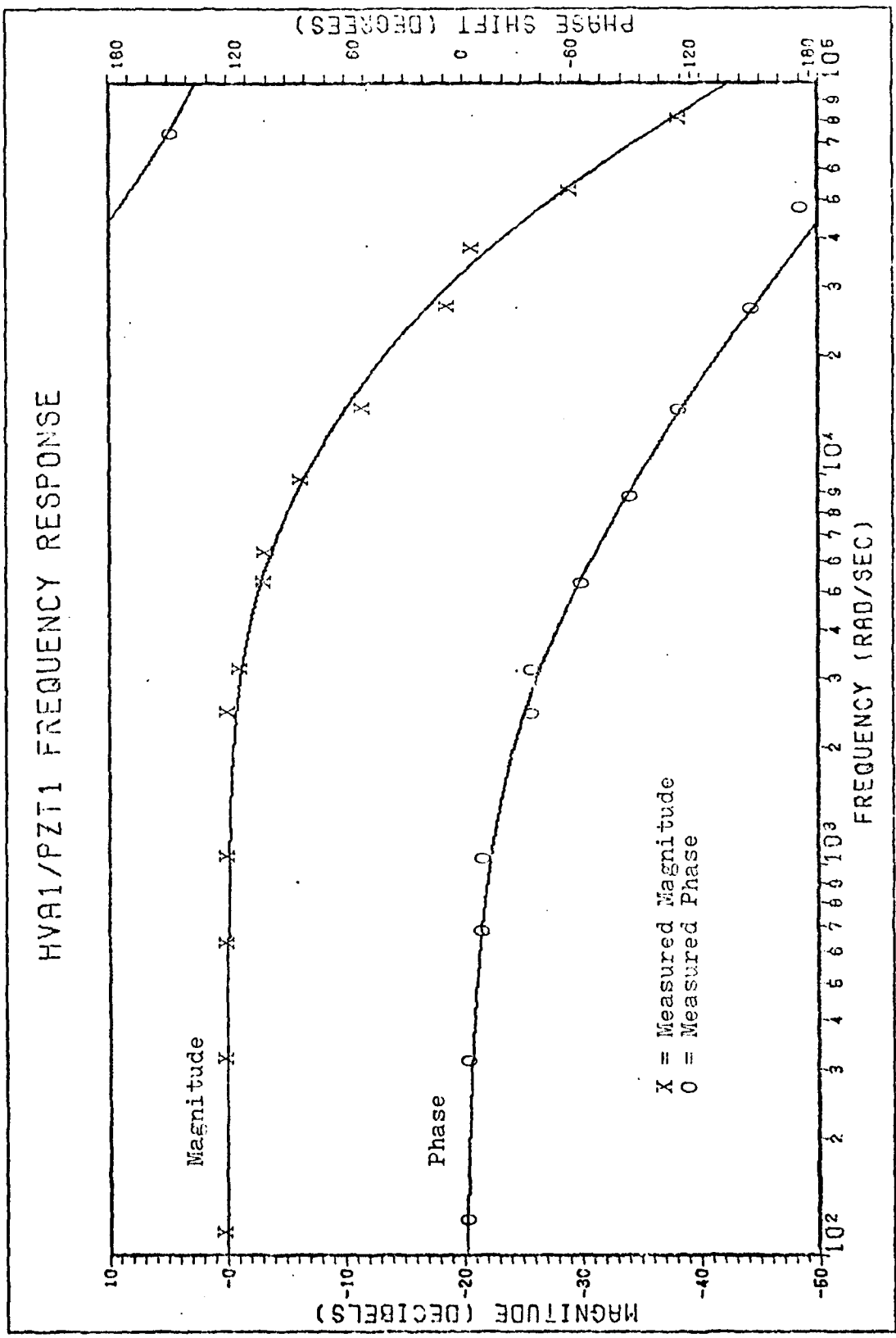

Figure 5.9 HVA_1/PZT_1 Frequency Response

microphone output signal to the oscillator signal on the oscilloscope as the signal generator frequency was increased.

From the results the frequency response of the HVA_1/PZT_1 combination was determined and is shown in Figure 5.9.

The transfer function for the HVA_1/PZT_1 combination was approximated as

$$G_{HVA1/PZT1} = \frac{(K_{HVA1})(\Delta\nu)_{PZT1})}{(s+5655)(s+38956)^2}$$

$$= \frac{(K_{HVA1})(0.1875\ MHz/volt)}{(s+5655)(s+38956)^2} \qquad (5.7)$$

where K_{HVA1} is the variable gain setting of HVA_1 and $\Delta\nu PZT_1$ is the PZT_1 sensitivity taken from Eq (5.2).

HVA_2/PZT_2 Frequency Analysis and Transfer Function

The combined frequency response of HVA_2/PZT_2 was determined in the same manner as it was for HVA_1/PZT_1. The estimated frequency response for HVA_2/PZT_2 is shown in Figure 5.10.

The transfer function for the HVA_2/PZT_2 combination, is

$$G_{HVA2/PZT2} = \frac{(K_{HVA2})(\Delta\nu_{PZT2})}{(s+3142)(s+119380)^2}$$

$$= \frac{(K_{HVA2})(-0.482\ MHz/volt)}{(s+3142)(s+119380)^2} \qquad (5.8)$$

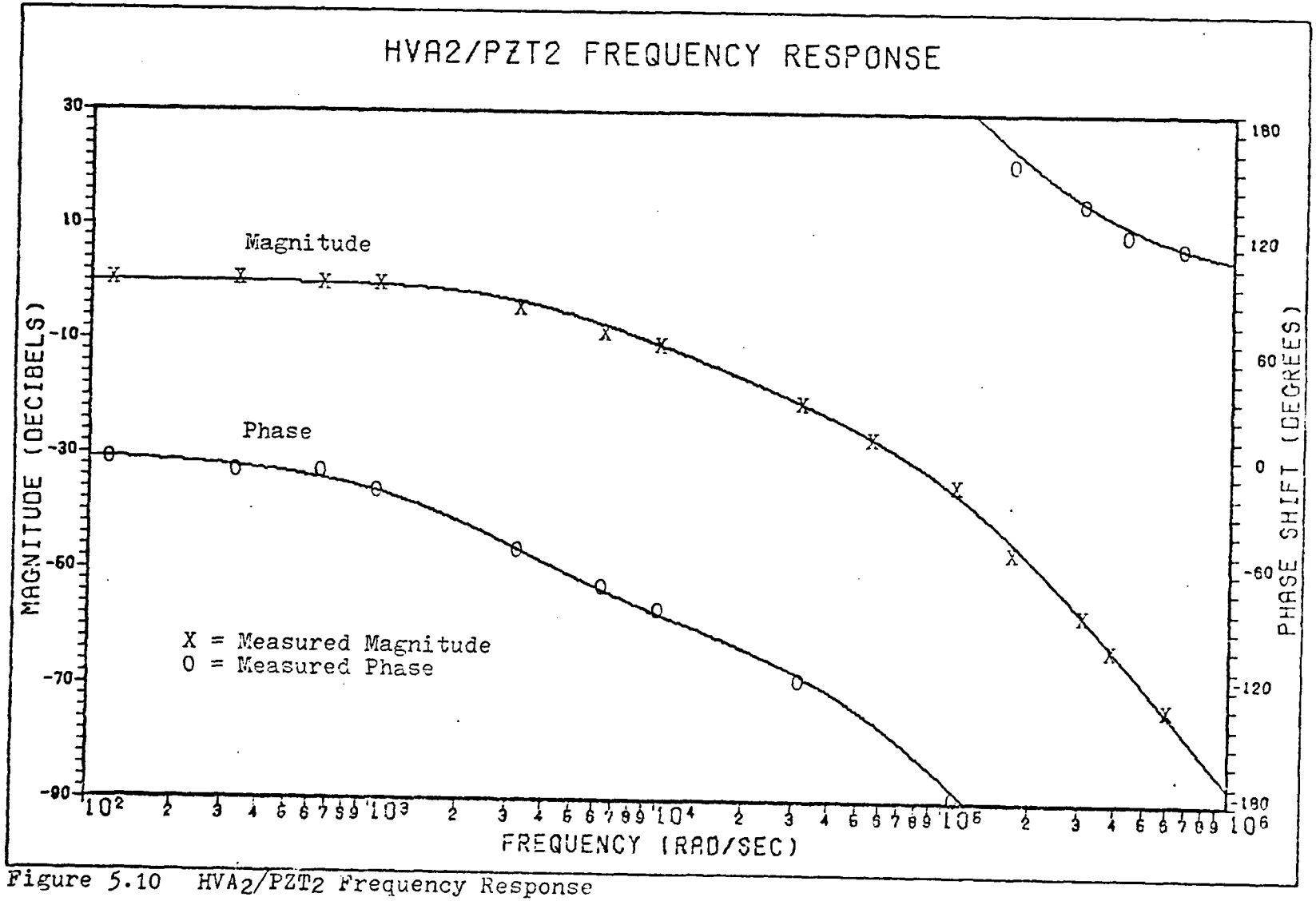

Figure 5.10 HVA_2/PZT_2 Frequency Response

where K_{HVA2} is the variable gain setting of HVA_2 and PZT_2 is the PZT_2 sensitivity from Eq (5.3).

VI Compensator Design

General Discussion

Two compensators were designed for use with control method I and a third was designed for use with method II. The first compensator was designed using only steady-state analysis. The second compensator is more sophisticated and was designed using frequency analysis for a closed loop bandwidth of 2.0 KHz. The third compensator was also designed using frequency analysis for a closed loop bandwidth of 2.0 KHz. In the design of the third compensator, the compensator in the PZT_1 loop was designed first for a closed loop bandwidth of 100 Hz neglecting the presence of the loop to PZT_2. This low bandwidth is well within the limits that a longer PZT would have put on the system. The compensator in the loop to PZT_2 was then designed taking into account the design of the other loop. The system models from Figures 2.2 and 2.4 are redrawn in Figures 6.1 and 6.2 to include the transfer function of each component as found in Chapter V. Design of compensator Gc_1 for variation 1 of control method II is shown in the next section.

Compensator $Gc_1(s)$ for Variation 1 of Control Method I Using Steady State Analysis

The open loop transfer function, $Gc_1(s)$, for the

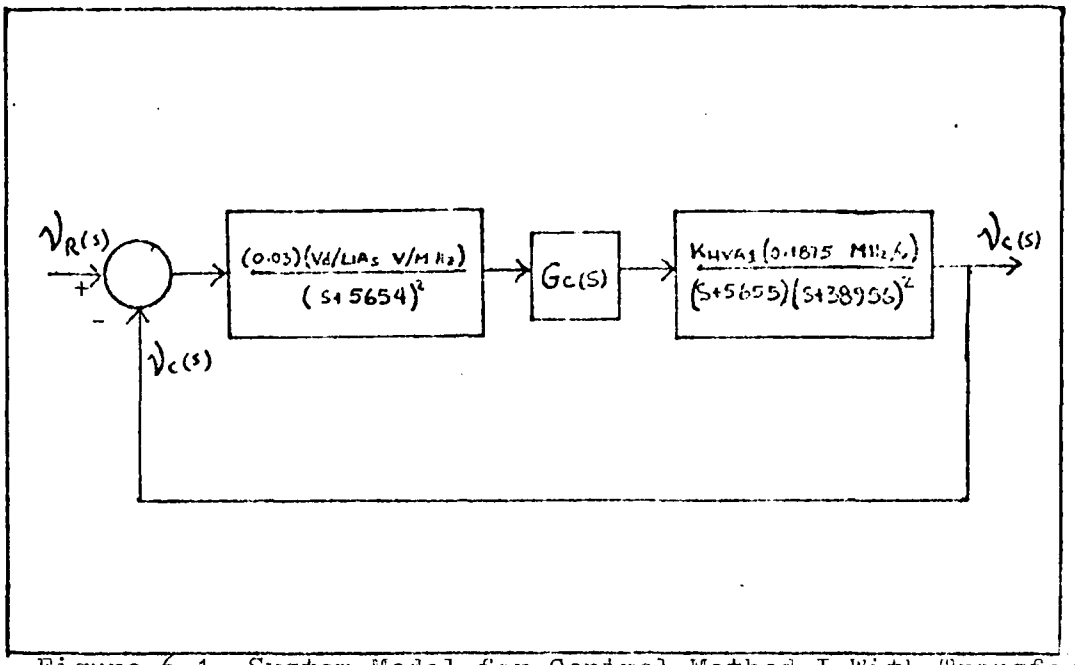

Figure 6.1 System Model for Control Method I With Transfer Functions

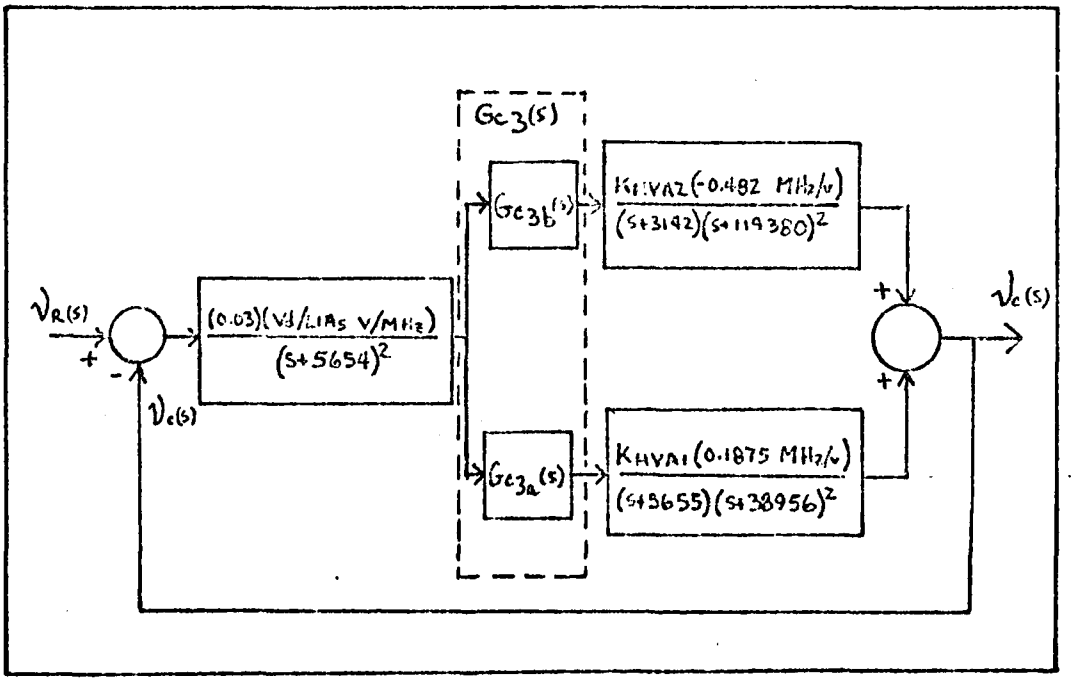

Figure 6.2 System Model for Control Method II With Transfer Functions

system shown in Figure 6.1, without the compensator is

$$G_{x1}(s) = \frac{K_{x1}}{(s+5655)^3(s+38956)^2} \tag{6.1}$$

where

$$K_{x1} = \frac{(0.0056)(Vd)(K_{HVA1})}{LIA_S} \tag{6.2}$$

For most measurments Vd = 0.23v, K_{HVA1}=100, and LIA_S=500 $x10^{-6}$, then

$$K_{x1} = 257 \tag{6.3}$$

To design for a steady-state error equal to zero for a step input, the theory shown by D'Azzo and Houpis is used where (Ref 7:177)

$$e(t)_{ss} = \lim_{s\to 0}\left[sE(s)\right] = 0 \tag{6.5}$$

The control ratio for the loop shown in Figure 6.1 is

$$\frac{V_c(s)}{V_R(s)} = \frac{G_{x1}(s)\,G_{c1}(s)}{1 + G_{x1}(s)\,G_{c1}(s)} \tag{6.6}$$

where

$$V_c(s) = E(s)\,G_x(s) \tag{6.7}$$

Substituting $V_c(s)$ from Eq (6.7) into Eq (6.6) and solving for $E(s)$ yields:

$$E(s) = \frac{V_R(s)}{1 + G_{x1}(s)\, G_{c1}(s)} \tag{6.8}$$

where for a step input of magnitude 1

$$V_R(s) = \frac{1}{s} \tag{6.9}$$

Thus Eq (6.8) can be written as

$$E(s) = \frac{1}{s\left[1 + G_{x1}(s)\, G_{c1}(s)\right]} \tag{6.10}$$

Substituting Eq (6.10) into Eq (6.5) yields

$$e(t)_{ss} = \lim_{s \to 0} \frac{s}{s\left[1 + G_{x1}(s)\, G_{c1}(s)\right]}$$

$$= \lim_{s \to 0} \frac{1}{1 + G_{x1}(s)\, G_{c1}(s)} \tag{6.11}$$

Replacing $G_{x1}(s)$ with Eq (6.1) and setting $e(t)_{ss}$ equal to zero results in the following :

$$0 = \lim_{s \to 0} \frac{(s+5655)^3 (s+38956)^2\, G_{c1} D(s)}{(s+5655)^3 (s+38956)^2 G_{c1} D(s) + K_{x1} G_{c1} N(s)} \tag{6.12}$$

where $G_{c1}N(s)$ and $G_{c1}D(s)$ are the numerator and denominator of $G_{c1}(s)$. For this equation to hold true, $G_{c1}D(s)$

must contain a zero at the origin of the s plane, thus a first choice for the compensator is

$$G_{c_1}(s) = \frac{K_{c_1}}{s} \tag{6.13}$$

where K_{c_1} is the compensator constant. The open loop transfer function including $G_{c_1}(s)$ becomes

$$G'_{x_1}(s) = \frac{K_{x_1} K_{c_1}}{(s)(s+5655)^3(s+38956)^2} \tag{6.14}$$

Using $K_{x_1} = 257$ from Eq (6.3), thus yields the result

$$G'_{x_1}(s) = \frac{257\, K_{c_1}}{(s)(s+5655)^3(s+38956)^2} \tag{6.15}$$

To get an idea of the amount of gain achievable, a computer assisted root locus was generated as shown in Figure 6.3. An expansion of the branch starting at s=0 indicates that for a damping ratio of 0.7,

$$K_{c_1} = 3.46 \times 10^{18} \tag{6.16}$$

This value was used to generate the system open loop and closed loop frequency response plots shown in Figures 6.4 and 6.5.

From the open loop frequency plot of Figure 6.4, the system is seen to have about a 60db gain margin which shows it is very stable. The closed loop frequency

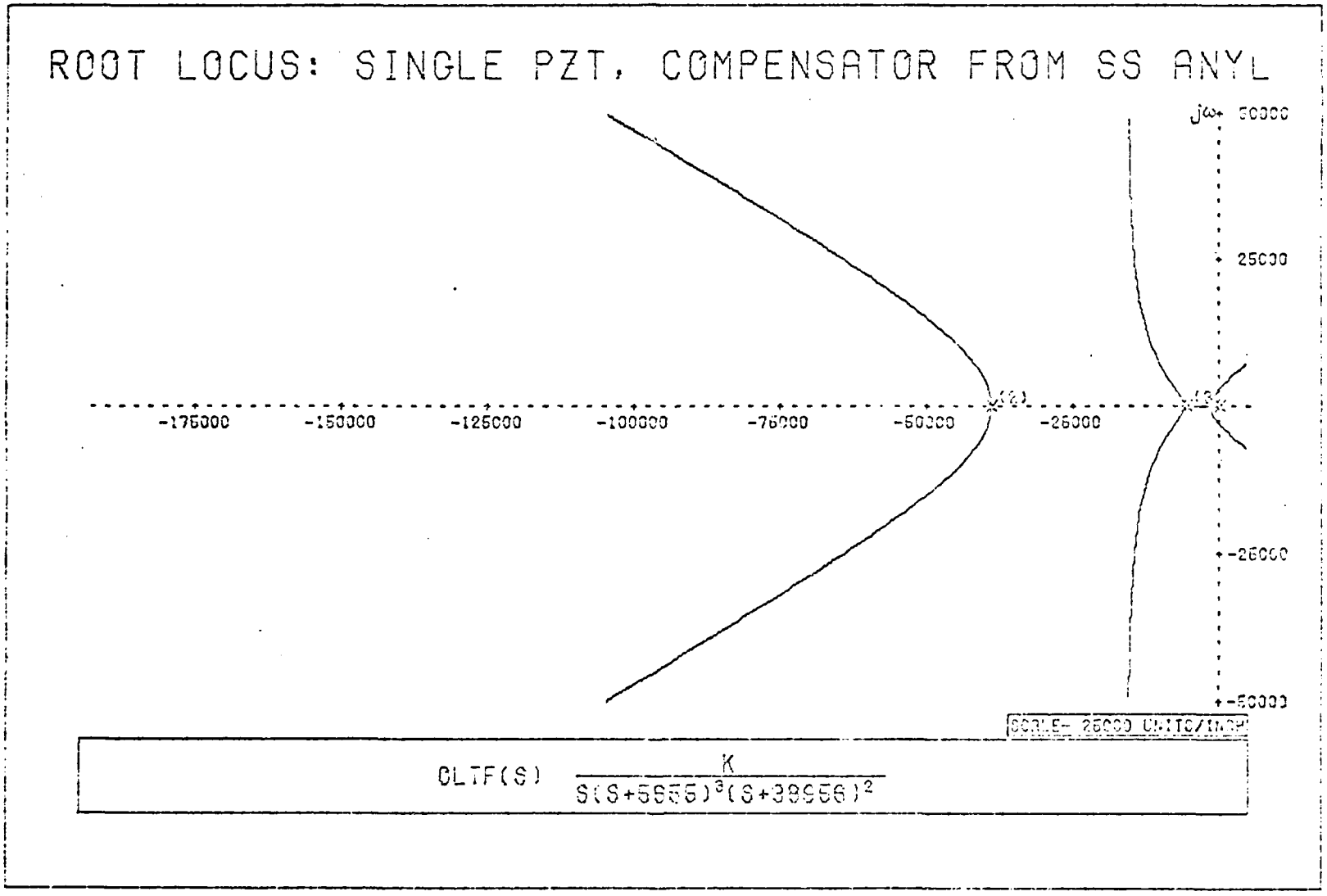

Figure 6.3 System Root Locus. Variation 1 of Control Method I, Using Compensator Gc_1

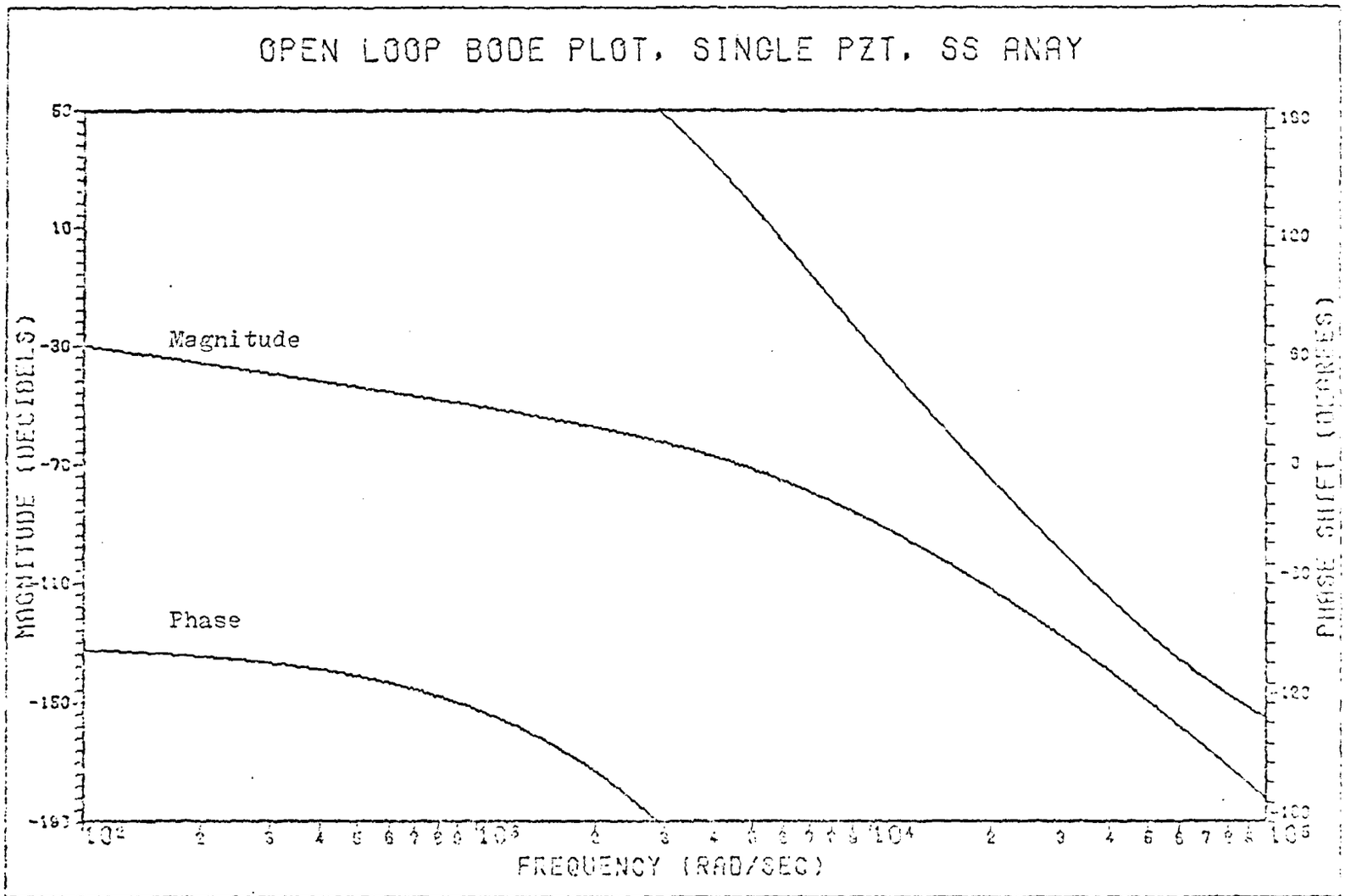

Figure 6.4 Open Loop Frequency Response. Variation 1 of Control Method 1, Using Compensator Gc_1

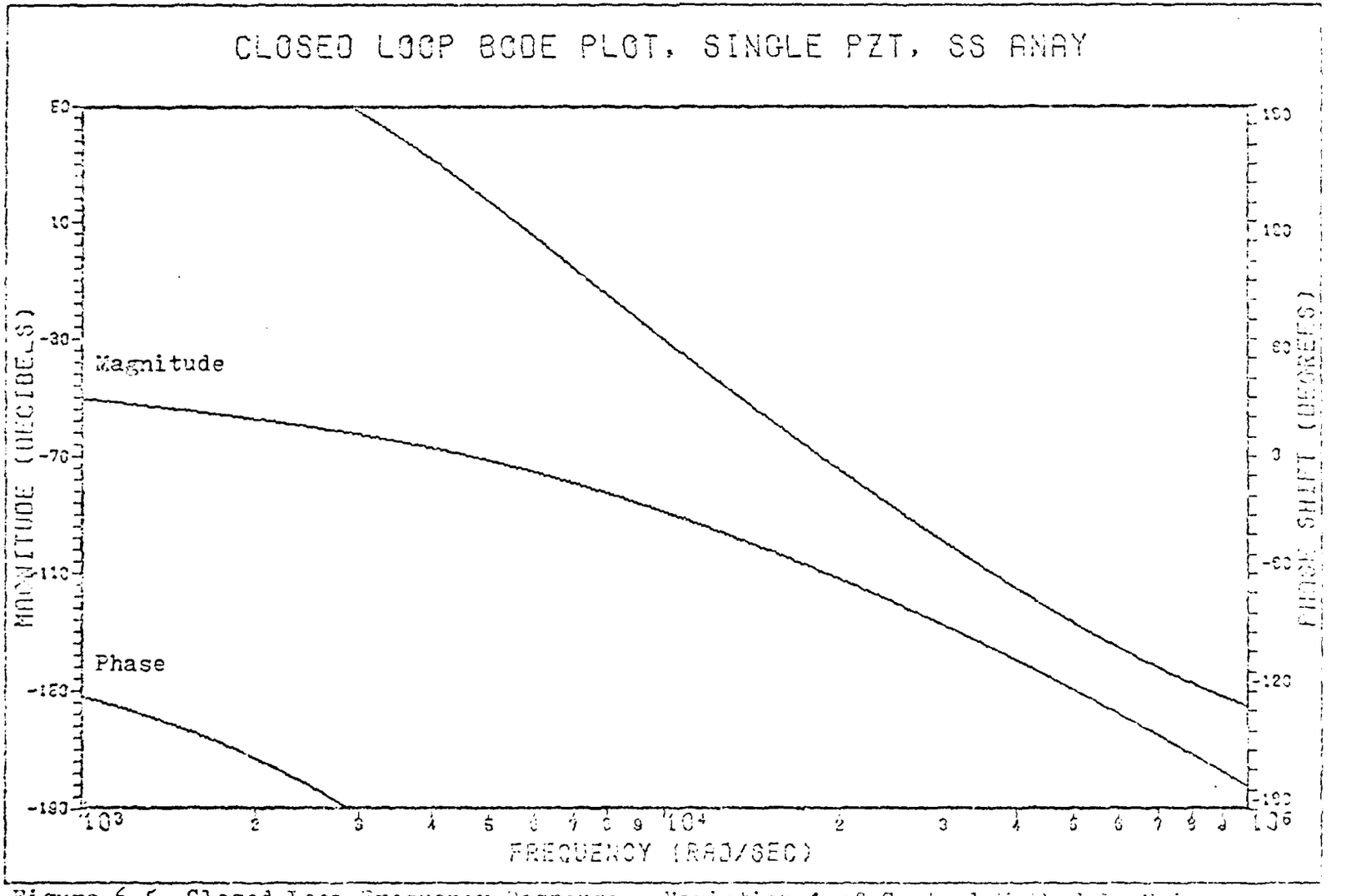

Figure 6.5 Closed Loop Frequency Response. Variation 1 of Control Method 1, Using Compensator G_{c1}

response shown in Figure 6.5 shows a 20 db/decade drop for low frequencies with a break frequency at about 2.0 KHz as would be expected.

The compensator circuit design was implemented using operational amplifiers as shown in Appendix B. The design of compensator Gc_2 for use with variation 2 of control method I is covered in the following section.

Compensator $Gc_2(s)$ for Variation 2 of Control Method I Using Frequency Analysis

The desired bandwidth of the closed loop system is 2.0 KHz. The Guileman-Truxal procedure as explained by D'Azzo and Houpis is followed during the design of this compensator (Ref 7:408).

The control ratio, $M_2(s)$, for the system shown in Figure 6.1 is

$$M_{2(s)} = \frac{V_{c(s)}}{V_{R(s)}} = \frac{N_{2(s)}}{D_{2(s)}} = \frac{G_{c2(s)}\ G_{x1(s)}}{1 + G_{c2(s)}\ G_{x1(s)}} \qquad (6.17)$$

where $N_2(s)$ and $D_2(s)$ are the desired control ratio numerator and denominator respectively. For a bandwidth of 2.0 KHz and a 20 db/decade roll-off with four nondominant poles, the control ratio can be rewritten as

$$M_{2(s)} = \frac{N_{2(s)}}{D_{2(s)}} = \frac{K_{m2}}{(s+12560)(s+75000)(s+80000)(s+105000)(s+90000)} \qquad (6.18)$$

The constant Km_2 required for a control ratio of unity for zero steady-state error is found by taking the limit of $M_2(s)$ as s approaches zero and setting it equal to unity. So,

$$1 = \lim_{s \to 0} M_2(s) = \lim_{s \to 0} \frac{K_{m2}}{(s+12560)(s+75000)(s+80000)(s+85000)(s+90000)}$$

$$= \frac{K_{m2}}{5.76 \times 10^{23}} \qquad (6.19)$$

thus,

$$K_{m2} = 5. \times 10^{23} \qquad (6.20)$$

Solving Eq (6.17) for $Gc_2(s)$ yields (Ref 7:408):

$$Gc_2(s) = \frac{N_2(s)}{[D_2(s) - N_2(s)]\, G_{x1}(s)} \qquad (6.21)$$

Using Eqs (6.1) and (6.18) to solve for $Gc_2(s)$ results in the following:

$$Gc_2(s) = \frac{K_{m2}(s+5655)^3(s+38956)^2}{[(s+12560)(s+75000)(s+80000)(s+85000)(s+90000) - K_{m2}]\, K_{x1}} \qquad (6.22)$$

Expanding the denominator, using Eq (6.20) and factoring the results, Eq (6.22) becomes

$$Gc_2(s) = \frac{5.7 \times 10^{23}(s+5655)^3(s+38956)^2}{K_{x1}(s)(s+52440 \pm j46400)(s+118800 \pm j31080)} \qquad (6.23)$$

The compensator is further simplified by setting the damping ratio equal to 1.0 which moves the poles to the real axis for ease of implementation.

$$G_{c_2}(s) = \frac{5.7\times10^{23}(s+5600)^3(s+38900)^2}{K_{x1}(s)(s+70021)^2(s+122800)^2} \qquad (6.24)$$

Using Eq (6.3) to substitute for K_{X1} yields

$$G_{c_2}(s) = \frac{7.2\times10^{21}(s+5600)^2(s+38900)^2}{(s)(s+70021)^2(s+122800)^2} \qquad (6.25)$$

The open loop transfer function then becomes

$$G''_{x1}(s) = \frac{5.7\times10^{23}(s+5600)^3(s+38900)^2}{(s)(s+70021)^2(s+122800)^2(s+5600)^3(s+38956)^2} \qquad (6.26)$$

A root locus plot is shown in Figure 6.6. Figures 6.7 and 6.8 show the system open and closed loop frequency response plots. The frequency plots were generated using the numerator constant shown in Eq (6.25). Note that the gain margin in Figure 6.7 is about 17 db indicating a stable system. The closed loop frequency response shown in Figure 6.8 is flat with a breakpoint at about 2.0 KHz as designed.

This compensator circuit design was also implemented using operational amplifiers and is shown in Appendix C. The design of compensator G_{c_3} for use with control method II is covered in the following section.

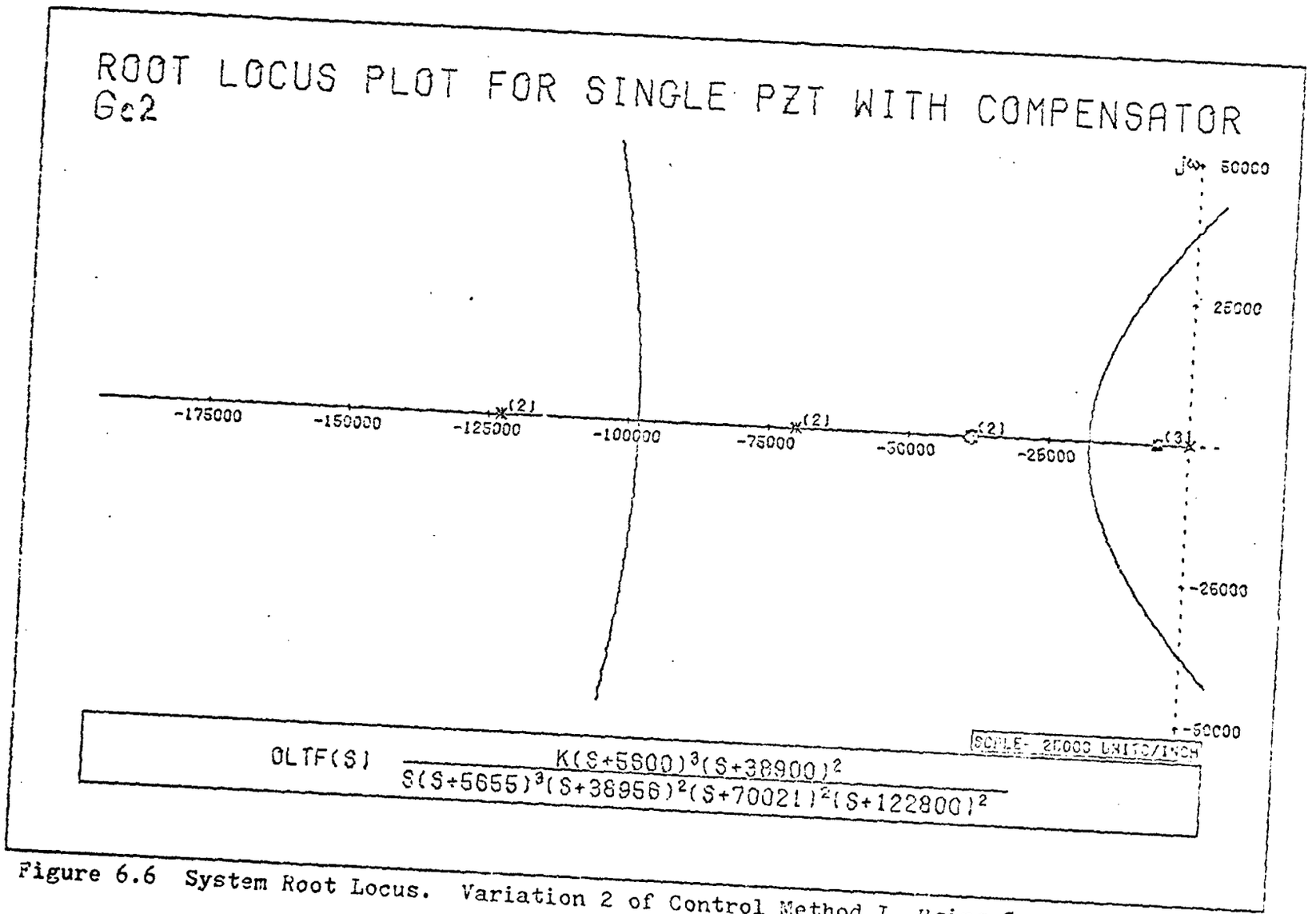

Figure 6.6 System Root Locus. Variation 2 of Control Method I, Using Compensator G_{c2}

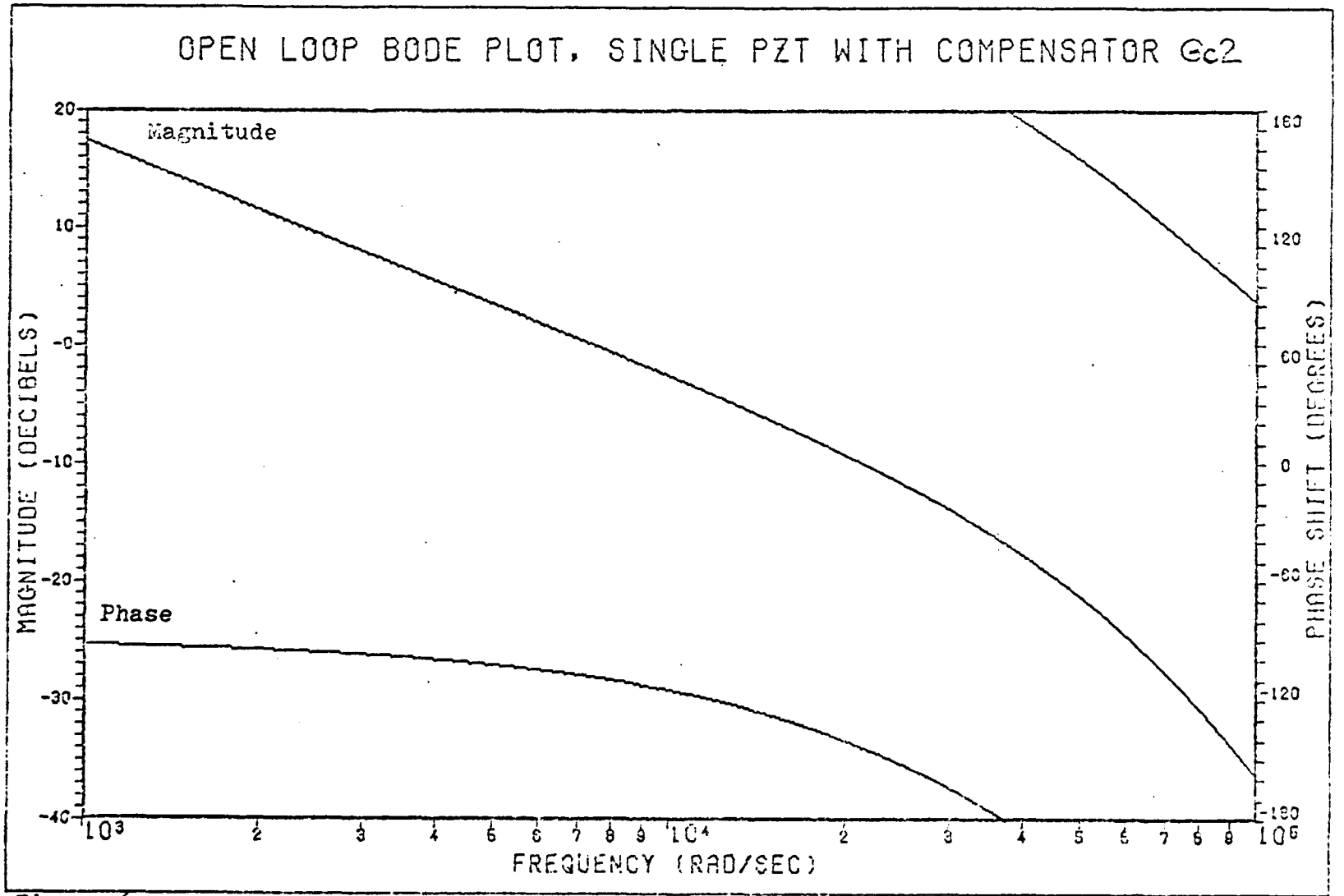

Figure 6.7 Open Loop Frequency Response. Variation 2 of Control Method 1, Using Compensator Gc_2

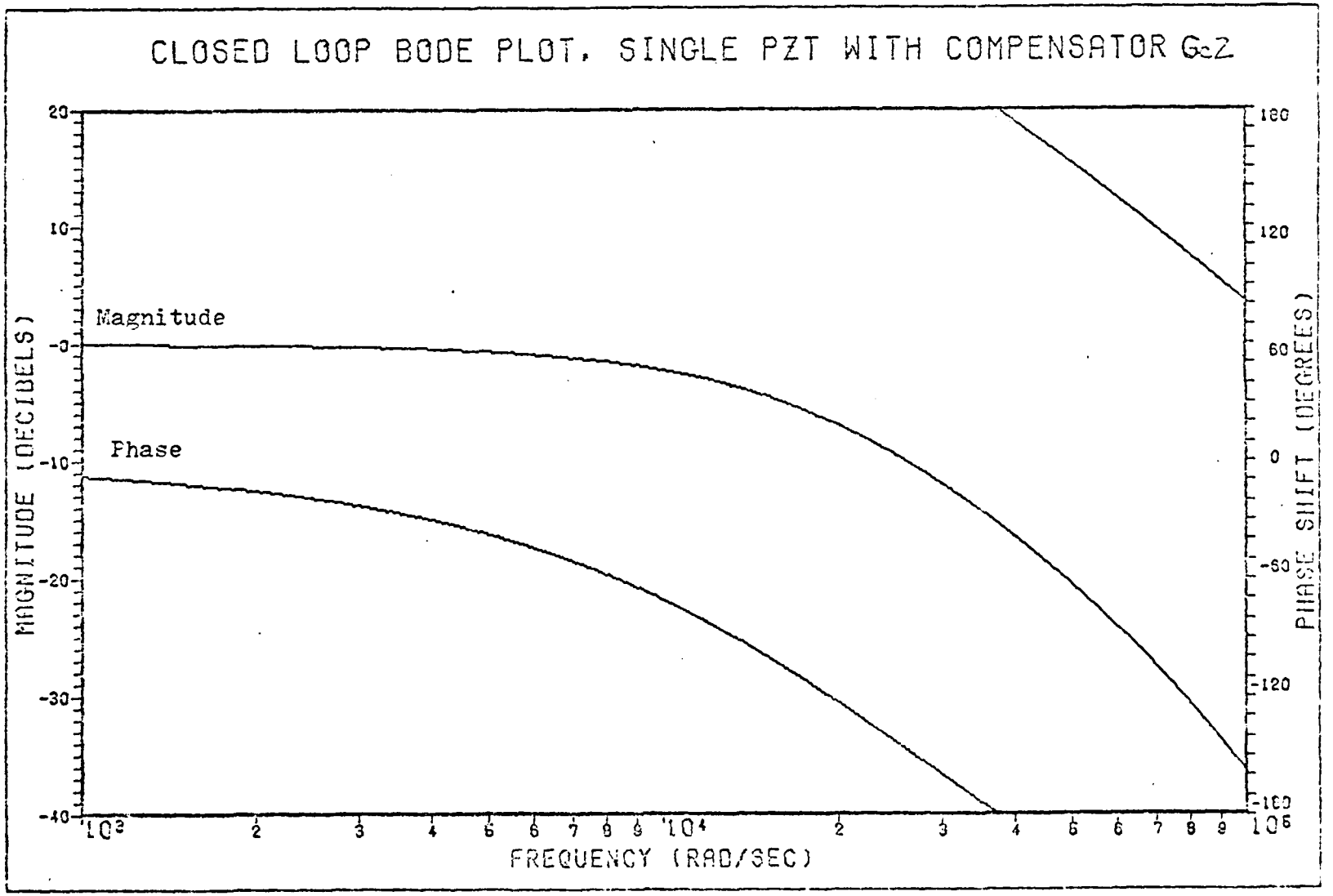

Figure 6.8 Closed Loop Frequency Response. Variation 2 of Control Method I, Using Compensator G_{c_2}

Compensator $Gc_3(s)$ for Control Method II Using Frequency Analysis

The compensator $Gc_3(s)$ is designed in two steps. First, the loop to PZT_2 is ignored and a compensator, $Gc_{3a}(s)$, is designed for a closed loop bandwidth of 100 Hz with a 40 db roll-off and a 0.6 damping coefficient. Using Figure 6.1, and the same procedure as used in the last section, the closed loop control ratio is

$$M_{3a}(s) = \frac{N_{3a}(s)}{D_{3a}(s)} = \frac{Km_{3a}}{(s^2+691s+394384)(s+40000)(s+45000)(s+50000)} \qquad (6.27)$$

where $M_{3a}(s)$ is the control ratio of Figure 6.1 using $Gc_{3a}(s)$ in place of $Gc(s)$. $N_{3a}(s)$ and $D_{3a}(s)$ are the desired numerator and denominator of $M_{3a}(s)$. The constant Km_{3a} required for a control ratio of one to achieve zero steady-state error is found using the same method as in the previous section. Then,

$$Km_{3a} = 3.5 \times 10^{19} \qquad (6.28)$$

Using Eq (6.21), the equation for compensator $Gc_{3a}(s)$ is,

$$Gc_{3a}(s) = \frac{N_{3a}(s)}{[D_{3a}(s) - N_{3a}(s)]\, G_{x1}(s)} \qquad (6.29)$$

Using Eqs (6.27) and (6.1) to substitute for $N_{3a}(s)$, $D_{3a}(s)$, and $G_{x1}(s)$, the compensator equation becomes

$$Gc_{3a}(s) = \frac{3.5\times10^{19}(s+5655)^3(s+38956)^2}{\left[(s^2+691s+394384)(s+40000)(s+45000)(s+50000)-3.5\times10^{19}\right]K_{x1}} \qquad (6.30)$$

Expanding Eq (6.30) and factoring the results, the compensator becomes

$$Gc_{3a}(s) = \frac{3.5\times10^{19}(s+5655)^3(s+38956)^2}{K_{x1}(s)(s+719)(s+49740)(s+39550)(s+45690)} \qquad (6.31)$$

$Gc_{3a}(s)$ is simplified by cancelling nondominant poles and zeros which leaves

$$Gc_{3a}(s) = \frac{3.5\times10^{19}(s+5600)^3}{K_{x1}(s)(s+719)(s+49740)} \qquad (6.32)$$

The second part of compensator $Gc_3(s)$ is designed using $Gc_{3a}(s)$ of Eq (6.32) and the system diagram from Figure 6.2. The desired closed loop bandwidth is 2 KHz with a 20 db/decade roll-off. The desired closed loop transfer function with four nondominant poles is

$$\frac{N_3(s)}{D_3(s)} = \frac{Km_3}{(s+12560)(s+120000)(s+125000)(s+130000)(s+135000)} \qquad (6.33)$$

For zero steady state error, the numerator constant must be

$$Km_3 = 3.3\times10^{24} \qquad (6.34)$$

If $G_{X2}(s)$ is the open loop transfer function of the system, then the system control ratio, $M_3(s)$, is

$$M_{3(s)} = \frac{G_{X2}(s)}{1 + G_{X2}(s)} \tag{6.35}$$

where $G_{X2}(s)$ includes both compensators $Gc_{3a}(s)$ and $Gc_{3b}(s)$. Solving for $G_{X2}(s)$ using Figure 2.4,

$$G_{X2}(s) = \left[G_{LIA}(s)\right]\left[\frac{Gc_{3b}N(s)}{Gc_{3b}D(s)} G_{HVA2/PZT2}(s) + Gc_{3a}(s)\, G_{HVA1/PZT1}(s)\right] \tag{6.36}$$

where $Gc_{3b}N(s)$ and $Gc_{3b}D(s)$ are the numerator and denominator of $Gc_{3b}(s)$. $Gc_{3b}(s)$ can be found by substituting Eq (6.36) into Eq (6.35) and setting the results equal to Eq (6.33). We then get

$$Gc_{3b}(s) = \frac{5\times10^{21}(s)(s+665)(s+3142)(s+5654)^2(s+39900\pm j1786)(s+49800)(s+118000\pm j0.0187)}{(s)^2(s+719)(s+38960)^2(s+49740)(s+83760\pm j63030)(s+177500\pm j43630)} \tag{6.37}$$

The compensator is simplified so that $Gc_{3b}(s)$ becomes

$$Gc_{3b}(s) = \frac{5\times10^{21}(s+3142)(s+5606)^2}{(s)(s+83760\pm j63030)} \tag{6.38}$$

Again, a damping factor of unity is used to move the poles to the real axis for ease of implementation so the final design of $Gc_{3b}(s)$ is

$$Gc_{3b}(s) = \frac{5\times10^{21}(s+3142)(s+5606)^2}{(s)(s+104833)^2} \tag{6.39}$$

The system open loop transfer function $G_{X2}(s)$ becomes

$$G_{XZ}(s) = \frac{3.1\times10^{25}(s+741)(s+5000)^3(s+39810)(s+39810)(s+49710)}{(S)(s+719)(s+5655)^3(s+38960\pm j0.02839)(s+49770)(s+119400\pm j0.326)(s+409800\pm j0.361)} \quad (6.40)$$

This derivation assumes HVA gain settings of 100, LIAs= 500 mv, and Vd = 0.23v

A root locus plot is shown in Figure 6.9. Figure 6.10 and 6.11 show the system open-loop and closed-loop frequency response plots. As seen in Figure 6.9 the root locus plot shows an improvement over both of the plots previously seen. The open loop frequency response, as shown in Figure 6.10, shows a phase margin of about 10.0 db which indicates that the system is stable. The degree of stability is less however than for method I as seen by comparing Figures 6.11, 6.5, and 6.8. The closed loop frequency response from Figure 6.11 is flat to about 2.0 KHz as was designed. The circuit design of the compensator, G_{c3}, is shown in Appendix D.

Final Design of Each Compensator

Figure 6.12 shows all three compensators taken from equations 6.13, 6.25, 6.32, and 6.39 respectively.

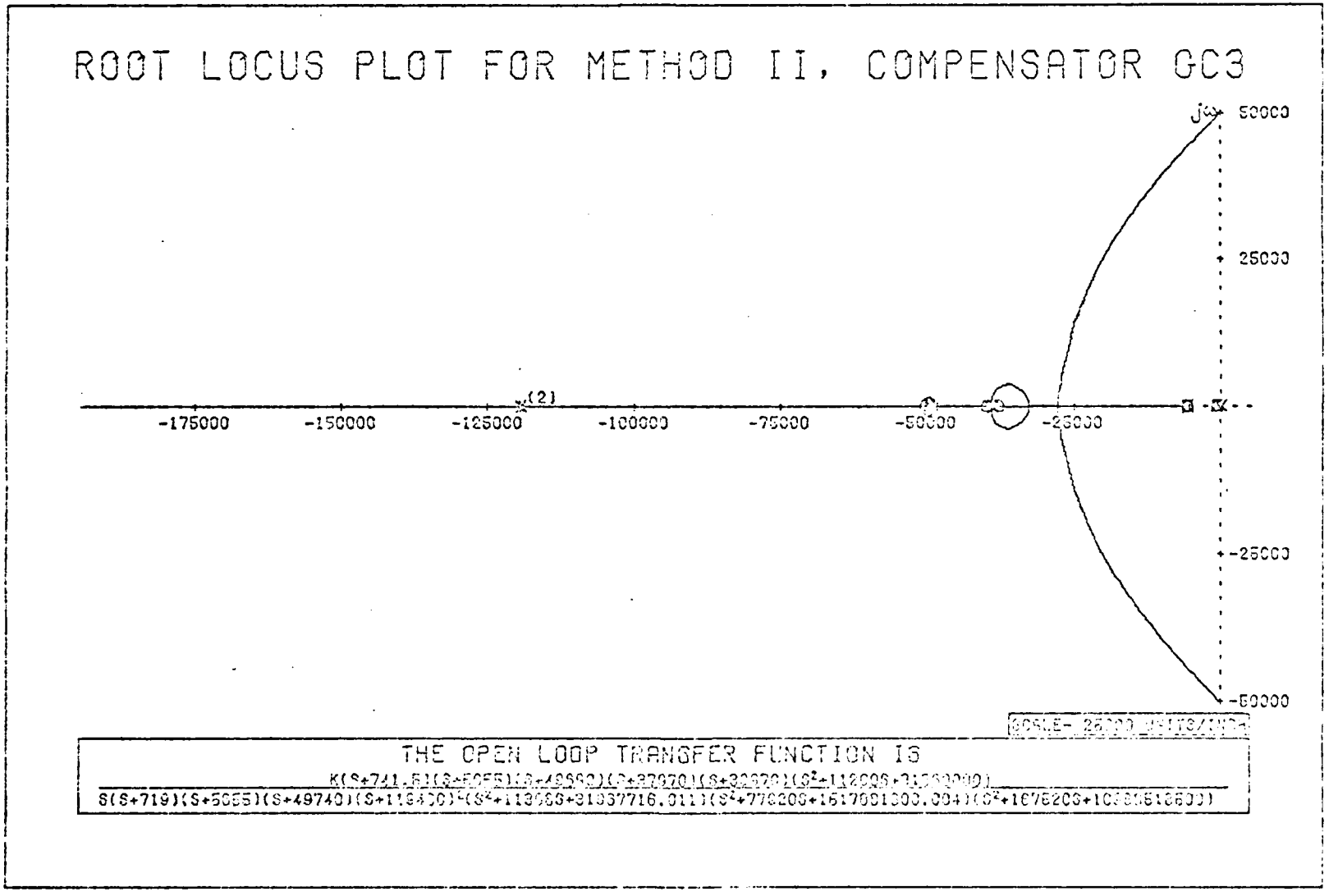

Figure 6.9 System Root Locus. Control Method II Using Compensator G_{C3}

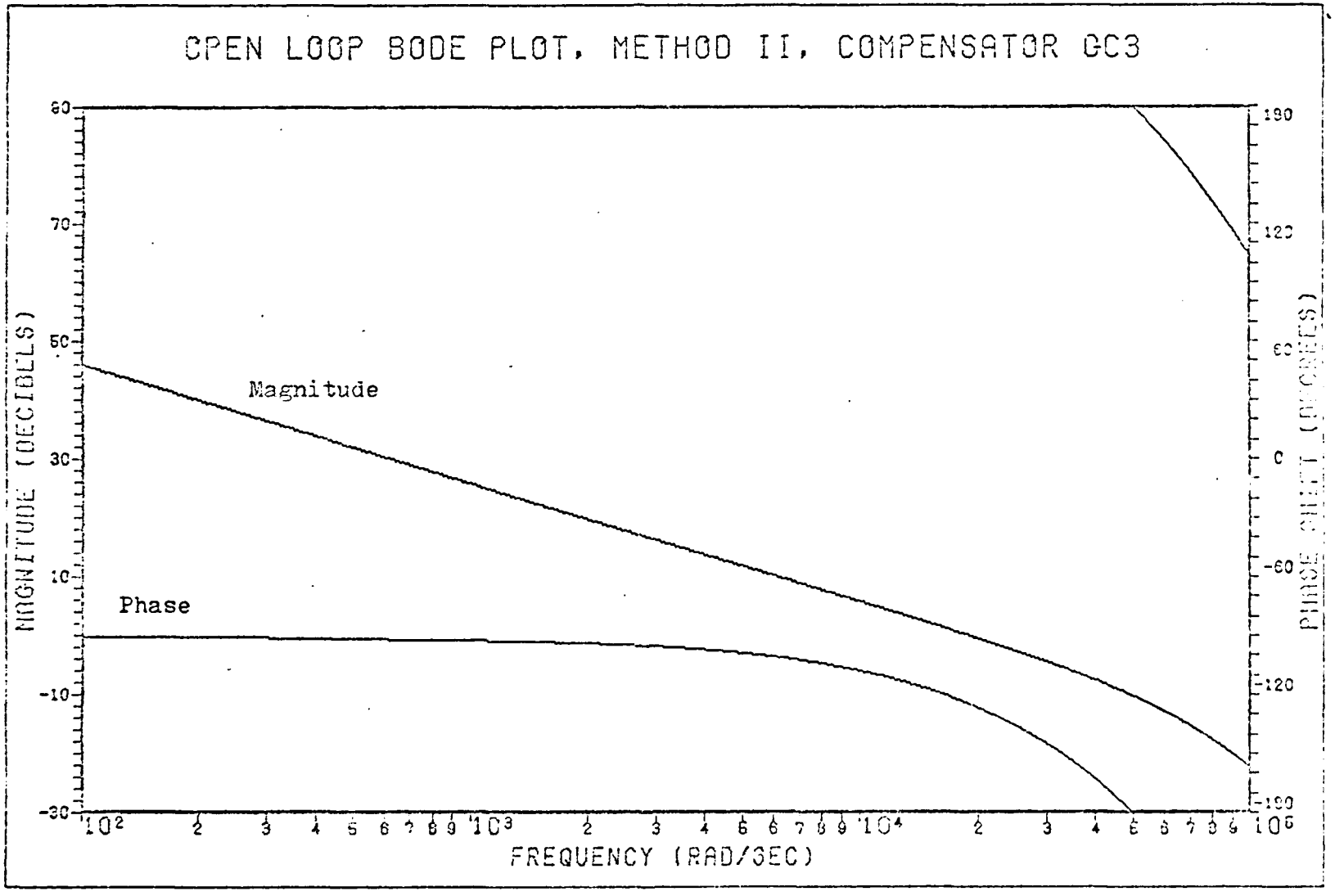

Figure 6.10 Open Loop Frequency Response. Control Method II Using Compensator Gc3

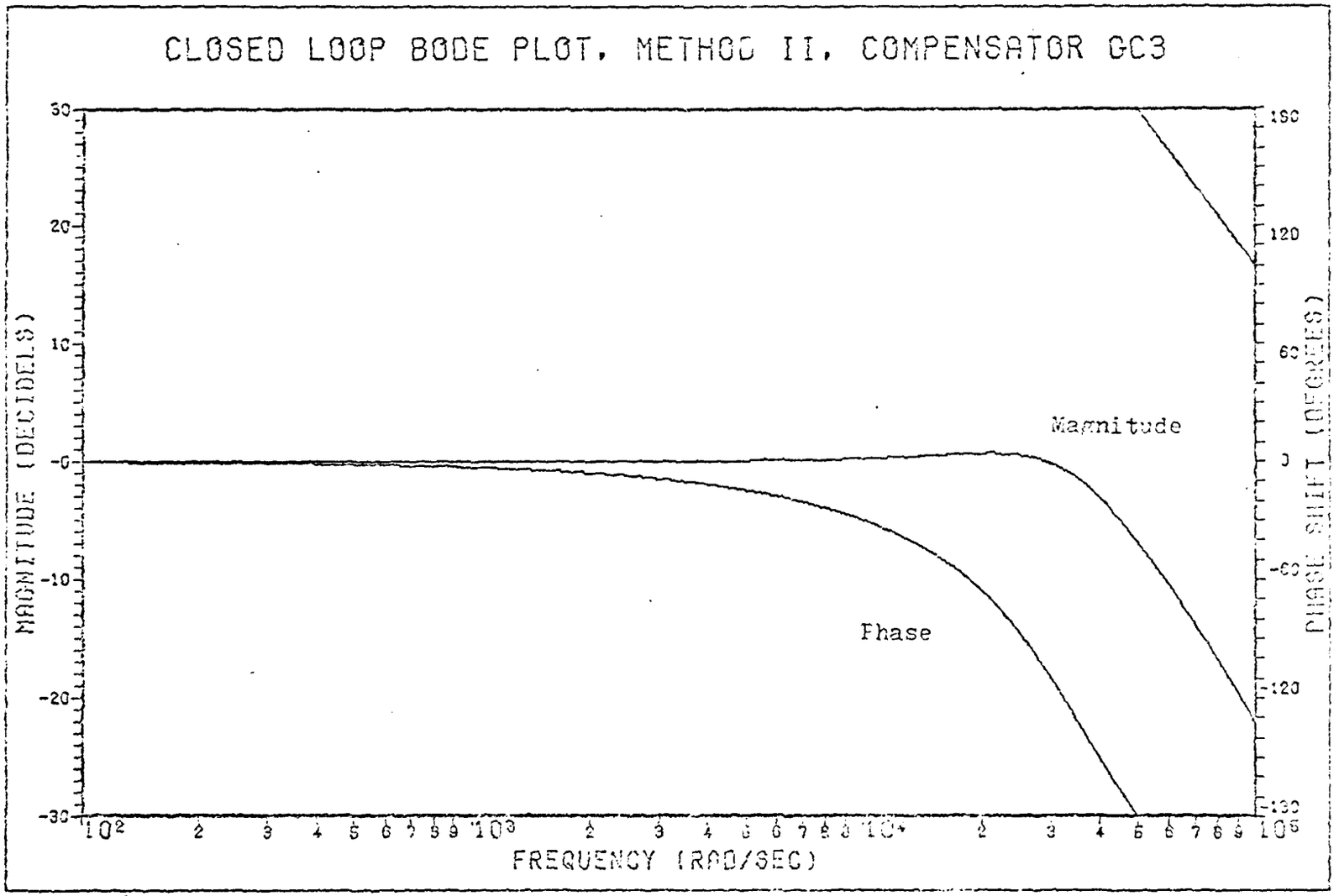

Figure 6.11 Closed Loop Frequency Response. Control Method II Using Compensator G_{C3}

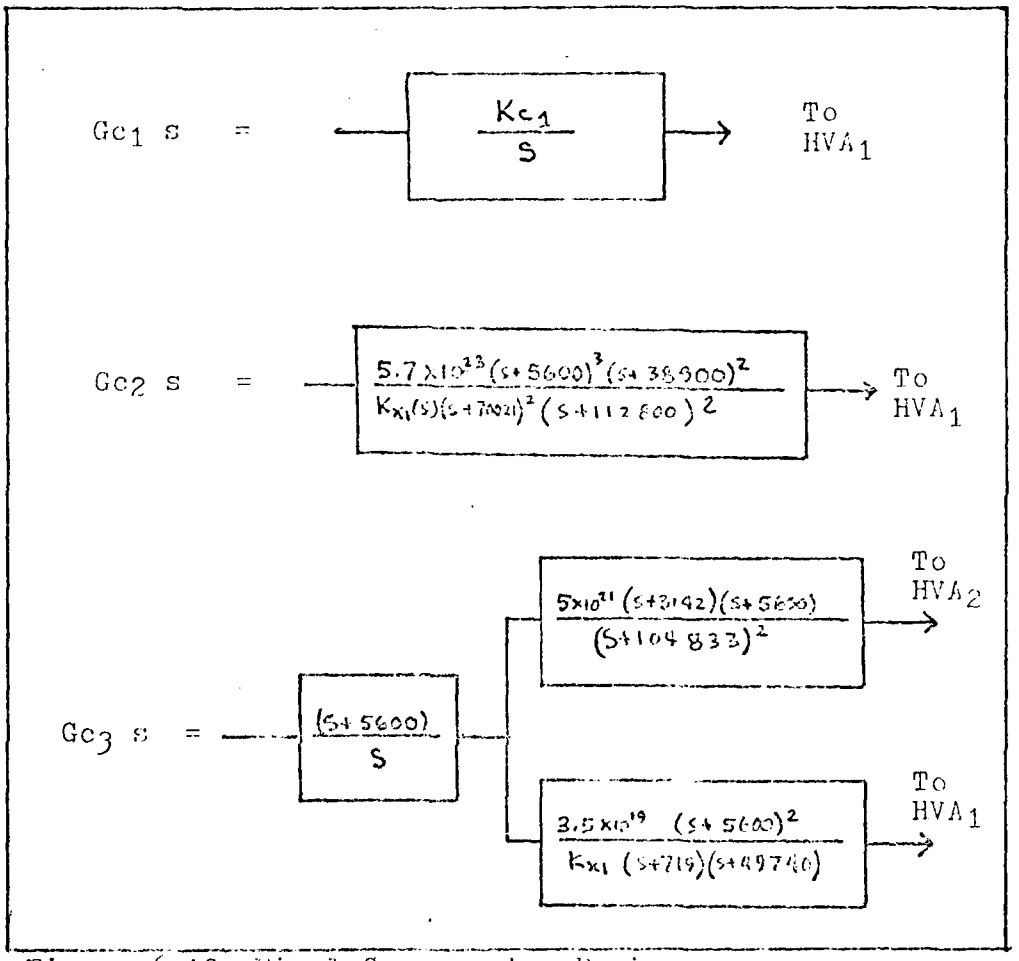

Figure 6.12 Final Compensator Designs

AD-A085 707 AIR FORCE INST OF TECH WRIGHT-PATTERSON AFB OH SCHOO--ETC F/G 20/5
COMPARISON OF CONTROL METHODS IN A FREQUENCY STABILIZED LASER.(U)
JAN 80 R D LUZITANO
UNCLASSIFIED AFIT/GE/EE/80-2 NL

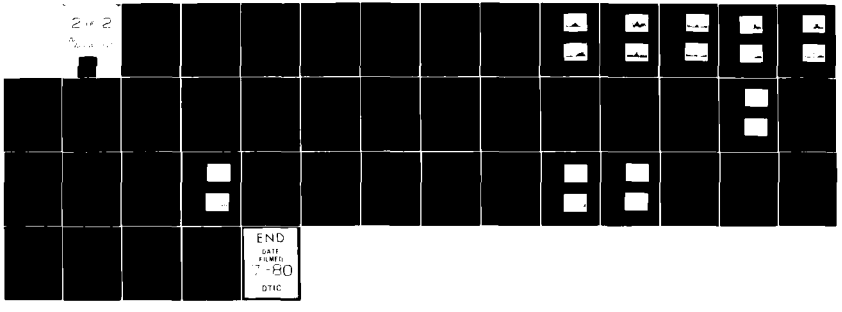

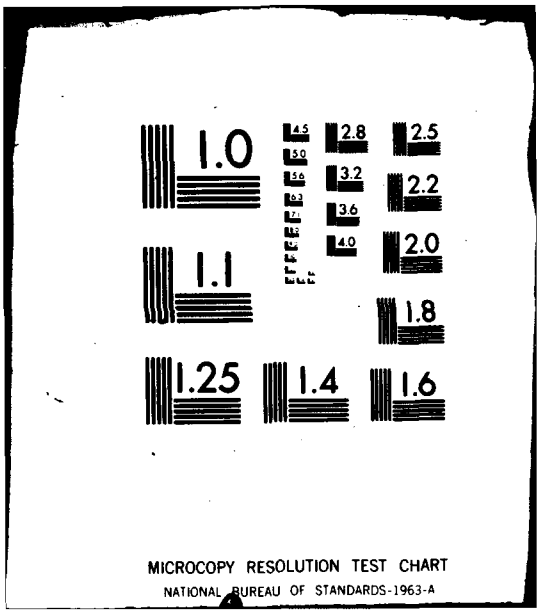
1.0
1.1
1.25
1.4
1.6
1.8
2.0
2.2
2.5
2.8
3.2
3.6
4.0
4.5
5.0
5.6
6.3
MICROCOPY RESOLUTION TEST CHART
NATIONAL BUREAU OF STANDARDS-1963-A

VII Performance Comparisons

General Discussion

System performance data is contained in this chapter for control methods I and II that can be used to frequency stabilize a laser. A comparison is made between each method's controllable range of the laser cavity. A second comparison is then made between each control method's frequency spectrum of the system error signal. The control range comparisons are made in the next section.

Control Range Comparison

In order to estimate the difference in the long term control range between control methods I and II, a recording was made over a three minute time span of the correction voltages from HVA_1 and HVA_2. The experiment was performed while the room temperature was increasing so that a correction voltage drift could be observed. The entire experiment, using both control methods, only took ten minutes to perform and the room temperature drift was assumed to be constant over that short a period. For both control methods, a laser mode was positioned at the top of the laser output intensity curve using HVA_1. The interferometer resonance was then adjusted to match the laser mode frequency and the loop was closed.

Figure 7.1 shows the results obtained using the

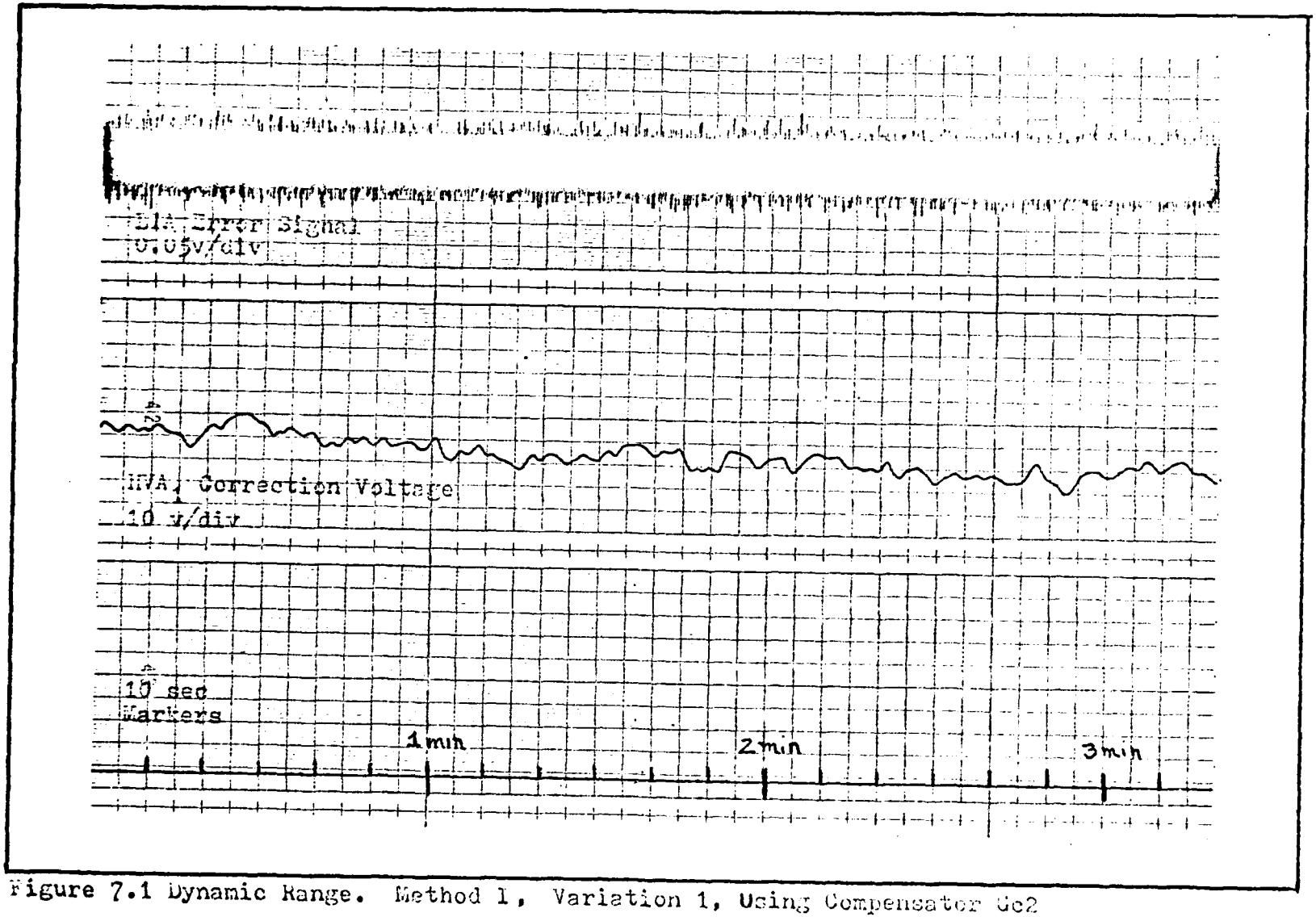

Figure 7.1 Dynamic Range. Method 1, Variation 1, Using Compensator Ge2

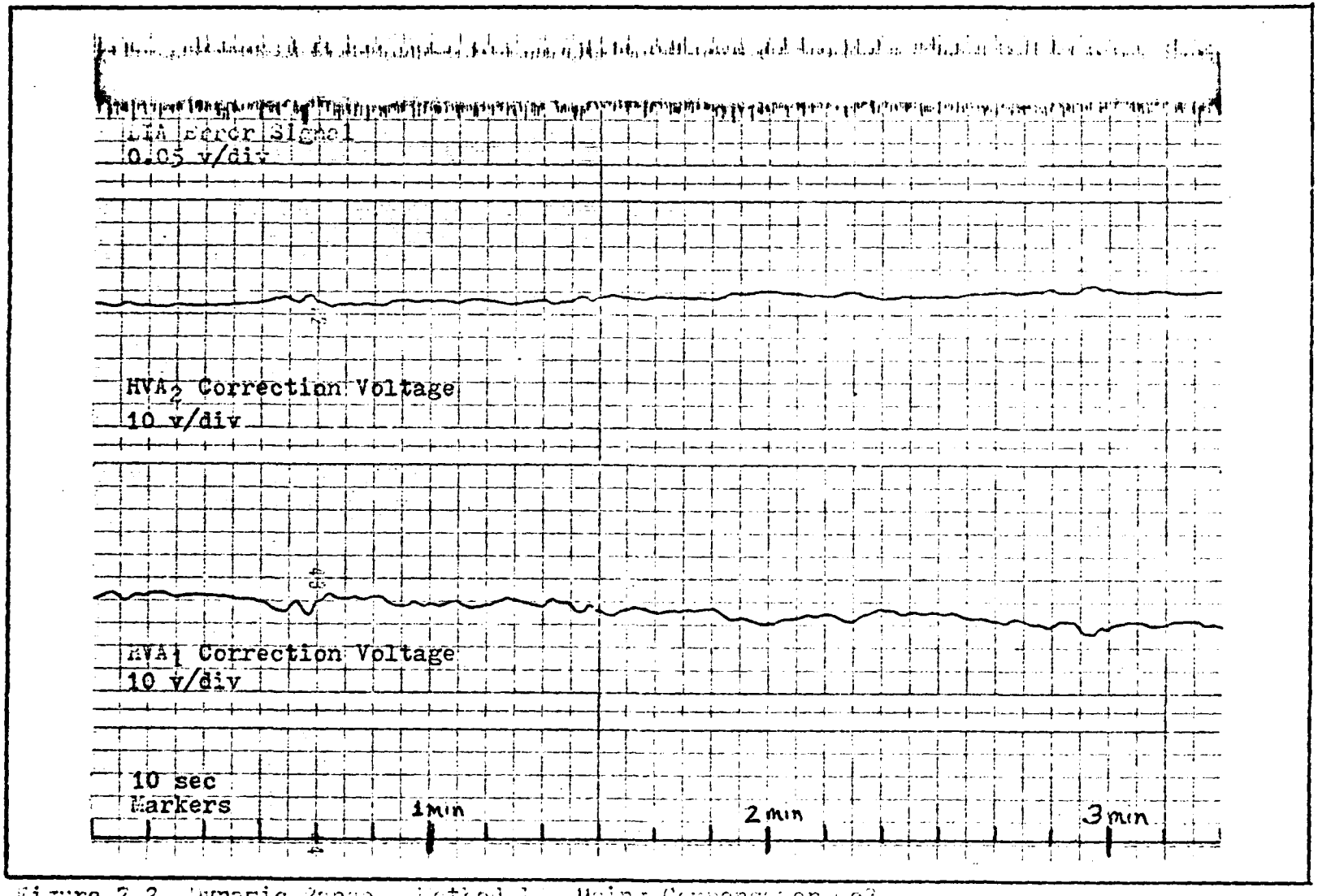

Figure 7.2 Dynamic Range. Method II, Using Compensator #3

second variation of control method I. The LIA error signal and ten second time markers are also shown in the figure. For the period shown, the HVA_1 correction voltage slowly drops. The maximum voltage shown occurs around 27 seconds with a minimum occurring just before 3 minutes. The difference between the maximum and minimum voltage is 150 volts.

Figure 7.2 shows the results of the same experiment using control method II. Figure 7.2 again shows a slow decrease in the correction voltage from HVA_1, however, the drift is not as great. This is because the control is split between each PZT as seen by the slowly increasing voltage from HVA_2. The voltages are of opposite sign because of the negative sensitivity of PZT_2 as shown in Chapter V. The maximum correction voltage from HVA_1 occurs at about ten seconds with the minimum occurring just before three minutes. The difference between maximum and minimum voltage is 90 volts. The difference in HVA_2 maximum and minimum voltage is about 50 volts.

From the results, it is evident that for a large temperature drift saturation will occur a lot sooner for control method I than it will for control method II. From this it is evident that the dynamic range of the control system has been increased by using dual PZT controllers.

The reason for making PZT_2 short is to provide a

fast response time to control high frequency noises. Theoretically, this will allow PZT_1 to be lengthened to further increase the dynamic range of the control loop. The next section compares the frequency spectrum of the error signal, e(t), between control methods I and II.

Frequency Spectrum of the LIA Error Signal

Performance results were obtained for each control method by recording the noise spectrum of the error signal, e(t), from the LIA. Figures 7.3 - 7.12 show the results of the performance tests and are grouped at the back of this section for ease of comparison.

Figures 7.3 through 7.4 show the frequency spectrum of the open loop error signal and are used for comparisons of the noise reduction when the loop is closed. What appears to be noise on the left side of Figures 7.3 through 7.4 is actually trace blur. This was due to the high sweep rate required because the laser frequency would not stay matched very long to the interferometer resonance in the open loop configuration.

Figures 7.5 through 7.8 when compared to Figure 7.3 show the amount of noise reduction achieved when the loop is closed. Noise reduction for each control method is tabulated in Table 7.1. Fourteen db has been added to the noise reduction figures of Table 7.1 because for Figures 7.5 through 7.12 the LIA sensitivity setting was increased

Table 7.1
Noise Reduction for Each Control Method
(0-250 Hz Range

Method	Compensator	Noise Level	Noise Reduction in db
____	open loop	greater than 7v	____
I	Gc_1	greater than 0.8v	less than -32.8 db
I	Gc_2	0.4v	-38.9 db
II	Gc_3	0.2v	-44.9 db

from 500 μv to 100 μv. This results in a 14 db increase in the magnitude of the error signal.

From Table 7.1 it is evident that for the low frequency range (0Hz - 250 Hz) control method II provides a greater noise reduction than does control method I. Also note that variation 2, using compensator Gc_2, is much better than variation 1 using compensator Gc_1.

In order to make an objective comparison of the two control methods, the frequency range of the spectrum analyzer was increased from 50 Hz/cm to 200 Hz/cm as seen in Figures 7.9 to 7.12. By comparing this set of figures, showing the expanded frequency spectrum, method II is seen to provide the best overall noise reduction.

To compare the high frequency noise reduction achieved

by each control method, Figure 7.4 must first be perused. From Figure 7.4, the noise content of the error signal is seen to be below 1000 Hz. Figure 7.9 shows that variation 1 of control method I is effective to about 400 Hz. Figure 7.10 indicates that variation 2 reduces the higher frequency noise as designed. As seen in Figure 7.12, method II also reduces the noise for the higher frequencies and is even more effective.

Figure 7.11 is a picture of the results obtained when only the PZT_1 portion of the control loop is closed using control method II. This simulates the use of a very long PZT for variation 2 of control method I. As seen in Figure 7.12, when the PZT_2 portion of the loop is closed reduction of the higher frequency noises is significant. Conclusions formed from these test results are discussed in the following chapter.

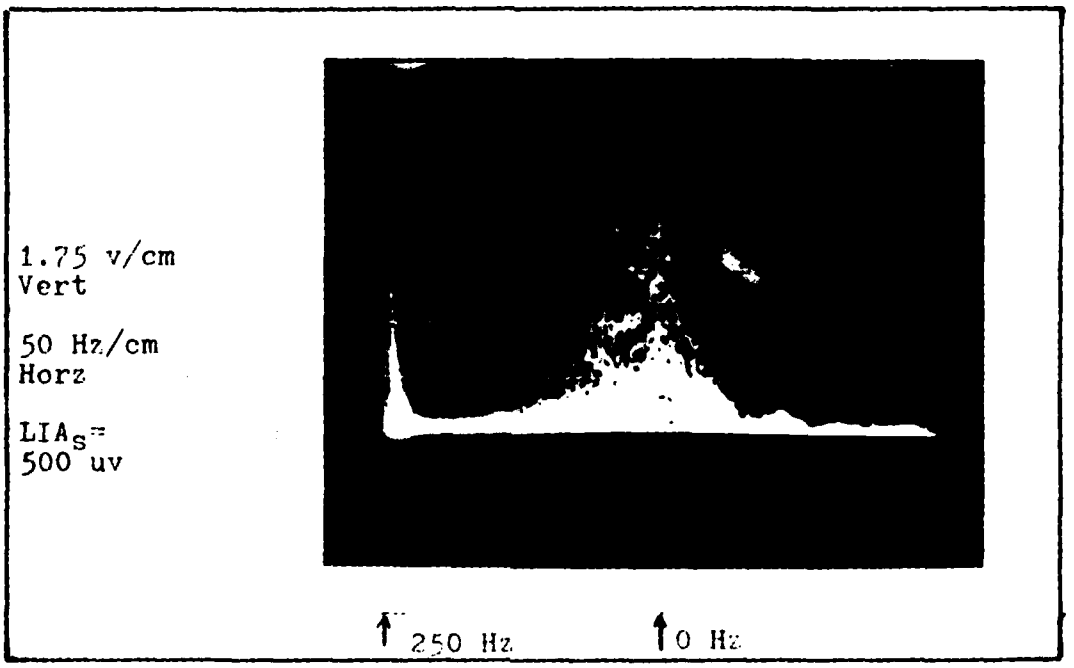

Figure 7.3 Spectral Content of the Open Loop Error Signal (0 Hz - 250 Hz)

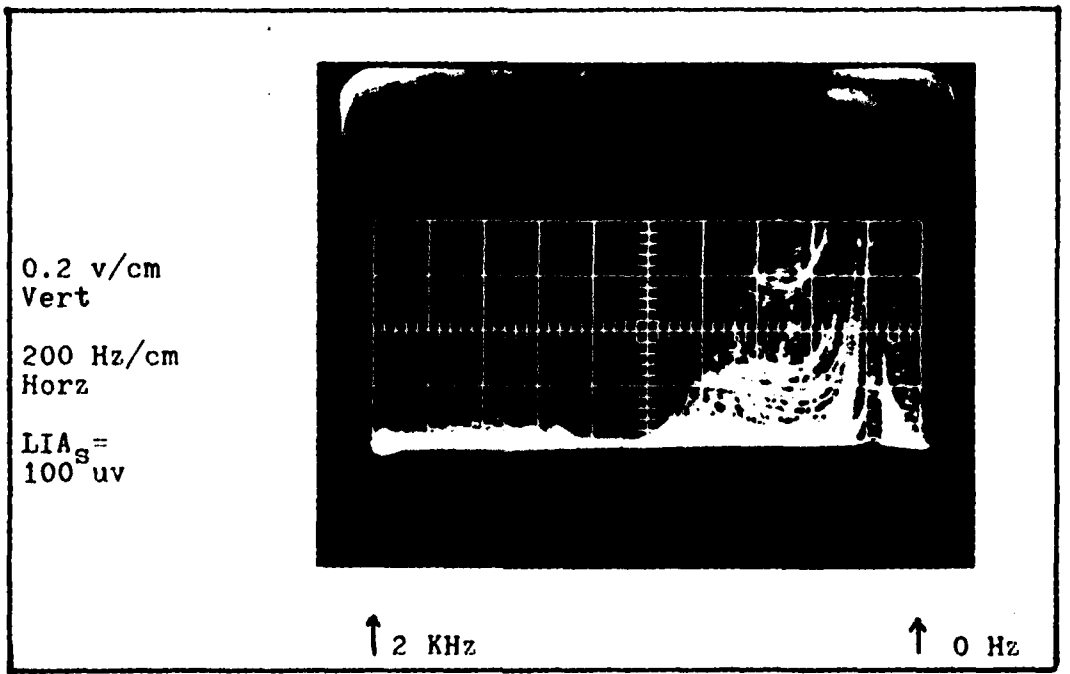

Figure 7.4 Spectral Content of the Open Loop Error Signal (0 Hz - 2 KHz)

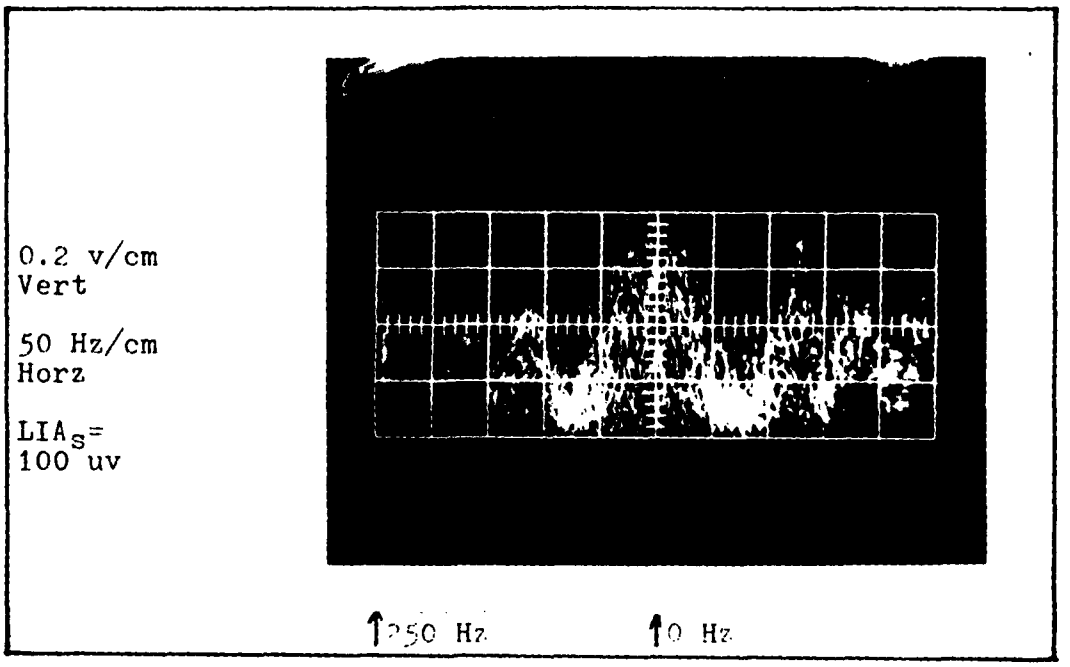

Figure 7.5 Spectral Content of the Closed Loop Error Signal. (0 Hz - 250 Hz) Method I, Variation 1

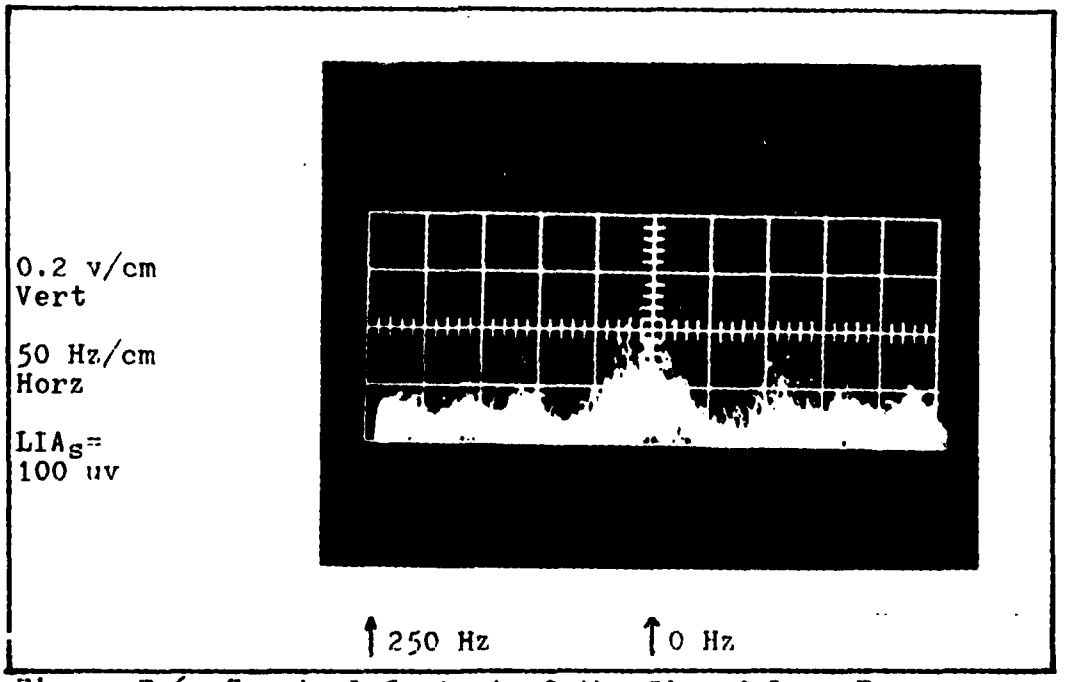

Figure 7.6 Spectral Content of the Closed Loop Error Signal (0 Hz - 250 Hz). Method I, Variation 2, Using Compensater Gc_2

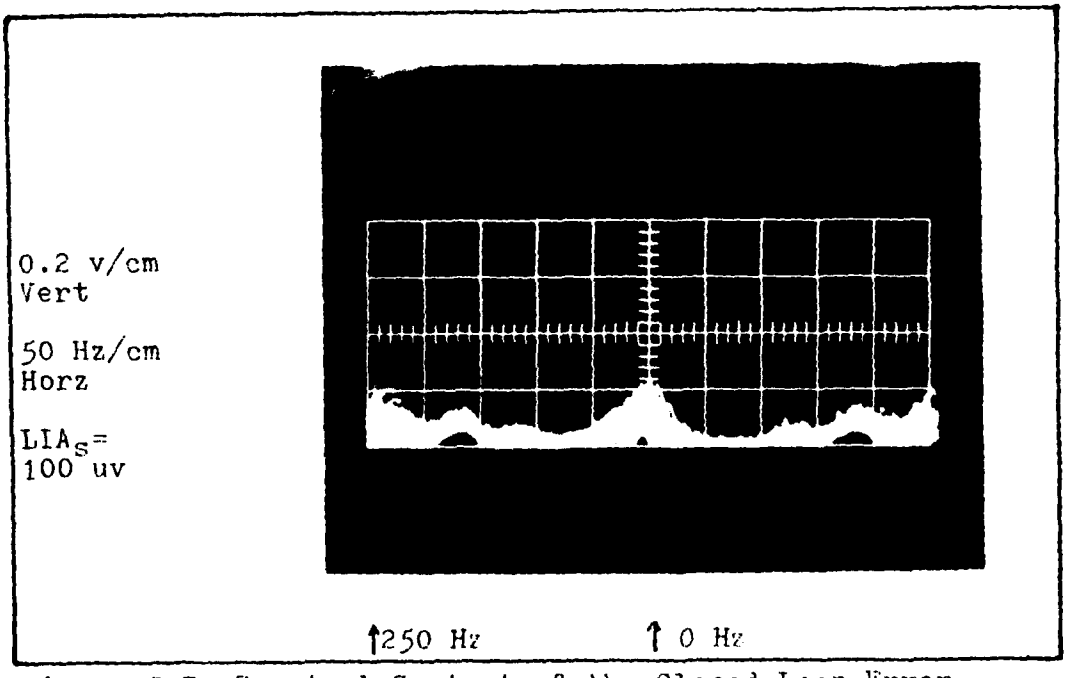

Figure 7.7 Spectral Content of the Closed Loop Error Signal (0 Hz - 250 Hz) Using the Gc_{3a} Portion of Compensator Gc_3

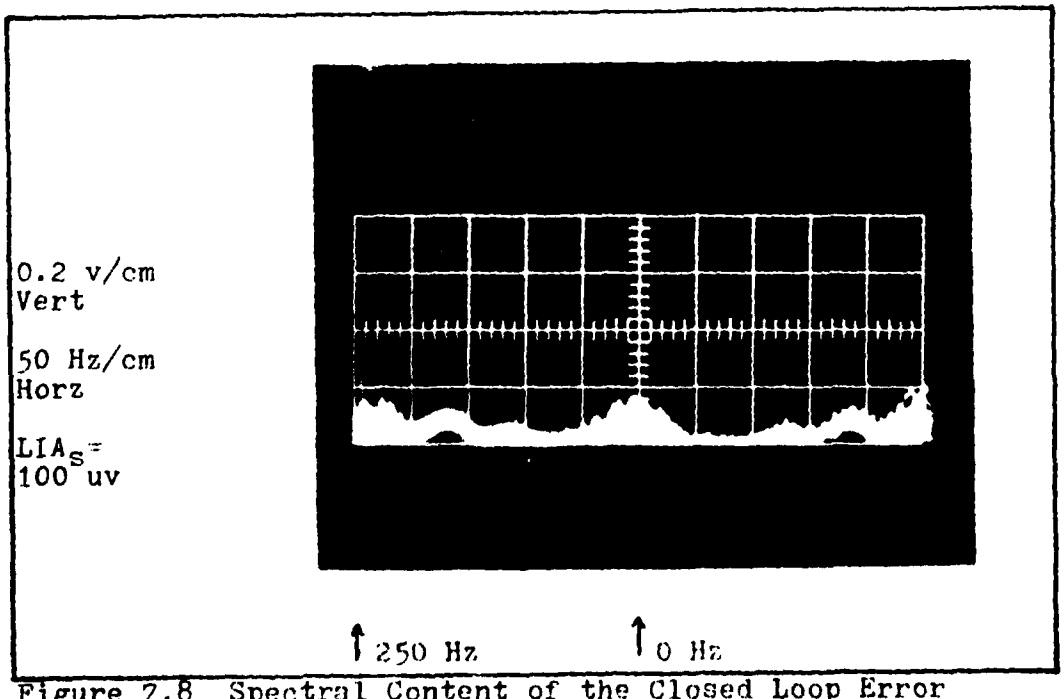

Figure 7.8 Spectral Content of the Closed Loop Error Signal (0 Hz - 250 Hz). Method II

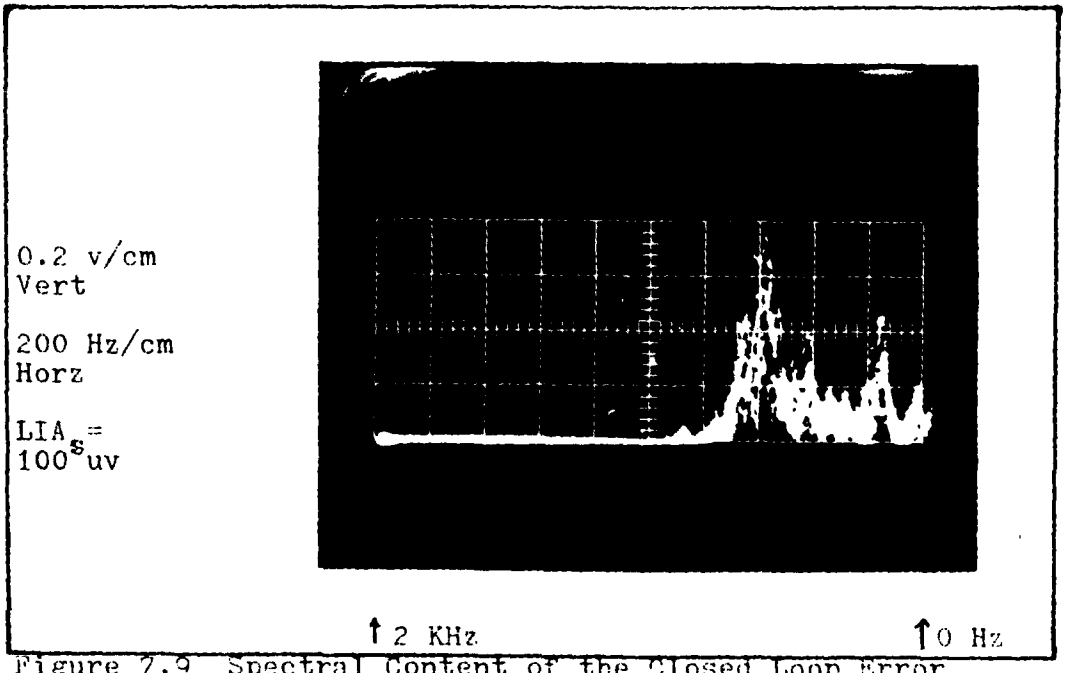

Figure 7.9 Spectral Content of the Closed Loop Error Signal (0 Hz - 2 KHz). Method I, Variation 1

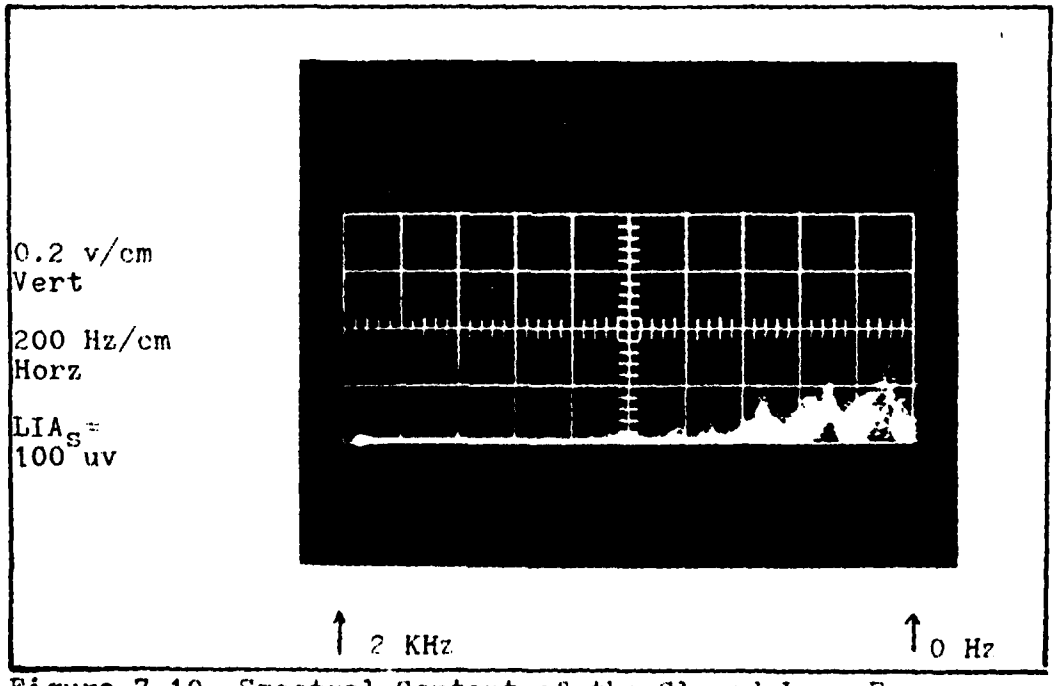

Figure 7.10 Spectral Content of the Closed Loop Error Signal (0 Hz - 2 KHz). Method I, Variation 2

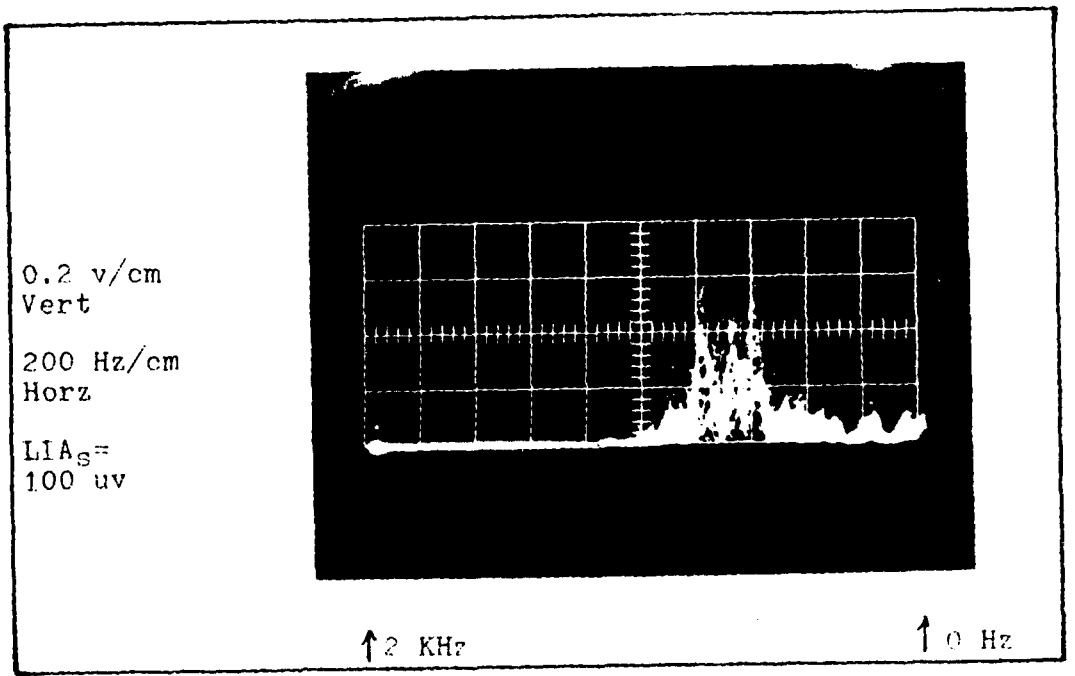

Figure 7.11 Spectral Content of the Closed Loop Error Signal (0 Hz - 2 KHz), Using the Gc_{3a} Portion of Compensator Gc_3

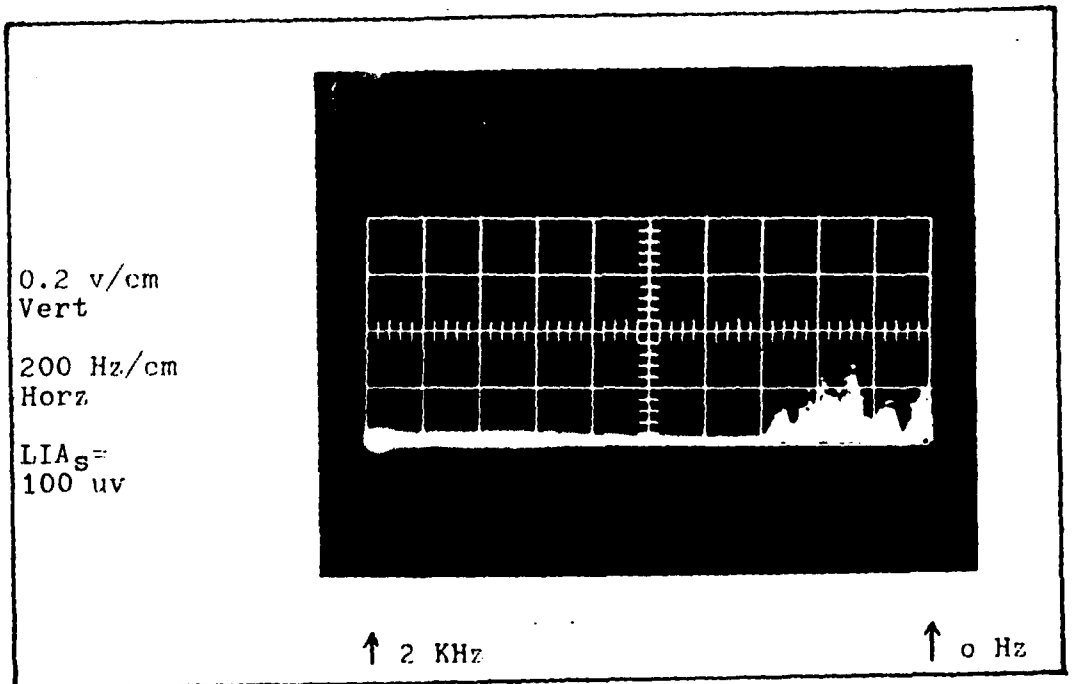

Figure 7.12 Spectral Content of the Closed Loop Error Signal (0 Hz - 2 KHz). Method II

VIII Conclusions and Recommendations

General Discussion

The purpose of this research was to compare two methods that can be used to frequency stablize a laser. Control method I consisted of a feedback loop that used a single PZT controller to correct the laser cavity length. Two variations of method I were used in the research. Variation 1 used a control loop compensator designed from steady state analysis. The compensator used in variation 2 was more sophisticated and was designed from frequency analysis. Control method II deviates from the standard approach used in method I. Two PZTs of different lengths were used to control the laser cavity. A long PZT was used to provide a large dynamic range while a short PZT was used to provide a fast response time.

The results from use of the two control methods were obtained by first recording the difference in the controllable range and second, by recording and comparing the frequency spectrum of the error signal produced by each method.

Conclusions

From the comparisons made in Chapter VII, control method II is superior to control method I. From the Control Range section of Chapter VII it is clearly evident that the control system limits will be reached much sooner when

control method I is used. This is very important when the system is used in a temperature varying environment. From the Frequency Spectrum section of Chapter VII, it is also evident that the noise reduction for control method II is greater than for control method I. Also, control method II is more effective at high frequencies than control method I.

In conclusion, the use of dual PZT controllers looks very promising and should be adopted where both a large dynamic range and fast response time are desired. Recommendations regarding this research are discussed in the following section.

Recommendations

One of the major problems encountered during this research was due to large temperature drifts in the laboratory. As shown earlier, the single PZT controller was only expected to compensate for $0.3^{\circ}F$ temperature change before reaching the limit of the high voltage amplifier. Due to the temperature variations in the laboratory, this limit was reached after about 30 minutes using control method II, and even less using control method I. To help solve this problem, a piezoelectric transducer with a much greater sensitivity should be used. It is also recommended that a longer PZT be used that will further increase the dynamic range of the control system. To further reduce the temperature drift problem, the use of super-invar is

recommended for all of the laser hardware along with a much shorter laser.

Large temperature drifts not only cause the laser cavity to change length, but also causes the interferometer cavity length to change. Thus, while the laser frequency may indeed be locked to the interferometer resonance, the actual frequency could be varying with temperature. A solution to this problem is to use a laser gain tube that displays a Lamb dip at the peak of the output intensity curve. The laser frequency could then be locked to the Lamb dip and the interferometer would not be needed in the control loop (Ref 2:351).

Bibliography

1. Holland, Charles R. and David J. Olkowski. Evaluation of Errors in a Passive Ring Laser Gyroscope. MS Thesis Wright-Patterson AFB, Ohio: Air Force Institute of Technology, December 1978.

2. White, A. D. "Frequency Stabilization of Gas Lasers", IEEE Journal of Quantum Electronics, QE-1, 8:349-357 (November 1965).

3. Smith, P. W. "Stabilized Single-Frequency Output from a Long Laser Cavity", IEEE Journal of Quantum Electronics, QE-1, 8:343-348 (November 1965).

4. O'Shea, Donald C., W. Russel Callen, and William T. Rhodes. Introduction to Lasers and Their Applications. Massachusetts: Addison-Wesley Publishing Company, 1977.

5. Datu, C. A. "Frequency Stabilization by Phase Control of a Single Frequency-Single Mode CO_2 Laser", DDC ADB0 14310L, September 1975.

6. Nagai, Haruhiko. "Laser Frequency Fluctuations Due to Mechanical Vibrations", IEEE Journal of Quantum Electronics, QE-8, 12:857-865 (December 1972).

7. D'Azzo, John J. and Constantine H. Houpis. Linear Control System Analysis and Design: Conventional and Modern. New York: McGraw Hill Inc, 1975.

8. Jodon Engineering Associates Inc. Optical Spectrum Analyzer Model SA 1500 Instruction Manual. Michigan: Jodon Engineering Associates Inc, August 1969.

Appendix A

Laser/Interferometer Hardware Designs

The material in Appendix A consists of drawings for the laser and interferometer hardware as referenced in Chapter III. Figures D.1 - D.4 include drawings for the laser end plates, the laser gain tube support blocks, the PZT mounting blocks, and the interferometer mount respectively.

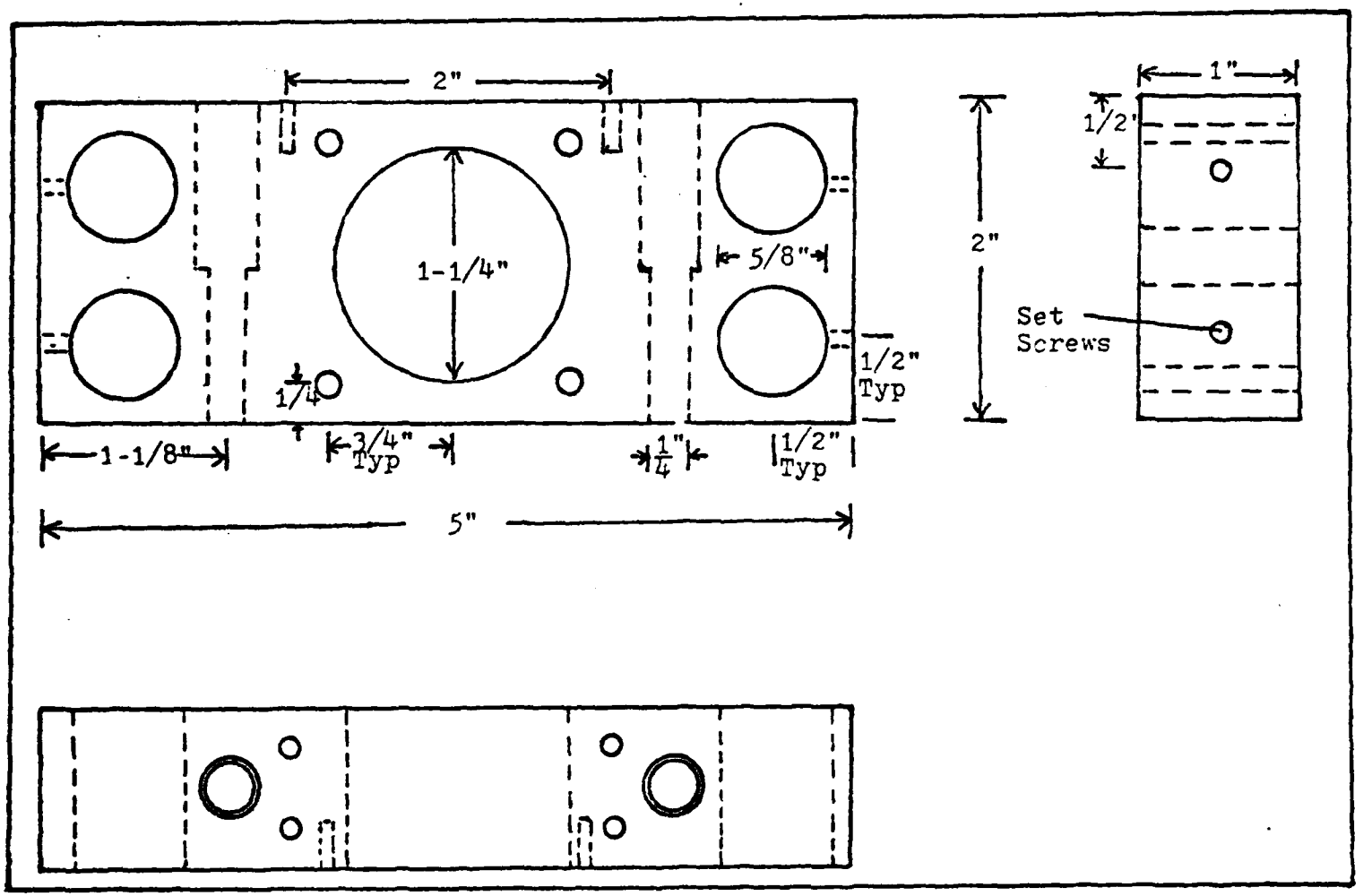

Figure A.1 Laser End Plates

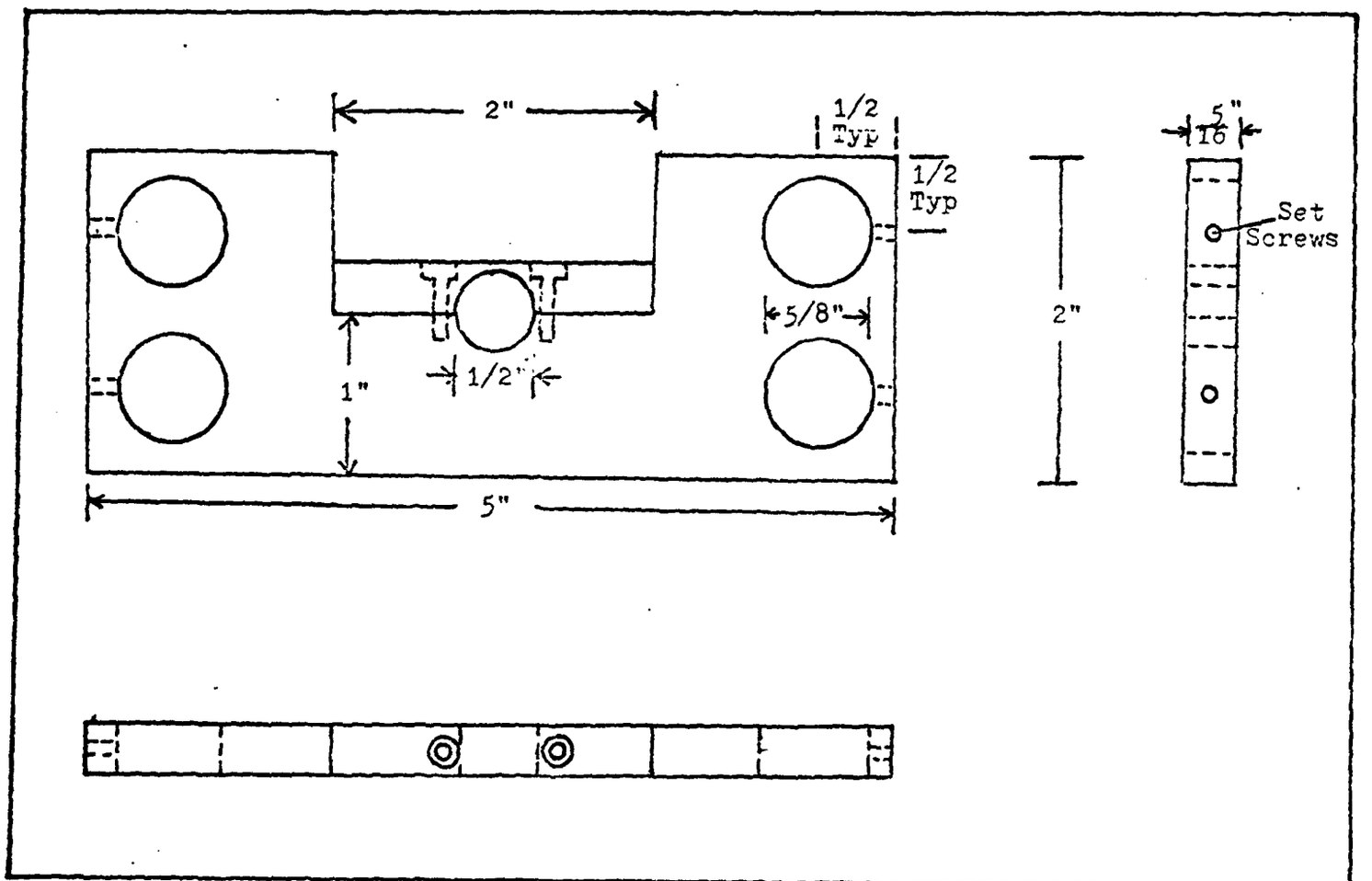

Figure A.2 Laser Gain Tube Support Blocks

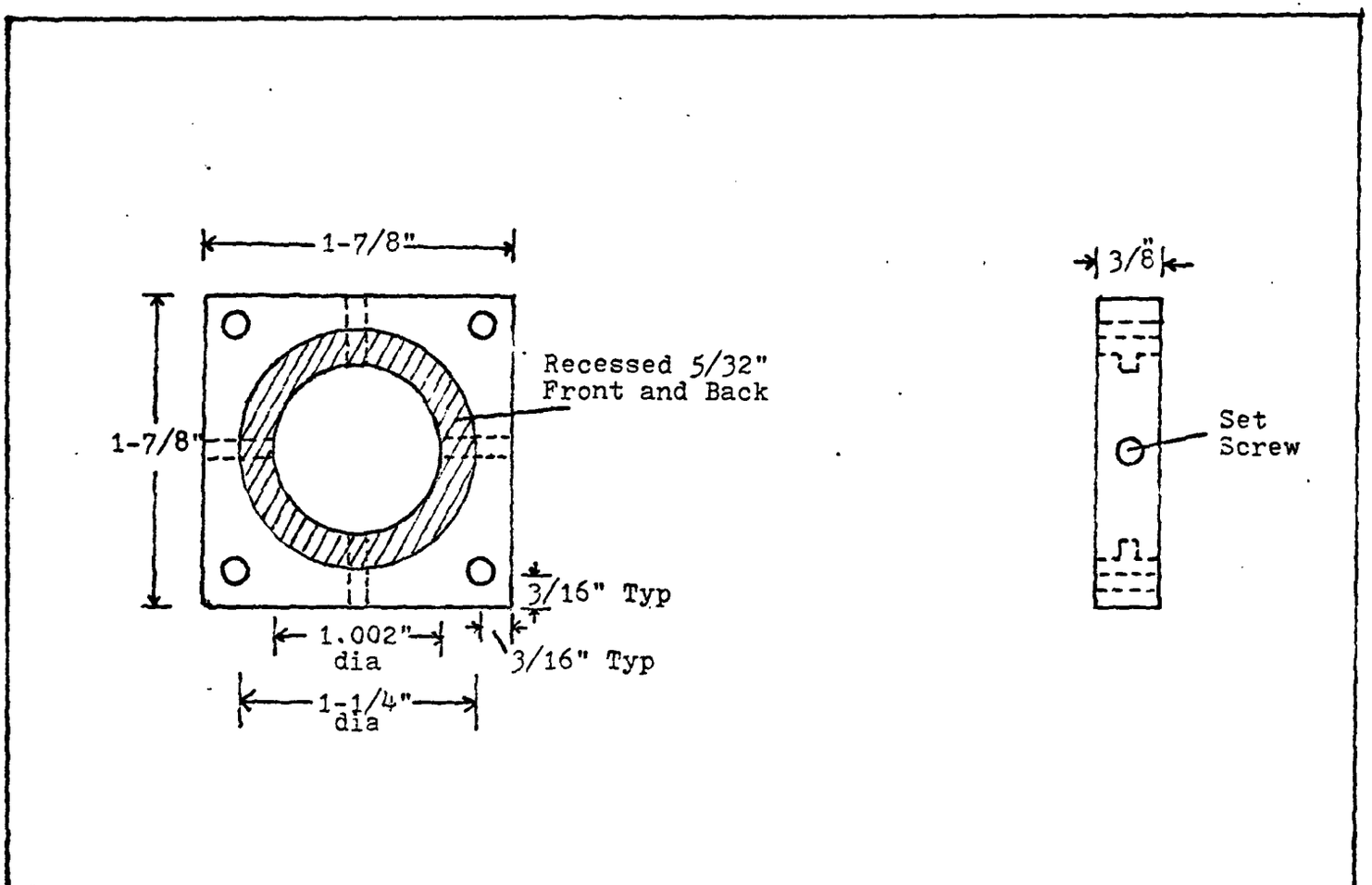

Figure A.3 PZT Mounting Blocks

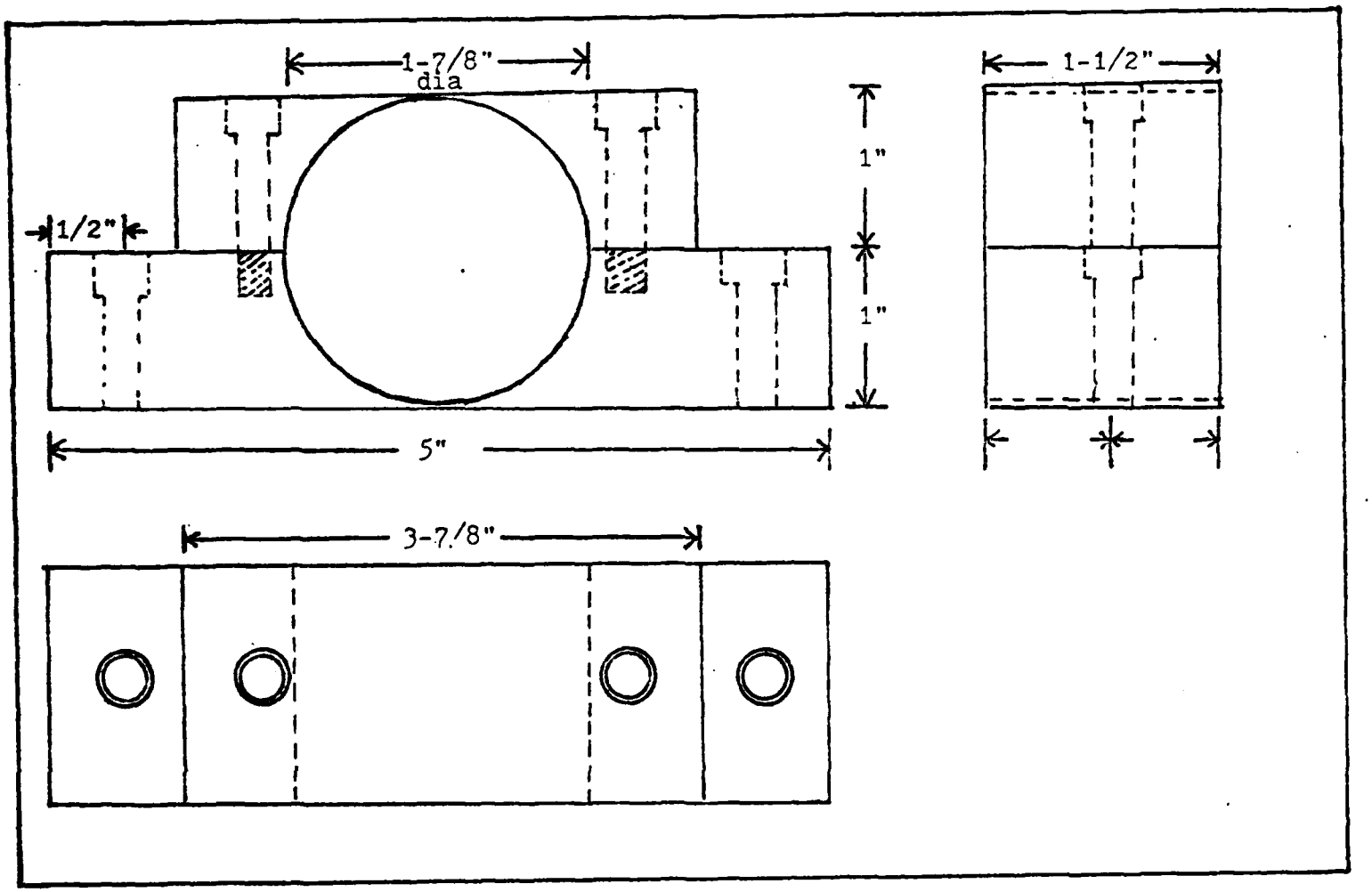

Figure A.4 Interferometer Mount

Appendix B

Circuit Design and Tests for Compensator Gc_1

The material in Appendix B consists of the circuit design procedure, a schematic diagram, and test results for compensator Gc_1 as referenced in Chapter VI.

Circuit Design

From Figure 6.12, the compensator Gc_1 is broken into two parts, a gain stage, and an integrator. A summing stage is also included to combine the modulation signal from the LIA, with the compensator signal for input to the HVA. Figure B.5 is a schematic diagram of the compensator and summer. The transfer function for the compensator is

$$\frac{K_{c_1}}{S} = \left(\frac{K'}{C100 \cdot R104}\right)\left(\frac{1}{S}\right) \qquad (B.1)$$

where K' will remain as a variable gain adjustable by R100 and the first stage shown in Figure B.5.

Operational Tests

Figure B.2 shows the expected frequency response plot for the compensator. The compensator was tested using the equipment configuration shown in Figure B.1.

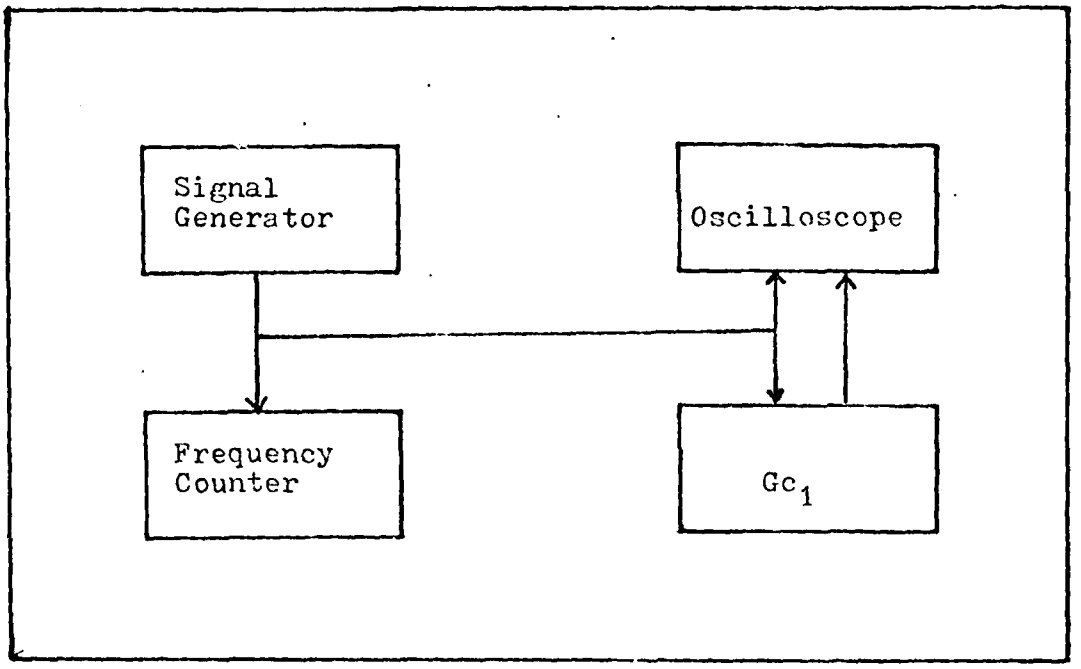

Figure B.1 Block Diagram of Equipment Used to Test Compensator Gc_1

The frequency from the signal generator was adjusted while the output of Gc_1 was viewed on the oscilloscope. The phase and amplitude of Gc_1 was compared to the input signal with results as plotted in Figure B.2. The solid lines in Figure B.2 indicate the expected phase and magnitude of the results while X indicates the measured magnitude and O represents the measured phase.

As shown by the results, the compensator works as designed. Figures B.3 and B.4 show the amplitude and spectral content of the noise from Gc_1 with the input shorted. As seen in Figure B.3, the noise amplitude is very small and has little affect on the laser for the same reasons as stated in Chapter IV.

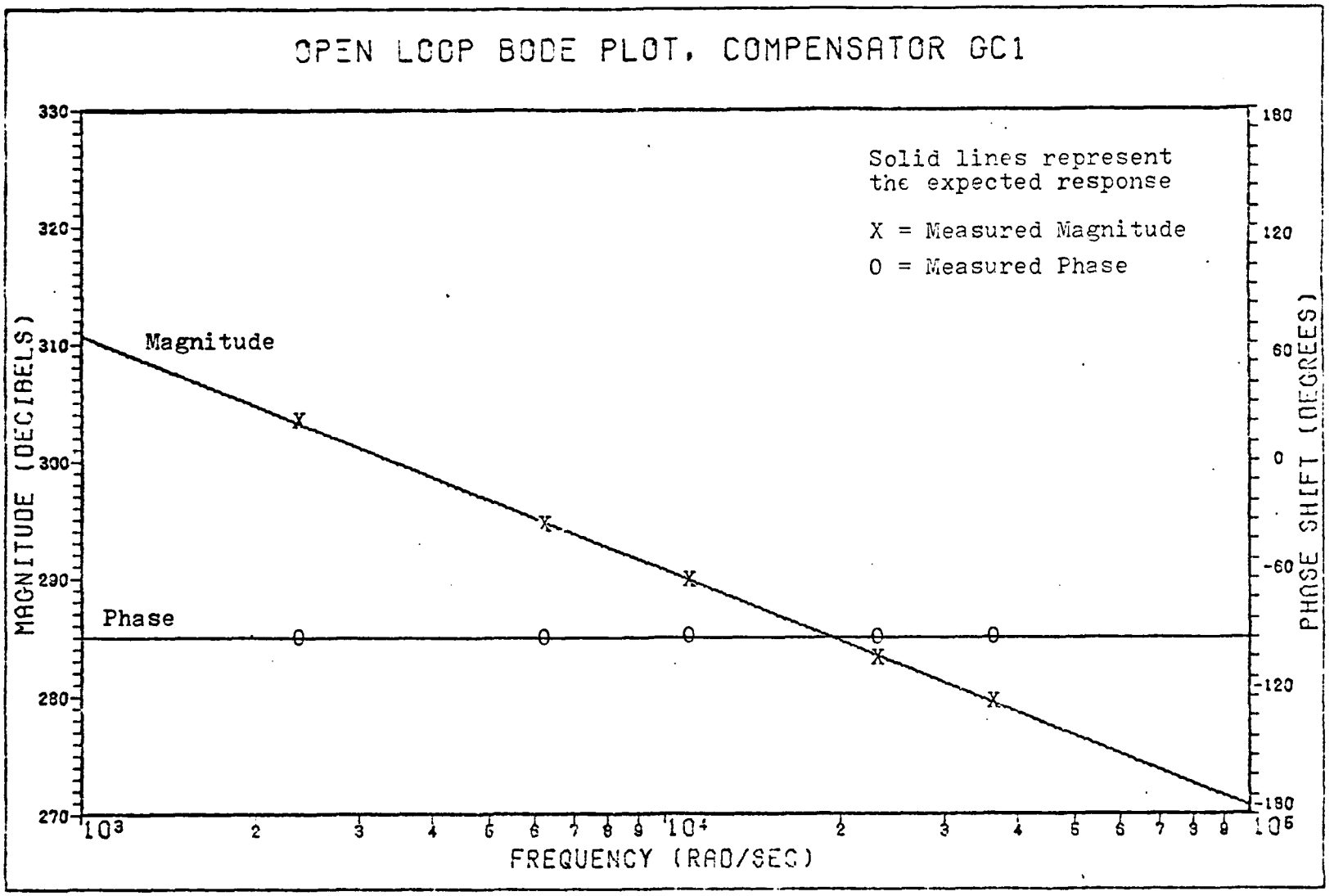

Figure B.2 Measured vs Expected Frequency Response Plot for Compensator G_{c_1}

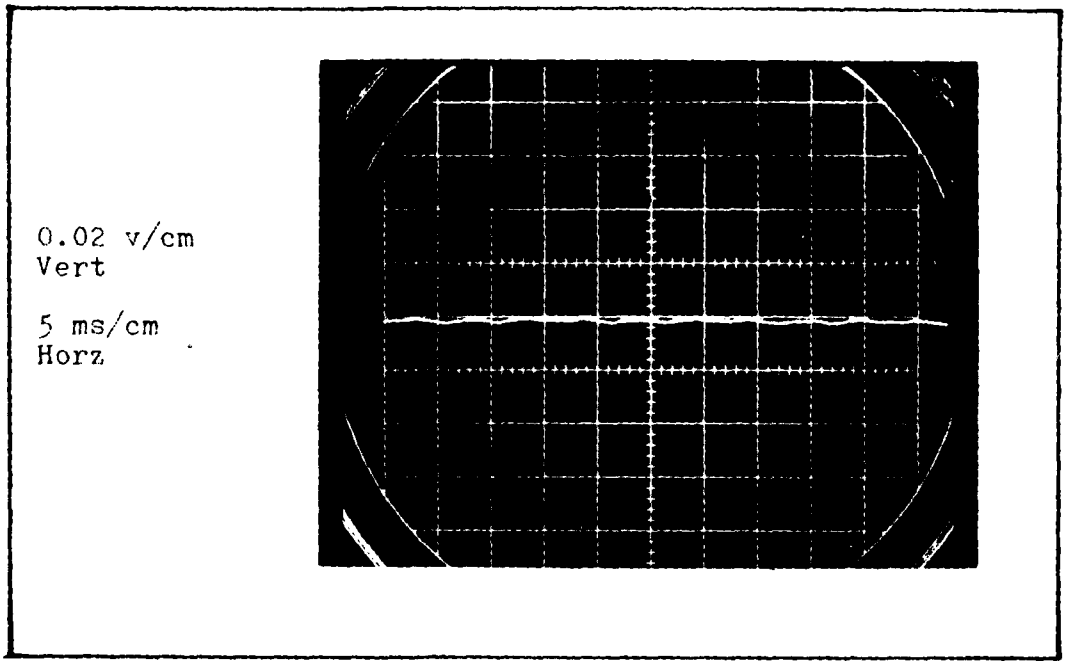

Figure B.3 Noise from Compensator Gc_1

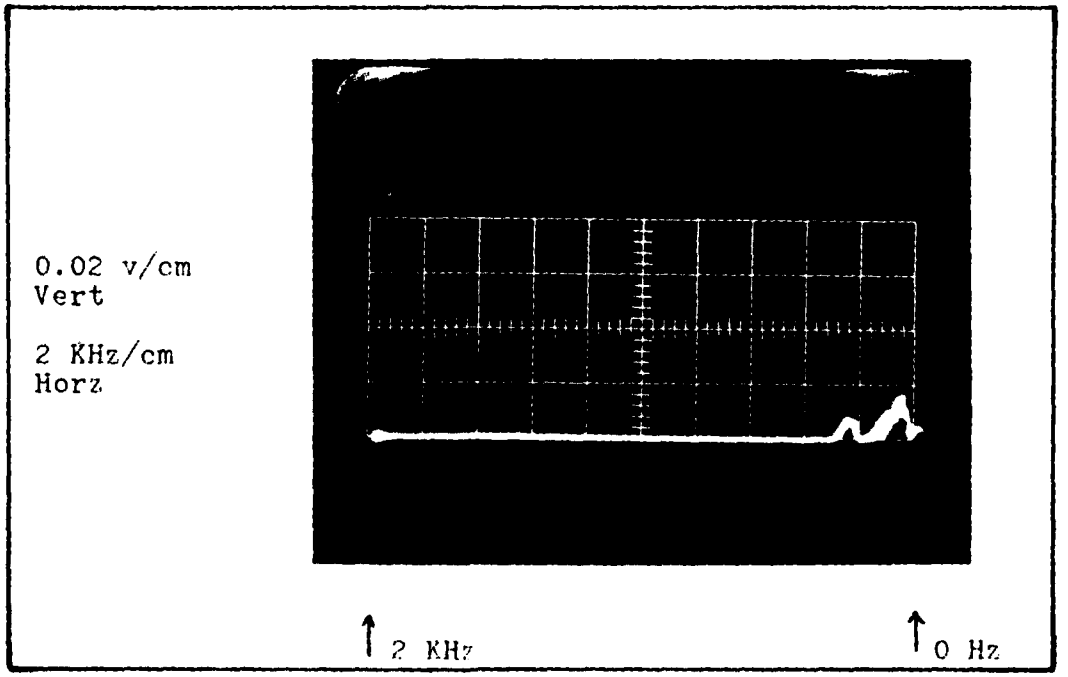

Figure B.4 Spectral Content of Noise from Compensator Gc_1

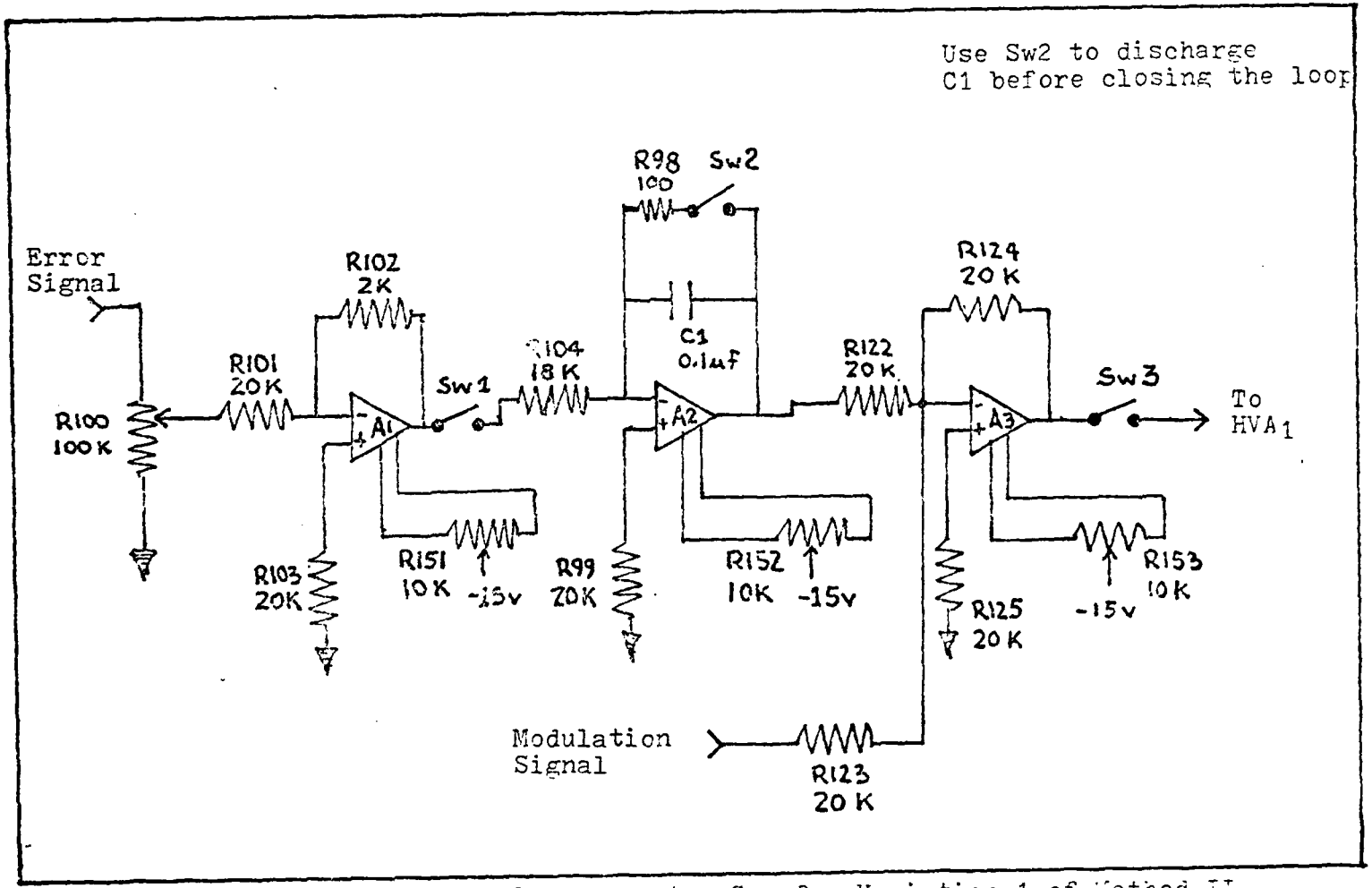

Figure B.5 Schematic Diagram of Compensator Gc_1 for Variation 1 of Method II

Appendix C

Circuit Design and Tests for Compensator Gc_2

The material in Appendix C consists of the circuit design procedure, a schematic diagram, and operational test results for compensator Gc_2 as referenced in Chapter VI.

Circuit Design

The transfer function for Gc_2 from Eq (6.25) is shown again here with a variable gain K'':

$$Gc_2 = \frac{K''(s+5600)^3(s+38900)^2}{(s)(s+70021)^2(s+112800)^2} \qquad (C.1)$$

Eq (C.1) was broken into six parts and amplifier transfer functions G_{A4} to G_{A9} were assigned to each part as shown in Figure C.1. The schematic diagram shown in Figure C.5 was determined from Figure C.1. Component values were found by finding the ratio of each stage's output impedance to input impedance and equating the ratio to the respective transfer function.

Operational Tests

The same tests that were performed on Gc_1 were also performed on Gc_2 with results plotted in Figure C.2. The

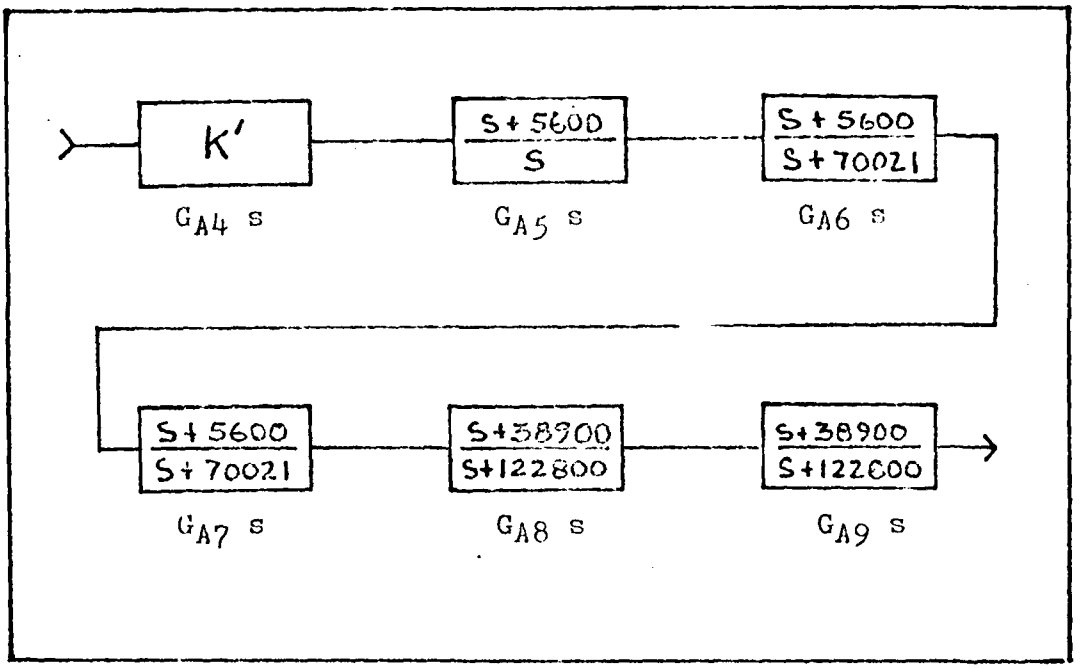

Figure C.1 Amplifier Assignment to Compensator Gc_2

solid lines in Figure C.2 are the expected phase and magnitude of the test results while X indicates the measured magnitude and O indicates the measured phase.

As shown by the results, the compensator works as designed. Figures C.3 and C.4 show the amplitude and spectral content of the noise from Gc_1 with the input shorted. The maximum peak-to-peak amplitude shown in Figure C.3 is 0.07 volts and results in a very high signal-to-noise ratio as explained in Chapter IV. Therefore, the noise has very little affect on the laser frequency.

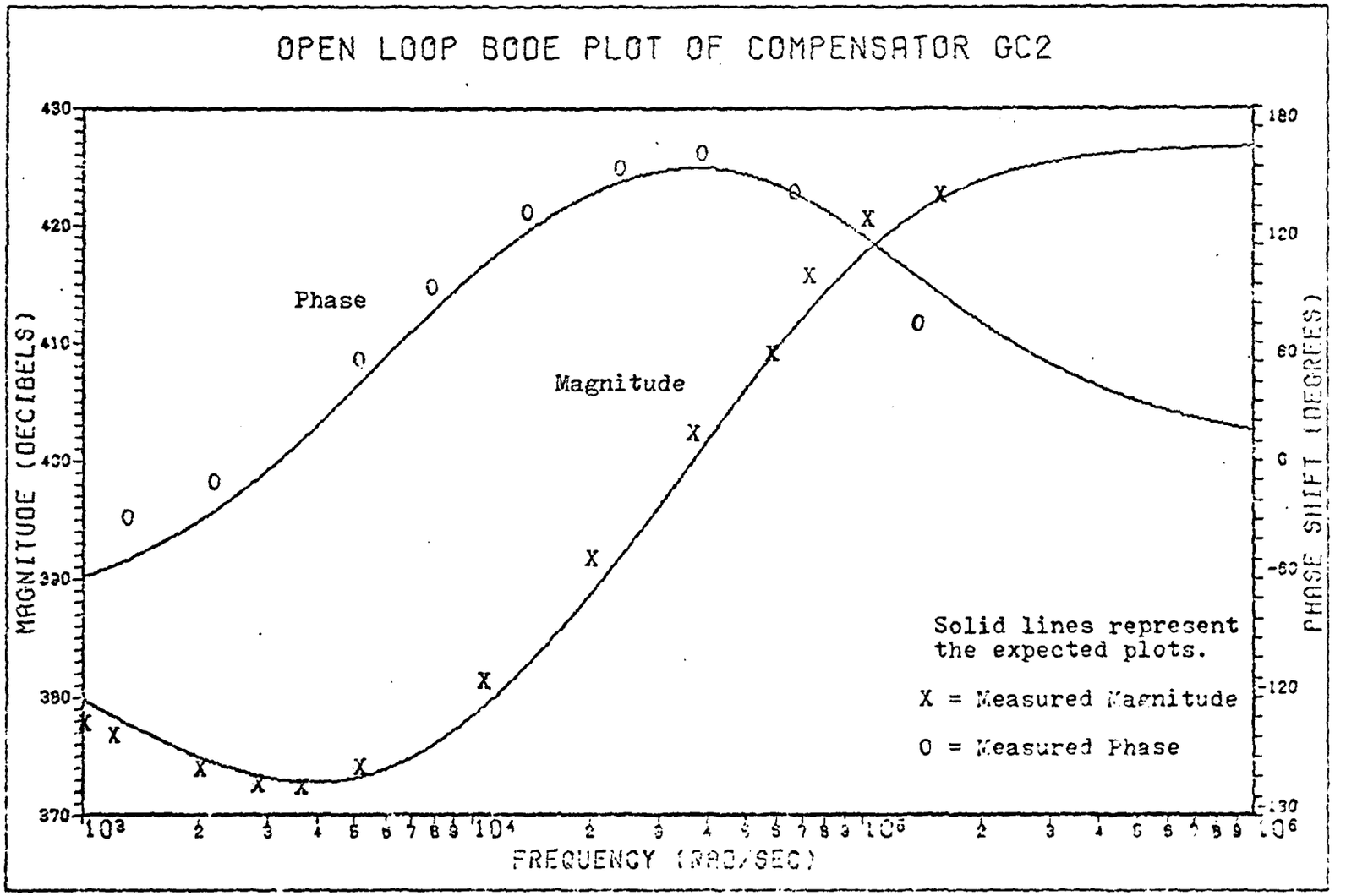

Figure C.2 Measured vs Expected Frequency Response for Compensator Gc_2

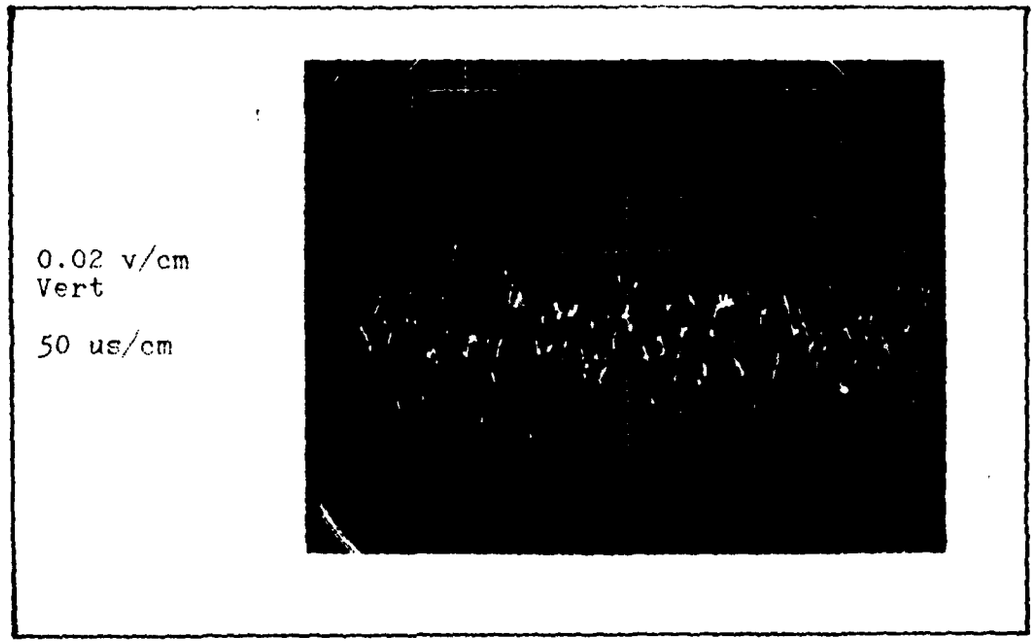

Figure C.3 Noise from Compensator Gc_2

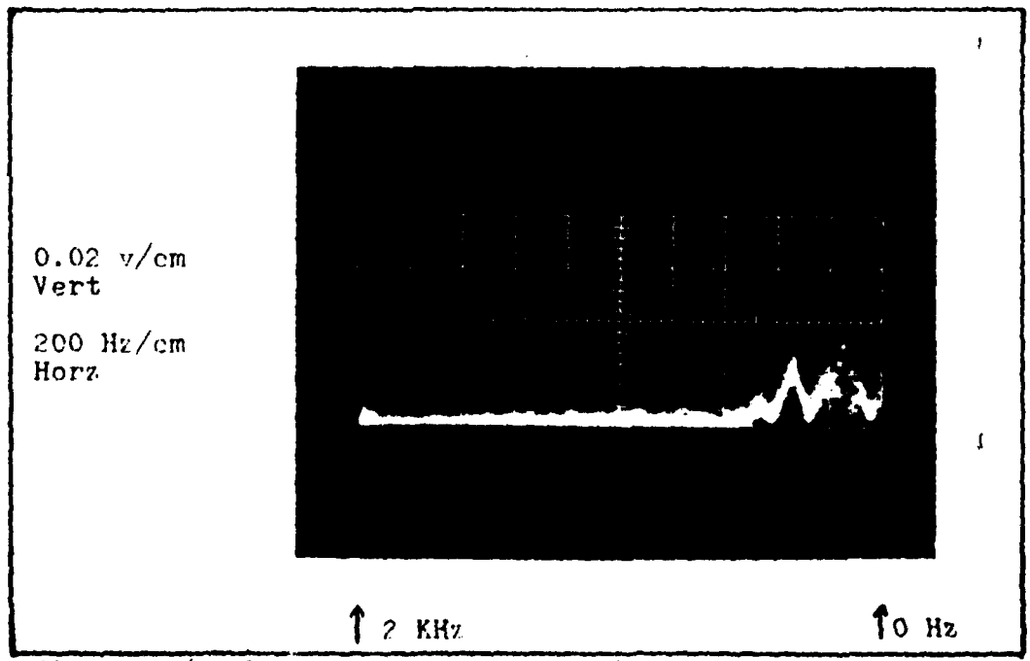

Figure C.4 Spectral Content of Noise from Compensator Gc_2

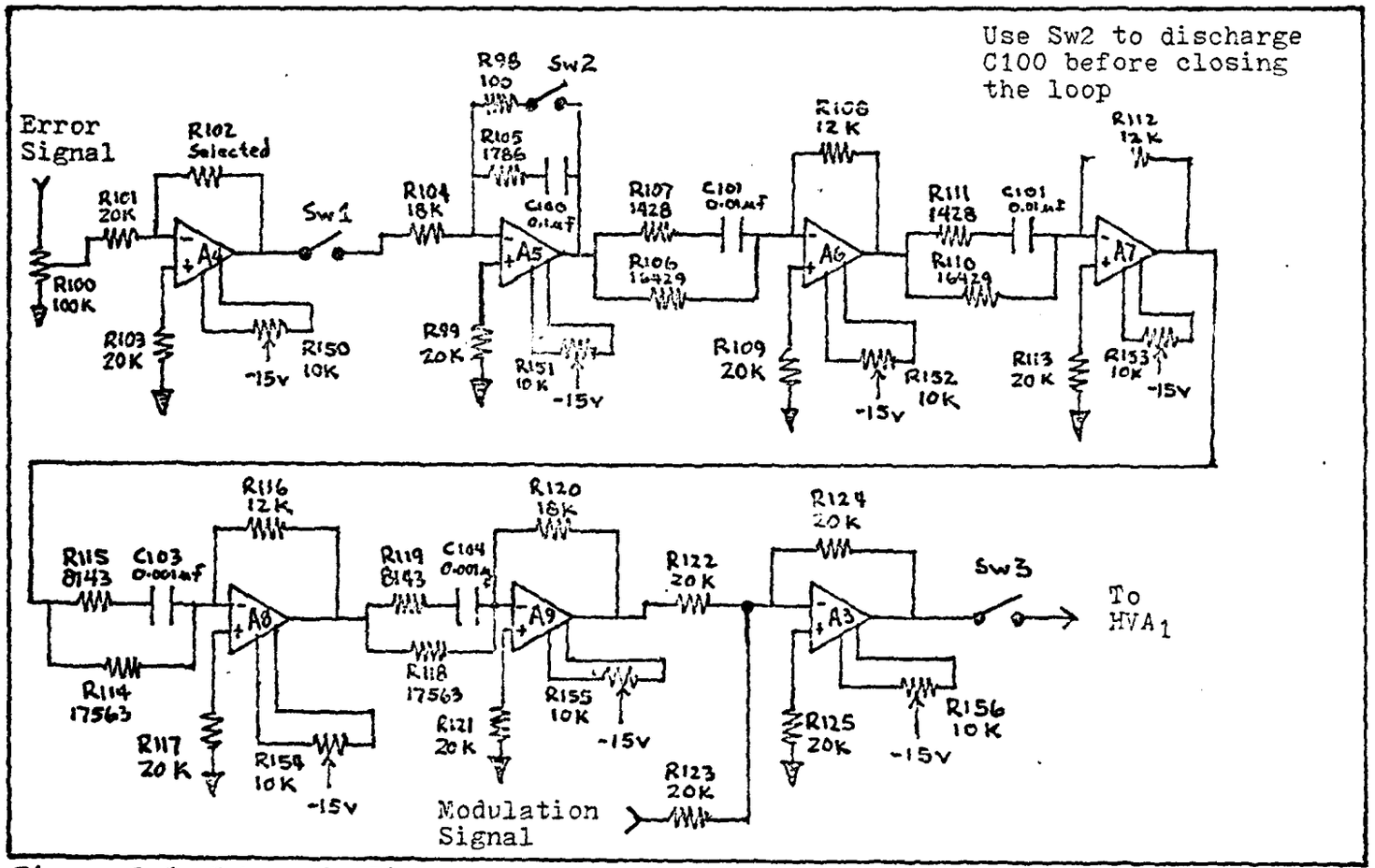

Figure C.5 Schematic Diagram of Gc_2, Variation 2 of Method I

Appendix D

Circuit Design and Tests for Compensator Gc_3

The material in Appendix D consists of the circuit design, a schematic diagram, and operational test results for compensator Gc_3 as referenced in Chapter VI.

The transfer function for Gc_3 is divided into two parts, Gc_{3a} and Gc_{3b} as shown in Chapter VI. The circuit design for both parts will be covered in the next section.

Circuit Design of Gc_{3a} and Gc_{3b}

The transfer functions for Gc_{3a} and Gc_{3b}, from Figure 6.12, are shown again here with variable gains K'''_a and K'''_b

$$Gc_{3a} = \frac{K'''_a (s+5600)^3}{(s)(s+719)(s+49740)} \qquad (D.1)$$

$$Gc_{3b} = \frac{K'''_b (s+3142)(s+5600)}{(s+104833)^2} \qquad (D.2)$$

Eqs (D.1) and (D.2) are broken into seven parts and amplifier transfer functions G_{A10} through G_{A15} are assigned to each part as shown in Figure D.1. The schematic diagram shown in Figure D.8 was determined from Figure D.1. Component values were found by finding the ratio of each stage's output impedance to input impedance and equating the results to the respective transfer function.

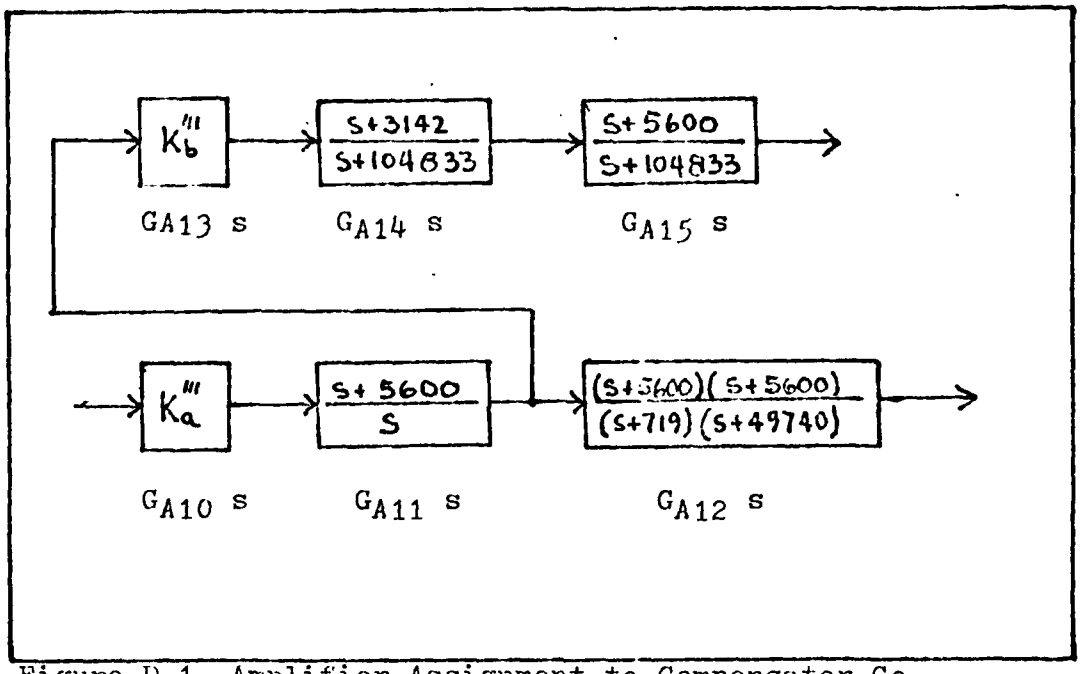

Figure D.1 Amplifier Assignment to Compensator Gc_3

Operational Tests

The same tests that were performed on Gc_1 in Appendix B, were also performed on both compensator Gc_{3a}, and the upper portion of Gc_3 shown in Figure D.1. The measured frequency responses of the compensators are plotted in Figures D.2 and D.3. The solid lines represent the expected phase and magnitude while the Xs and Os show the measured magnitude and phase respectively. As shown by the results, the compensator works as designed.

Figures D.4 through D.7 show the amplitude and spectral content of the noise from Gc_{3a} and Gc_{3b} with the input shorted. In both cases, the noise is relatively small and results in a very high signal-to-noise ratio as explained in Chapter IV, therefore, the noise has very little affect on the laser frequency.

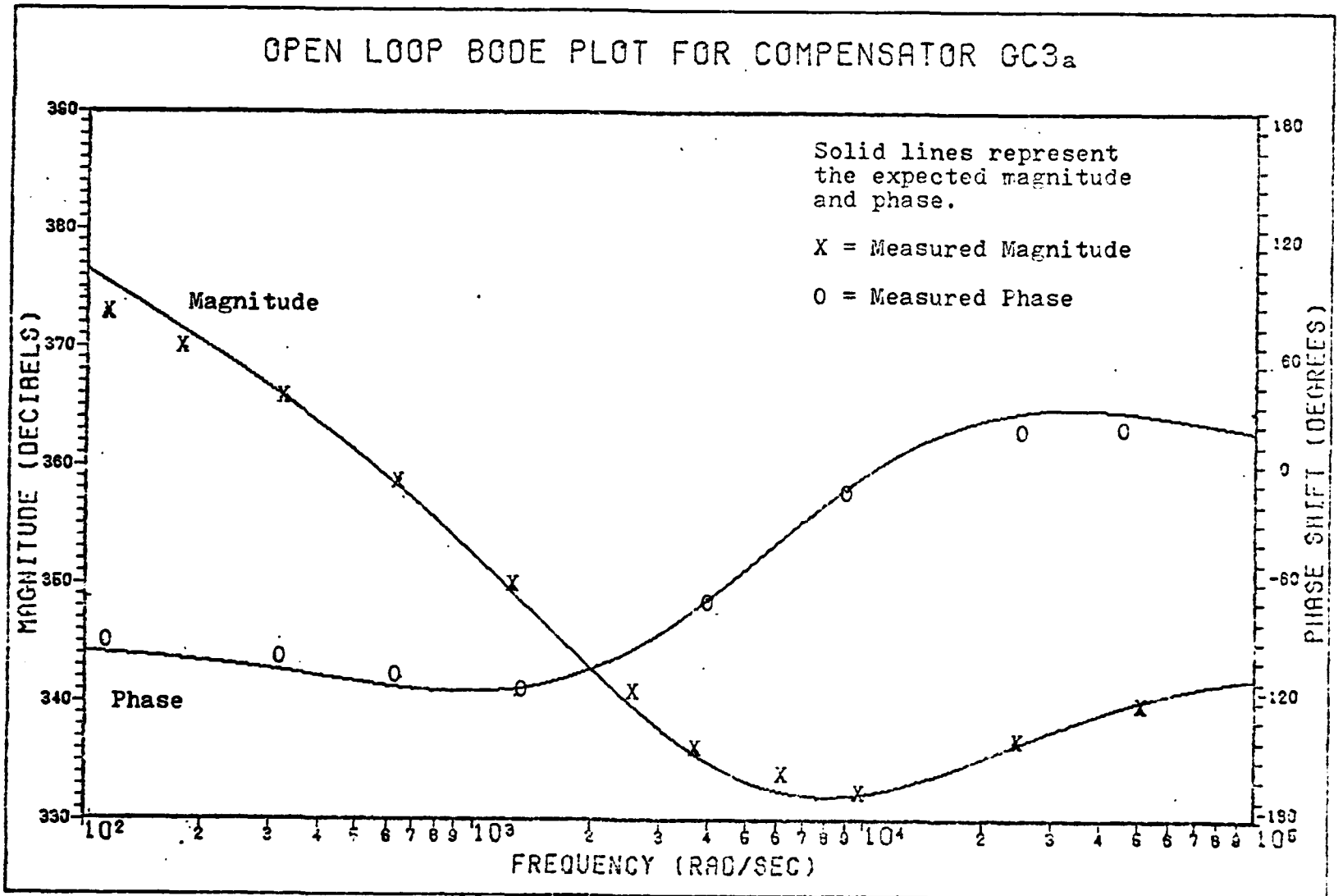

Figure D.2 Measured vs Expected Frequency Response of Compensator Gc_{3a}

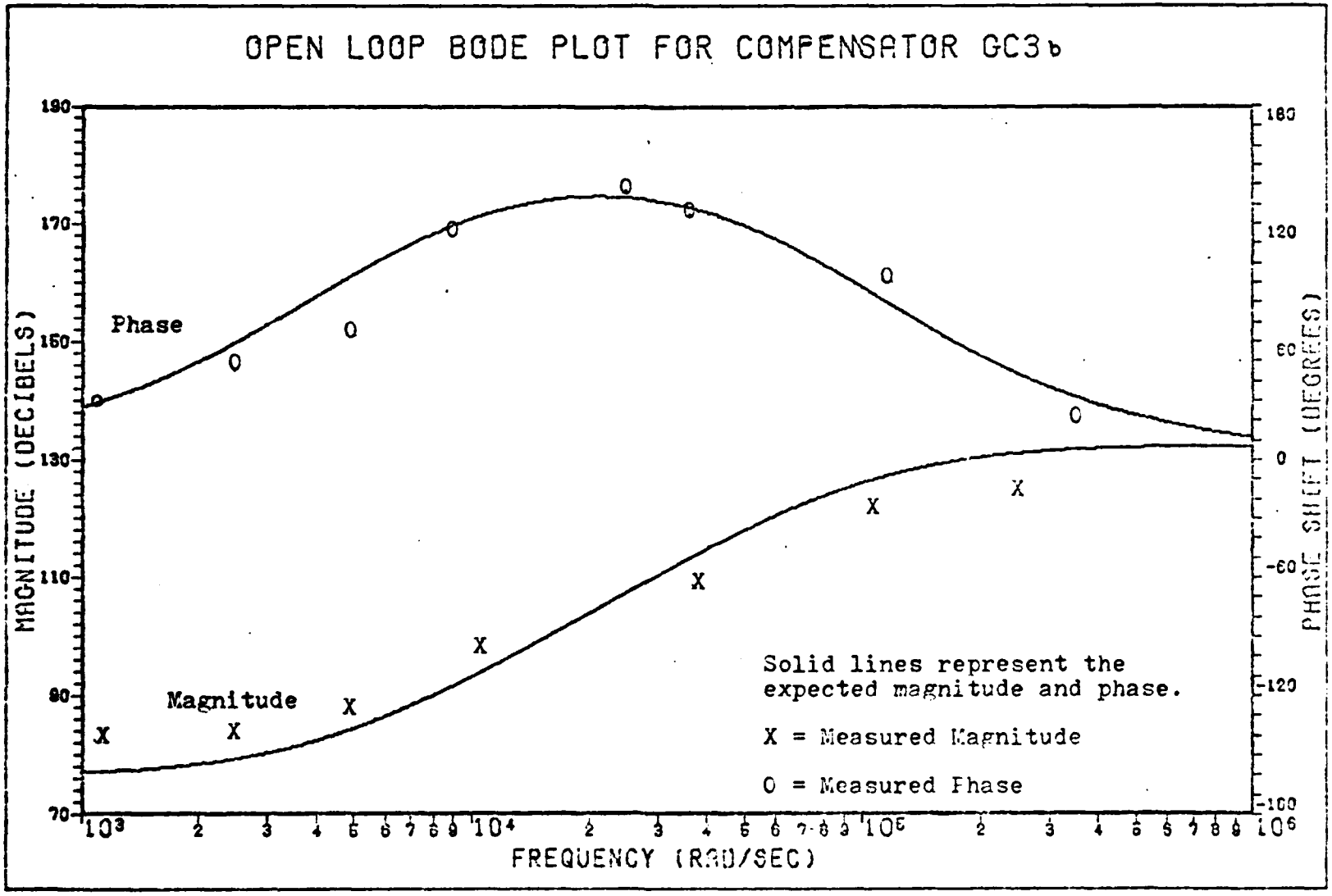

Figure D.3 Measured vs Expected Frequency Response of the Upper Portion of Compensator Gc_3 as seen in Figure D.1

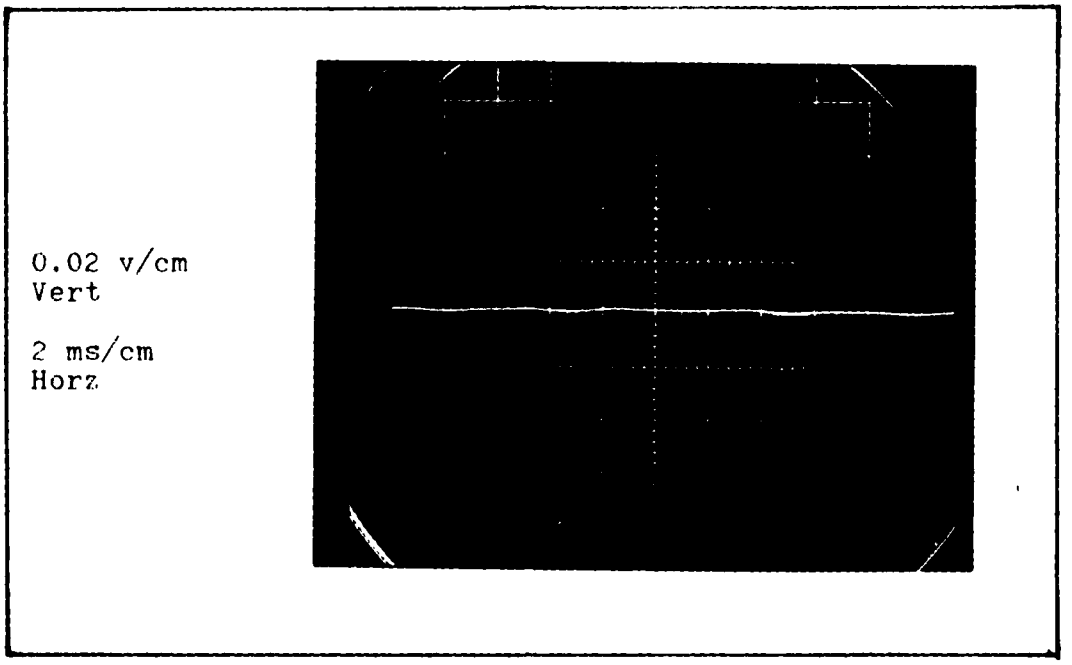

Figure D.4 Noise from Compensator Gc_{3a}

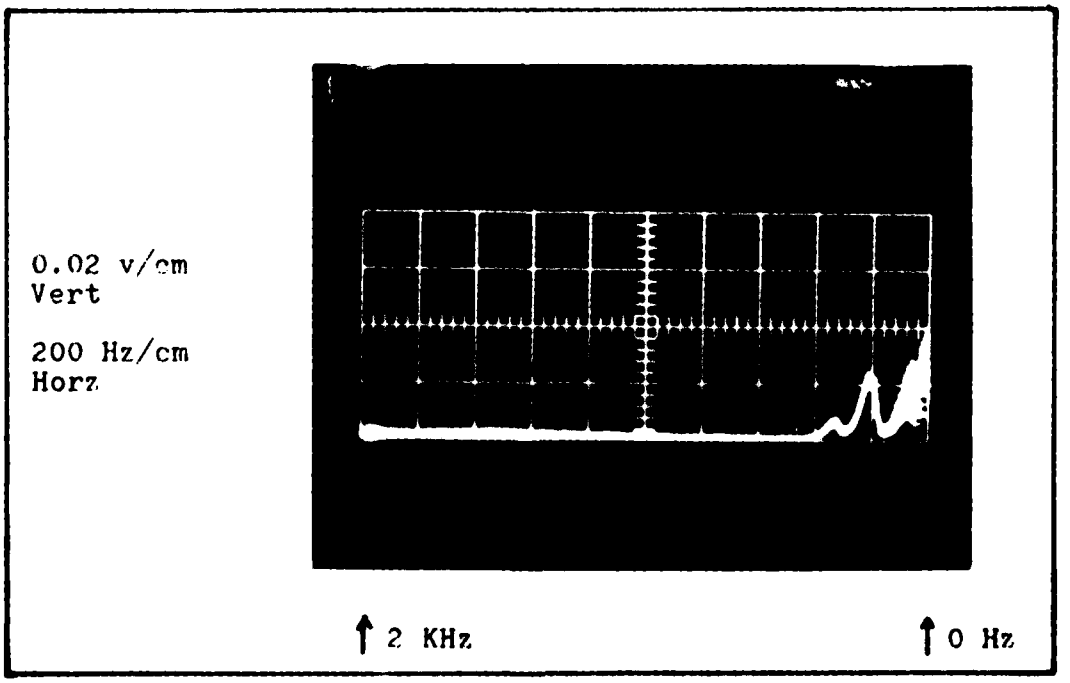

Figure D.5 Spectral Content of Noise from Compensator Gc_{3a}

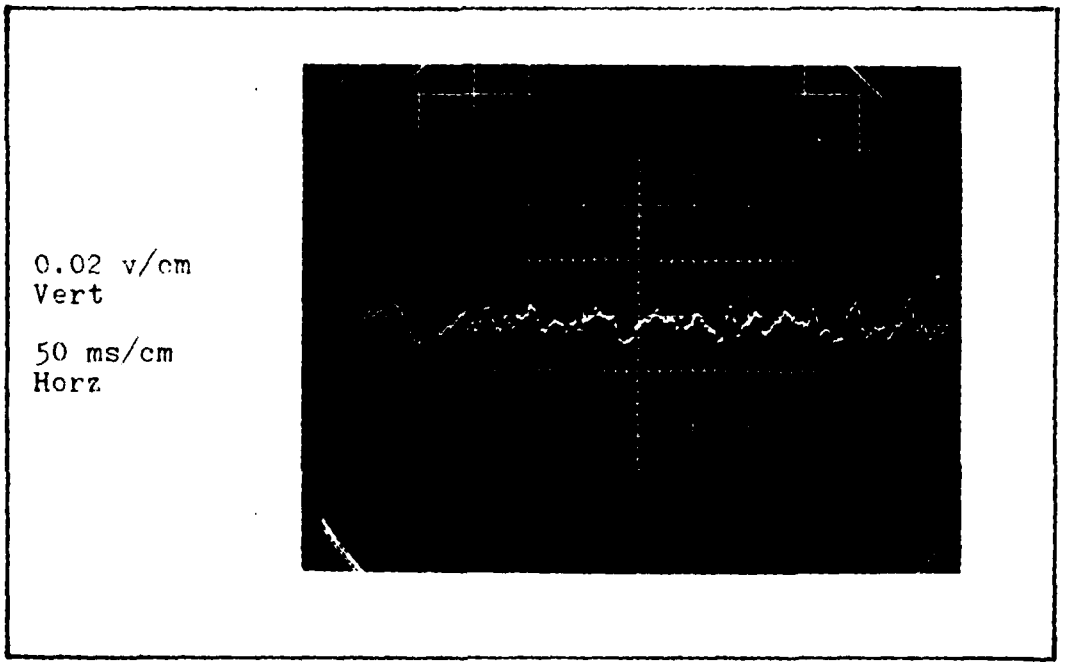

Figure D.6 Noise from Compensator Gc_{3b}

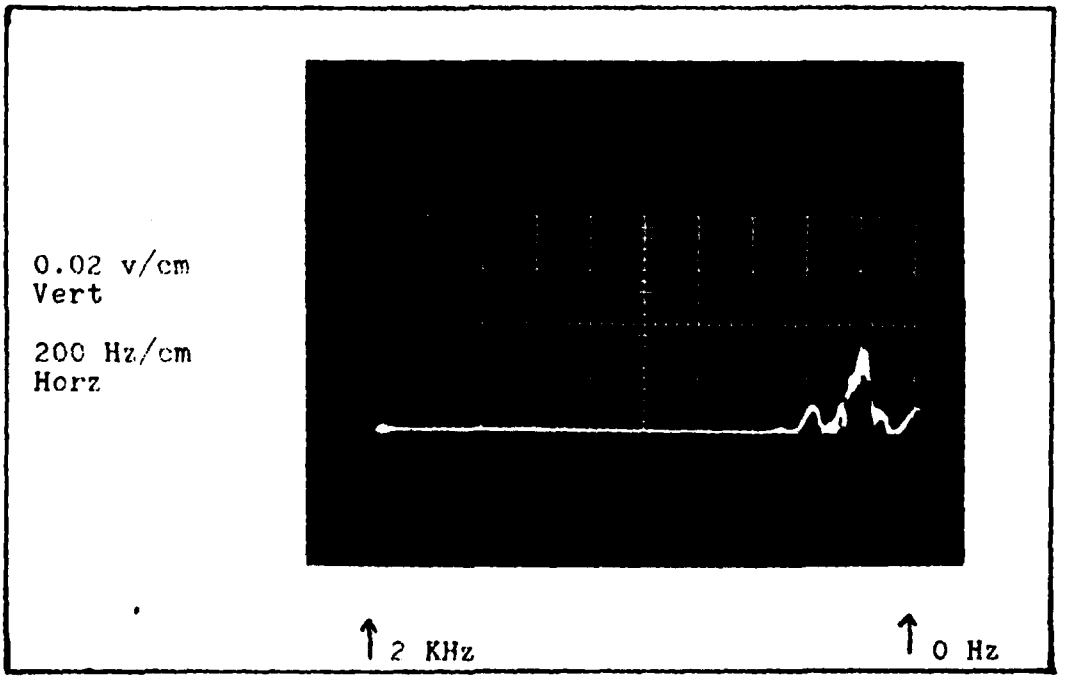

Figure D.7 Spectral Content of the Noise from Compensator Gc_{3b}

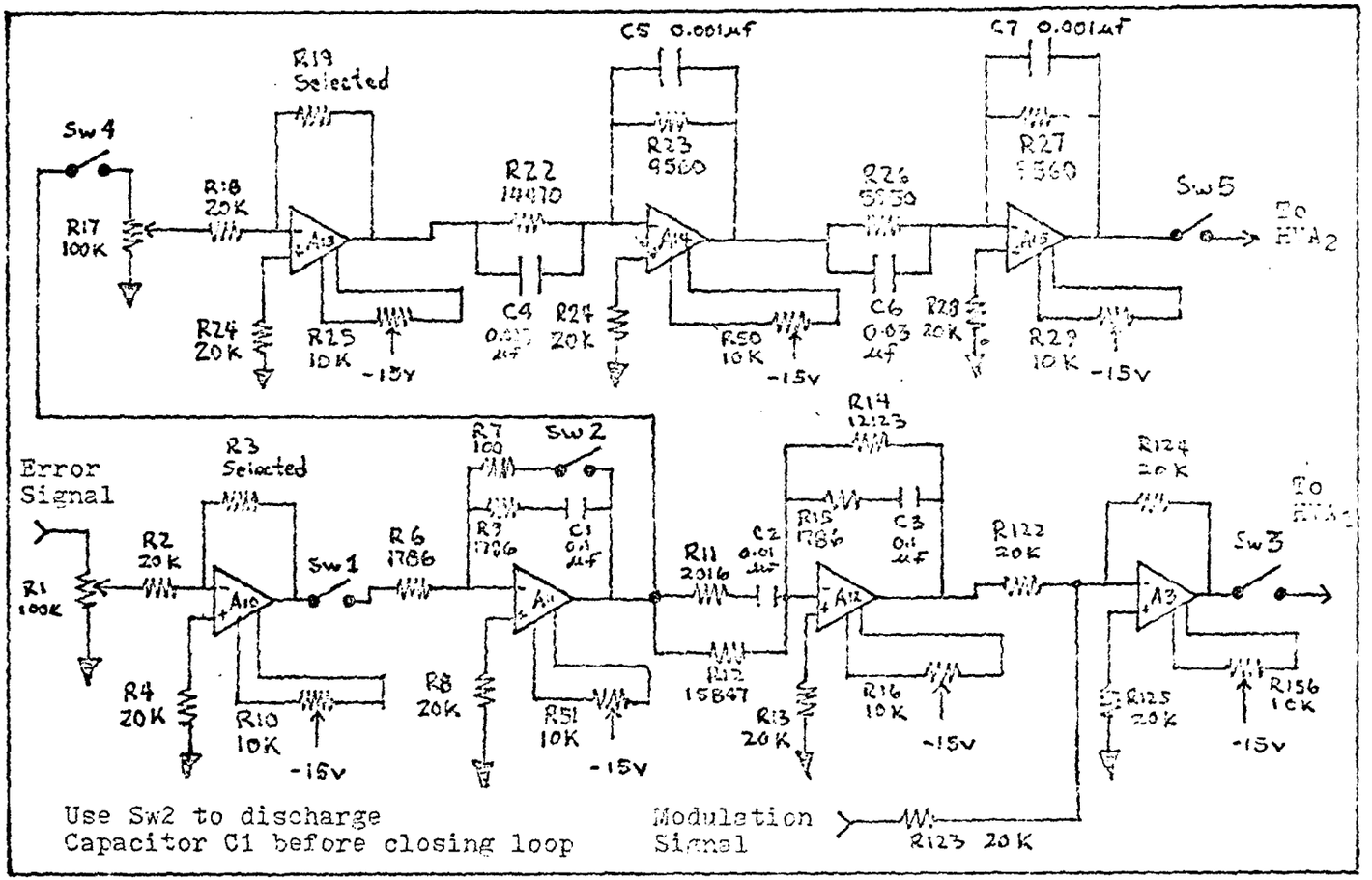

Figure D.8 Schematic Diagram of Compensator Gc_3 for Method II

Appendix E

Experimental Procedure

Test Set-up

The laboratory and test site used in this experiment are located in the Air Force Institute of Technology Building 640, room 238, at Wright Patterson AFB, Ohio. Within the laboratory, the laser and interferometer were mounted on a one inch thick aluminum plate and placed on a layer of foam rubber to isolate them from table vibrations. The laser was also covered with a plastic shield to reduce the affects of acoustical noise and air currents. The interferometer was wrapped with styrofoam and tape to isolate it from temperature variations.

Test Procedure

The following is the test procedure to use in order to lock the laser to the interferometer resonance.

Step 1. With the system in a closed loop configuration, turn all of the compensator switches to off. This opens the loop and discharges the integrator capacitors.

Step 2. Connect the oscilloscope horizontal output to the summing amplifier side of the compensator output switch.

Step 3. Adjust HVA_1 bias and gain control so that

a laser mode is detected on the oscilloscope from the detector output. With the LIA output also connected to the oscilloscope, the error signal will appear as a derivative of the detector signal.

Step 4. Maximize the error signal by adjusting the modulation frequency around 41 KHz.

Step 5. Rotate the LIA phase control to 90^{o} and adjust the phase for a minimum error signal.

Step 6. Rotate the phase control to 0^{o} and disconnect the oscilloscope horizontal output from the summing amplifier input.

Note: Steps 2 through 5 are accomplished to assure that the maximum derivative signal is achieved. It only needs to be performed about once a day.

Step 7. Manually adjust the interferometer power supply until the interferometer resonance matches a laser mode as seen by watching the detector output on the oscilloscope. If more than one mode is present, select the largest.

Step 8. Turn on all of the compensator switches.

With the above procedure completed, the laser will be locked to the interferometer resonance.

Appendix F

Equipment Listing

Equipment	Number Required
Laser Gain Tube, Spectra-Physics Model 120	1
Mirrors, Dielectric	
Laser - 35 cm Radius of Curvature, 98% Reflective	1
- Flat, 99.9% Reflective	1
Piezoelectric Length Transducer, Channel Devices	
Navy Type 54, 1-1/2 inch	1
Navy Type 54, 1/2 inch	1
Laser Exciter, Spectra-Physics Model 249	1
Interferometer, Jodon Model SA 1500	1
Compensator Circuits (See Figures B.5, C.5, and D.8)	1
Chart Recorder, Gould Brush 200 Eight Channel	1
Lock-In-Amplifier, Princeton Applied Research Model HR-8	1
High Voltage DC OP Amp, Burliegh Model PZ-70	2
Electronic Counter, Hewlett Packard Model 5212 A	1
Oscilloscope, Tecktronix Model 565	1
Oscilloscope, Lavoi Model 265 A	1
Spectrum Analyzer, Nelson-Ross PSA-016 Oscilloscope Plug-In Unit	1
Signal Generator, Wavetek Model 186	1
Neutral Density Filter, Oriel Corp. Density Factor 1.2	1
Power Supply, John Fluke Model 405B	1

Vita

Robert D. Luzitano was born on 28 December 1944 in Fall River, Massachusetts. He graduated from San Bernardino High School in 1962 and entered the United States Air Force a month later. He received an Associate of Arts degree in Liberal Arts from Victor Valley College in 1969. He graduated from California State University at Sacramento in 1973 with a Bachelor of Science degree in Electrical Engineering. He received his commission from Officer Training School in December 1973 and worked as an avionics maintenance officer for the 93rd Avionics Maintenance Squadron at Castle AFB, California. He entered the School of Engineering, Air Force Institute of Technology, in June 1978 and pursued studies towards a Master of Science degree in Electrical Engineering. Captain Luzitano is scheduled to be assigned to the 6514th Test Squadron at Hill AFB, Utah upon completion of his studies.

UNCLASSIFIED
SECURITY CLASSIFICATION OF THIS PAGE (When Data Entered)

REPORT DOCUMENTATION PAGE	READ INSTRUCTIONS BEFORE COMPLETING FORM
1. REPORT NUMBER: AFIT/GE/EE/80-2	2. GOVT ACCESSION NO.: AD-A085707
3. RECIPIENT'S CATALOG NUMBER	
4. TITLE (and Subtitle): Comparison of Control Methods in a Frequency Stabilized Laser	5. TYPE OF REPORT & PERIOD COVERED: M.S. Thesis
	6. PERFORMING ORG. REPORT NUMBER
7. AUTHOR(s): ROBERT [redacted] LUZITANO, CAPT [redacted] USAF	8. CONTRACT OR GRANT NUMBER(s)
9. PERFORMING ORGANIZATION NAME AND ADDRESS: Air Force Institute of Technology (AFIT/EN), Wright-Patterson AFB Ohio 45433	10. PROGRAM ELEMENT, PROJECT, TASK AREA & WORK UNIT NUMBERS
11. CONTROLLING OFFICE NAME AND ADDRESS: Air Force Avionics Laboratory/RWA-2, Wright-Patterson AFB Ohio 45433	12. REPORT DATE: [redacted] 13. [redacted] 120
14. MONITORING AGENCY NAME & ADDRESS (if different from Controlling Office)	15. SECURITY CLASS (of this report): UNCLASSIFIED 15a. DECLASSIFICATION/DOWNGRADING SCHEDULE

16. DISTRIBUTION STATEMENT (of this Report)

Approved for public release; distribution unlimited

17. DISTRIBUTION STATEMENT (of the abstract entered in Block 20, if different from Report)

18. SUPPLEMENTARY NOTES

Approved for public release; IAW AFR 190-17

JOSEPH P. HIPPS
Director of Public Affairs

19. KEY WORDS (Continue on reverse side if necessary and identify by block number)

Frequency Stabilized Laser
Control of Laser Frequency

20. ABSTRACT (Continue on reverse side if necessary and identify by block number)

The purpose of this research is to compare two types of control methods that can be used to frequency stabilize a laser. The first method uses a single piezoelectric transducer (PZT) to control the cavity length of a heliumneon laser. The second method employs dual PZT controllers of different lengths so that a fast response time can be achieved with the benefit of a large dynamic range. Two variations of the first method are compared to the second method. The first variation uses an integrator with gain as a compensator in

DD FORM 1 JAN 73 1473 EDITION OF 1 NOV 65 IS OBSOLETE

012225

UNCLASSIFIED
SECURITY CLASSIFICATION OF THIS PAGE (When Data Entered)

electronic feedback control loop and is designed using steady state analysis. The second variation uses a more sophisticated compensator that is designed using frequency analysis. Frequency analysis is also used in the compensator design for the second method. Each compensator is tested in a laser control loop and the results of each method are compared.